ABSTRACT

Title of Document: ADVANCED MODELING AND REFRIGERANT FLOW PATH OPTIMIZATION FOR AIR-TO-REFRIGERANT HEAT EXCHANGERS WITH GENERALIZED GEOMETRIES

Zhenning Li, Doctor of Philosophy, 2019

Directed By: Reinhard Radermacher, Professor
Vikrant Aute, Research Scientist
Department of Mechanical Engineering

Air-to-refrigerant heat exchangers are key components of the heating, ventilation, air-conditioning and refrigeration systems. The evolving simulation and manufacturing capabilities have given engineers new opportunities in pursuing complex and cost-efficient heat exchanger designs. Advanced heat exchanger modeling tools are desired to adapt to the industrial transition from conventional refrigerants to low Global Warming Potential (low-GWP) refrigerants. This research presents an advanced heat exchanger performance prediction model which distinguishes itself as a cutting-edge simulation tool in the literature to have capabilities, such as to (i) model heat exchangers with variable tube shape and topology, (ii) improved numerical stability, (iv) multiple dehumidification models to improve evaporator prediction, and (v) CFD-based predictions for airflow maldistribution.

Meanwhile, HX performance is significantly influenced by the refrigerant flow path arrangements. The refrigerant flow path is optimized for various reasons such as to (i) mitigate the impact of airflow maldistribution, (ii) reduce material/cost, (iii) balance refrigerant state at the outlet of each circuit, and (iv) ensure overall stable performance under a variety of operating conditions. This problem is particularly challenging due to the

large design space which increases faster than n factorial with the increase in the number of tubes.

This research presents an integer permutation based Genetic Algorithm (GA) to optimize the refrigerant flow path of air-to-refrigerant heat exchangers. The algorithm has novel features such as to (i) integrate with hybrid initialization approaches to maintain the diversity and feasibility of initial individuals, (ii) use effective chromosome representations and GA operators to guarantee the chromosome (genotype) can be mapped to valid heat exchanger designs (phenotype), and (iii) incorporate real-world manufacturability constraints to ensure the optimal designs are manufacturable with the available tooling. Case studies have demonstrated that the optimal designs obtained from this algorithm can improve performance of heat exchangers under airflow maldistribution, reduce defrost energy and assure stable heat exchanger performance under cooling and heating modes in reversible heat pump applications. Comparison with other algorithms in literature shows that the proposed algorithm exhibits higher quality optimal solutions than other algorithms.

ADVANCED MODELING AND REFRIGERANT FLOW PATH OPTIMIZATION FOR AIR-TO-REFRIGERANT HEAT EXCHANGERS WITH GENERALIZED GEOMETRIES

By

Zhenning Li

Dissertation submitted to the Faculty of the Graduate School of the
University of Maryland, College Park, in partial fulfillment
of the requirements for the degree of
Doctor of Philosophy
2019

Advisory Committee:
Prof. Reinhard Radermacher (Chair/Advisor)
Dr. Vikrant Aute (Co-advisor)
Prof. Shapour Azarm
Prof. Peter Sunderland
Prof. Jelena Srebric
Prof. Bao Yang

DEDICATION

To my grandmother on my mother's side,

Without her infinite love, I could not have had the opportunity to grow up.

ACKNOWLEDGEMENTS

I would like to express my sincere gratitude to my co-advisors, Prof. Reinhard Radermacher and Dr. Vikrant Aute, for offering me the opportunity to carry out this thesis research at the Center for Environmental Energy Engineering. I benefited greatly from their advice, motivation, immense knowledge and innovative thoughts. I am also grateful to my committee members: Prof. Shapour Azarm, Prof. Peter Sunderland, Prof. Jelena Srebric, Prof. Bao Yang for their insightful comments to improve the quality of this work.

I would like to thank Dr. Jiazhen Ling who offered me tremendous help throughout my stay at CEEE. Among CEEE alumni, Dr. Hongtao Qiao and Dr. Moon Soo Lee have helped me to clear up doubts and understand this field. I would like to thank Ransisi Huang who is a wonderful colleague to work with. And thanks to Dr. Rohit Dhumane, who is a reliable friend and become a constant source of support and sanity during my graduate school life.

I feel especially privileged to have Dr. Arne Speerforck as my friend. His wisdom and kindness guide me to be a better person. Thanks to Dr. Xiaojie Lin who accompanied me to overcome various difficulties. Thanks to Song Wei Li for the wonderful tennis time. Thanks to Zhenyuan Mei for joining me to enjoy numerous concerts. Thanks to my friends, Anna Sotnikova and Julia Berhard for offering me their support mentally. I would like to thank my girlfriend, Ke Lan for her companion and the numerous happy moments we shared together. Brutally as she beats me on Ping-Pong every single match, she is always cheering me up during good times and bad times. Lastly, I am grateful to my parents for their patience and encouragement. The love they have offered me is more than what I could have asked for.

TABLE OF CONTENTS

1 Introduction 1

1.1 Background and Motivation 1

1.2 Literature Review 2

1.2.1 Review of tube-fin heat exchanger modeling 2

1.2.2 Review of tube-fin heat exchanger circuitry optimization 5

1.2.3 Review of microchannel heat exchanger pass arrangements optimization 10

1.2.4 Review of robust optimization 12

1.2.5 Review of heat exchanger airflow maldistribution 14

1.3 Research Objectives 18

2 Tube-Fin Heat Exchanger Circuitry Optimization Using Integer Permutation Based Genetic Algorithm 20

2.1 Integer Permutation based Genetic Algorithm 20

2.1.1 Representation of heat exchanger circuitry 20

2.1.2 Selection 23

2.1.3 GA operators 23

2.2 Constraint Handling 26

2.2.1 Manufacturability Constraints 26

2.2.2 Constraint Handling Method 27

2.3 Hybrid Initialization Approaches 29

2.3.1 Predefined circuitry patterns 29

2.3.2 Integer permutation sampling 30

2.3.3 Optimal solutions from sub-problem optimization 31
2.4 Case Study 32
2.4.1 Baseline heat exchanger 32
2.4.2 Objectives 34
2.4.3 Unconstrained optimization 35
2.4.4 Constrained optimization 36
2.5 Stability Test 39
2.6 Comparison with Methods from Literature 40
2.7 Exhaustive Search Verification 43
2.8 Summary 45
3 Applications of Integer Permutation Based Genetic Algorithm 46
3.1 Heat Exchanger Circuitry Optimization for Improved Performance under Air Flow Maldistribution 46
3.1.1 Methodology 47
3.1.2 Problem Formulations 48
3.1.3 Results 50
3.1.4 Performance of Optimal Circuitries 53
3.1.5 Analysis of Optimal Designs 55
3.1.6 Performance of Optimal Heat Exchanger Designs in a System 57
3.1.7 Summary 58
3.2 New Heat Exchanger Circuitry Optimization Problem Formulation for Improved Performance Under Frosting Conditions 59
3.2.1 Background 59

3.2.2 Problem Formulation 60
3.2.3 Baseline Outdoor Heat Exchanger 61
3.2.4 Circuitry Optimization Results 64
3.2.5 Heat Exchanger Simulation under Frosting Conditions 66
3.2.6 Summary 71
3.3 New Heat Exchanger Circuitry Optimization Problem Formulation for Improved Performance in Reversible Heat Pump Applications 72
3.3.1 Introduction 72
3.3.2 Problem Formulation 72
3.3.3 Bi-objective Optimization 74
3.3.4 Single Objective Optimization 75
3.3.5 Summary 78
4 Multi-bank Microchannel Heat Exchanger Pass Configuration Optimization Using Integer Permutation based Genetic Algorithm 79
4.1 Introduction 79
4.2 Chromosome Design for Microchannel Heat Exchanger Pass Arrangements 79
4.3 Selection Operator and Constraint Handling 81
4.4 GA Operators 81
4.5 Case Study 83
4.5.1 Baseline heat exchanger 83
4.5.2 Objectives and Constraints 85
4.5.3 Case study I: single-bank MCHX 86

4.5.4 Case study II: multi-bank MCHX 88
4.6 Summary 89
5 Modeling of Variable Geometry Tube-Fin Heat Exchanger 90
5.1 Concept of Variable Geometry 90
5.2 Modeling Assumptions 93
5.3 Tube Connections 93
5.4 Basic Solving Methodology 95
5.5 Air Side Propagation 97
5.6 Robust Wall Temperature and Heat Flux based Solution Scheme 98
5.7 Pressure Drop Calculation 100
5.8 Correlation Smoothing with User-defined Boundaries 101
5.8.1 Discontinuity in single phase correlation 101
5.8.2 Discontinuity in phase transition regions 103
5.8.3 Smoothing effect on simulation results 107
5.9 Modeling Validation 107
5.9.1 Conventional geometry tube-fin heat exchanger data 107
5.9.2 Variable geometry tube-fin heat exchanger data 108
5.10 Summary 110
6 A CFD Assisted Heat Exchanger Model for Simulation of Air Flow Mal-distribution for Air-to-Refrigerant Heat Exchanger 111
6.1 CFD Model 111
6.2 Segmented Heat Exchanger and CFD Model Co-simulation 115
6.3 Effect of Different Parameters on Air Flow Maldistribution 116

6.4 Effect of Air Maldistribution on Heat Exchanger Performance..... 123

6.5 Summary 128

7 List of Major Contributions and Future Work..... 130

7.1 Contributions Resulting from This Research 130

7.1.1 Tube-fin heat exchanger circuitry optimization using Integer Permutation based Genetic Algorithm 130

7.1.2 Tube-fin heat exchanger circuitry optimization problem formulation for improved performance under multiple air velocity profiles 130

7.1.3 Tube-fin heat exchanger circuitry optimization problem formulation for improved performance under frosting conditions..... 131

7.1.4 Tube-fin heat exchanger circuitry optimization problem formulation for heat exchangers used as condensers and evaporators in heat pump applications... 132

7.1.5 Multi-bank microchannel heat exchanger pass optimization using Integer Permutation based Genetic Algorithm..... 133

7.1.6 Development of the variable geometry air-to-refrigerant heat exchanger model with capability to simulate next generation heat exchanger and predict airflow maldistribution..... 134

7.2 Summary of Major Contributions 134

7.3 List of Publications..... 136

7.4 Future Work 138

References..... 140

LIST OF TABLES

Table 2-1: Structural Parameters and Operating Conditions of Baseline Evaporator 33

Table 2-2: Correlations Adopted in HX Simulation 33

Table 2-3: Evaporator Optimization Results with Different Constraints 38

Table 2-4: Comparison of Tube-fin Heat Exchanger Circuitry Optimization Methods 43

Table 2-5: Exhaustive Search Verification Results 45

Table 3-1: Structural Parameters of Baseline Evaporator 63

Table 3-2: Operating Conditions of Baseline Evaporator 63

Table 3-3: Correlations Adopted in HX Simulation 64

Table 3-4: Comparison of Baseline VS Optimal Design 66

Table 3-5: Summary of Optimization Results 77

Table 4-1: Structural Parameters and Operating Conditions of Baseline MCHXs 84

Table 4-2: Single Bank MCHX Optimization Results 87

Table 4-3: Multi-bank MCHX Optimization Results 88

Table 5-1: Comparison between Successive Substitution and Golden Section Search to Model a CO_2 Gas Cooler with Different Supercritical HTC Correlations 99

Table 5-2: Benchmark of Different Smoothing Techniques 105

Table 6-1: Air Side Pressure Drop Correlations Used in Current Study 112

Table 6-2: Variables for Parametric Study 118

Table 6-3: Different Fin Types and Momentum Resistance Coefficients for Parametric Study 118

Table 6-4: Refrigerant (R410A) Side Heat Transfer and Pressure Drop Correlations Used for Performance Study 123

Table 6-5: Heat Exchanger Specifications and Test Conditions for Performance Study 124

LIST OF FIGURES

Figure 1-1: Tube-fin HX (a) Conventional geometry; (b) Variable geometry 4

Figure 1-2: Examples of Circuitries: (a) One of CO2 Gas Cooler Circuitries from Zilio et al. (2007); (b) Counter-flow Circuitry; (c) Parallel-flow circuitry; (d) Interleaved circuitry 7

Figure 2-1: Chromosome Representation: (a) 15-tube heat exchanger example; (b) Corresponding two-part chromosome 21

Figure 2-2: Chromosome Representation: (a) 24-tube heat exchanger sample; (b) Split branch chromosome 22

Figure 2-3: (a) Gene sequence inversion; (b) Gene insertion 24

Figure 2-4: (a) In-branch transposition; (b) Cross-branch transposition 24

Figure 2-5: (a) Branch detachment; (b) Branch union 25

Figure 2-6: (a) Split operator; (b) Effect of split operator 25

Figure 2-7: (a) Merge operator; (b) Effect of merge operator 26

Figure 2-8: Manufacturability Constraints: (a) Inlet & Outlet on the same side; (b) Inlet & outlet on the opposite side; (c) Long U-bends; (d) U-bend crossings; (e) Tubes splitting or merging from a single tube 27

Figure 2-9: Illustration for Recurring Circuitry Patterns: (a) 4-circuit, parallel flow, inlet tube at top; (b) 4-circuit, counter flow, inlet tube at top; (c) 5-circuit, inlet tube at bottom; (c) 22-circuit, counter flow 29

Figure 2-10: Examples of Initial Individuals Generated by Integer Permutation Sampling: (a) Random permutation; (b) Latin Hypercube sampling 30

Figure 2-11: Sample Solutions from Sub-problem Optimization: (a) Optimize the small sectional HX and repeat its pattern; (b) Optimize the entire HX 32

Figure 2-12: (a) Baseline Circuitry; (b) Experiment Tests vs Simulations 34

Figure 2-13: (a) Optimal circuitry; (b) GA optimization progress; (c) Histogram of number of circuits 36

Figure 2-14: Optimal Circuitry Designs (a) Baseline; (b) Unconstrained; (c) With mfg. constraints; (d) With refrigerant DP constraint; (e) With mfg. and DP constraints . 38

Figure 2-15: Capacity Distribution of Optimal Designs under Different Constraints for 60 runs. 39

Figure 2-16: Refrigerant Pressure Drop Distribution of Optimal Designs under Different Constraints 40

Figure 2-17: Sensible Heat Ratio Distribution of Optimal Designs under Different Constraints 40

Figure 2-18: HX Circuitry Designs: (a) Baseline; (b) Domanski *et al.* (2004); (c) Wu *et al.* (2008a); (d) Proposed algorithm 42

Figure 3-1: Air Velocity Distribution Profiles Collected from Lab Measurements 48

Figure 3-2: Optimization results from Max (Min.Q): (a) GA Progress; (b) Optimal Circuitry; (c) Optimal vs Baseline 50

Figure 3-3: Optimization Results from Max(Avg.Q): (a) GA progress; (b) Optimal circuitry; (c) Optimal vs baseline 51

Figure 3-4: Optimization Results from Min(Std.Q): (a) GA progress; (b) Optimal circuitry; (c) Optimal vs baseline 52

Figure 3-5: Comparison of Conventional Optimal, New Optimal and Baseline 53

Figure 3-6: (a) A-coil Airflow Profiles for Different Air Flow Rate; (b) Performance Comparison of Circuitry Designs 55

Figure 3-7: Comparison of Conventional Optimal, New Optimal and Baseline: (a) Refrigerant mass flow distribution in each circuit; (b) Superheat at the outlets of each circuit; (c) Capacity offered by each circuit; (d) Air flow rate distribution..... 56

Figure 3-8: Performance Comparison of New Optimal, Conventional Optimal and Baseline in a Cycle: (a) Simulated cycle in VapCyc®; (b) R410A P-h diagram using three HX designs..... 58

Figure 3-9: Outdoor unit from FTVI..... 62

Figure 3-10: Experimental tests vs simulations 62

Figure 3-11: IPGA optimization progress..... 64

Figure 3-12: Optimal heat exchanger circuitry 65

Figure 3-13: Frosting experiment tests vs simulations (Qiao et al, 2017) 67

Figure 3-14: Evaporator capacity transients..... 67

Figure 3-15: Frost mass transients 68

Figure 3-16: Frost distribution on different banks 69

Figure 3-17: Tube-wise evolution of frost thickness (baseline)..... 70

Figure 3-18: Tube-wise evolution of frost thickness (optimal circuitry) 70

Figure 3-19: Transients of air flow rate 71

Figure 3-20: (a) Pareto Front of Bi-objective HX Optimization; (b) Optimal Design with Medium Performance as Evaporator; (c) Optimal Design with Medium Performance as Condenser 75

Figure 3-21: (a) GA Progress from Single Objective Optimization; (b) Optimal Circuitry from Optimization under AC mode; (c) Reversed Circuitry as a Condenser under HP mode 76

Figure 3-22: Comparison of Bi-objective Optimal vs Single Objective Optimal ... 77

Figure 4-1: Pass Arrangement Representation: (a) 20-tube MCHX; (b) Chromosome 80

Figure 4-2: GA Operators: (a) Circuit union; (b) Circuit split; (c) Pass union 82

Figure 4-3: GA Operators: (a) Pass split; (b) Pass sequence inversion; (c) Tubes redistribution 83

Figure 4-4: 1-bank MCHX (a) GA progress; (b) Optimal; (c) Best design in Mehendale et al. (2016) 86

Figure 4-5: 2-bank MCHX (a) GA progress; (b) Baseline; (c) Optimal design 88

Figure 5-1: (a) Tube-fin heat exchanger with staggered tube configuration; (b) Tube-fin heat exchanger with arbitrary tube layout 90

Figure 5-2: Accelerated air evaporator from Waltrich et al. (2011) 92

Figure 5-3: (a) Next generation heat exchanger with novel tube shapes; (b) Next generation heat exchanger made by additive manufacturing 94

Figure 5-4: (a)U-bend length calculation in Jiang et al. (2006); (b) Improved U-bend length calculation 95

Figure 5-5: Methodology for obtaining weights for mixing of air stream 97

Figure 5-6: Schematic to explain air propagation through heat exchanger 98

Figure 5-7: Iteration in 1 Segment of CO2 Gas Cooler 100

Figure 5-8: Pressure drop prediction for 5 sample evaporators 101

Figure 5-9: Continuities in Single Phase HTC Correlations 102
Figure 5-10: Discontinuities in Single Phase DP Correlations 103
Figure 5-11: Discontinuities in Phase Transition Regions 103
Figure 5-12: Benchmark of Different Smoothing Techniques 105
Figure 5-13: Continuity of Outlet Enthalpy Changing Inlet Mass Flow Rate 106
Figure 5-14: Continuity of Outlet Enthalpy Changing Inlet Pressure 106
Figure 5-15: Continuity of Outlet Enthalpy Changing Inlet Enthalpy 106
Figure 5-16: Correlation Smoothing Effect on Simulation Results 107
Figure 5-17: Verification of New Model against Jiang *et al.* (2006)'s Model 108
Figure 5-18: Illustration of Next Generation Heat Exchangers 109
Figure 5-19: (a) Cartesian grid of NTHX-001; (b) Capacity validation for NTHXs 109
Figure 6-1: Computational Domain and Mesh of the A-Type Heat Exchanger ... 114
Figure 6-2: Detailed Approach for Integrated CFD Solver with Heat Transfer Model 116
Figure 6-3: Concept for Integrated CFD - HX Model 116
Figure 6-4: Effect of Heat Exchanger Apex Angle on the Velocity Profile 119
Figure 6-5: Effect of Heat Exchanger Depth on the Velocity Profile 120
Figure 6-6: Effect of Heat Exchanger Height on the Velocity Profile 121
Figure 6-7: Effect of Mass Flow Rate on the Velocity Profile 121
Figure 6-8: Effect of Fin Types on the Velocity Profile 122
Figure 6-9: Upper Slab of A-coil Used in Simulation 124
Figure 6-10: Effect of Fin Type on Heat Exchanger Capacity Degradation 126

Figure 6-11: Effect of Coil Depth on Heat Exchanger Capacity Degradation..... 126

Figure 6-12: Effect of Coil Height on Heat Exchanger Capacity Degradation..... 127

Figure 6-13: Effect of Apex Angle on Heat Exchanger Capacity Degradation.... 127

Figure 6-14: Effect of Air Velocity on Heat Exchanger Capacity Degradation ... 128

Figure 6-15: Refrigerant Flow Mal-distribution at Different Apex Angle 128

NOMENCLATURE

Acronyms

AC	air conditioning
AFR	air flow rate
AHRI	Air-conditioning, Heating and Refrigeration Institute
ASHRAE	American Society of Heating, Refrigerating and Air-Conditioning Engineers
CFD	computational fluid dynamics
CFM	cubic feet per minute
COP	coefficient of performance
DP	pressure drop
EA	evolutionary algorithm
FPI	fins per inch
FTVI	flash tank vapor injection
GA	Genetic Algorithm
HP	heat pump
HTC	heat transfer coefficient
HVACR	heating ventilation air conditioning and refrigeration
HX	heat exchanger
IPGA	Integer Permutation based Genetic Algorithm
ISHED	Intelligent System of Heat Exchanger Design
LMTD	Logarithmic Mean Temperature Difference method
MCHX	microchannel heat exchanger

MST	Minimum Spanning Tree Problem
NTHX	next generation heat exchanger
PIV	particle image velocimetry
RMOGA	Robust Multi-objective Genetic Algorithm
STD	standard deviation
TFHX	tube-fin heat exchanger
TSP	Travelling Salesman Problem
UTFHX	unified tube-fin heat exchanger
VRP	Vehicle Routing Problem
ε -NTU	Effectiveness - Number of Transfer Unit method

English letters

A	surface area [m^2]
C_p	specific heat [$J \cdot kg^{-1} \cdot K^{-1}$]
D	diameter [m]
f	frictional loss coefficient [dimensionless]
G	mass flux [$kg \cdot s^{-1} \cdot m^{-2}$]
H	header
h	enthalpy [$J \cdot kg^{-1}$]
ID	inner diameter [m]
k	thermal conductivity [$W \cdot m^{-1} \cdot K^{-1}$]
$\dot{m}$	mass flow rate [$kg \cdot s^{-1}$]
Nu	Nusselt number [dimensionless]

Pr	Prandtl number [dimensionless]
Q	heat transfer rate [W]
R	absolute thermal resistance [$K \cdot W^{-1}$]
Re	Reynolds number [dimensionless]
T	temperature [K]
ΔT	temperature difference [K]
U	heat transfer coefficient [$W \cdot m^{-2} \cdot K^{-1}$]
x	position [m] or quality [dimensionless]
Δx	distance [m]

Greek letters

δ	thickness [m]
ε	effectiveness [dimensionless]
η	fin efficiency [dimensionless]
μ	dynamic viscosity [Pa·s]
ρ	density [$kg \cdot m^{-3}$]
φ	two-phase multiplier [dimensionless]

Subscripts

c	cross-section
cond	condensation
cr	critical point

eff	effective
evap	evaporation
g	gas
h	hydraulic
i	intermediate
in	inlet
max	maximum
min	minimum
out	outlet°
ref	refrigerant
wall	tube wall

1 INTRODUCTION

1.1 Background and Motivation

Air-to-refrigerant heat exchangers (HXs) are key components in air-conditioning, heat pump and refrigeration systems. The most common types of air-to-refrigerant heat exchangers are tube-fin heat exchangers (TFHXs) and microchannel heat exchangers (MCHXs). There is a great emphasis on understanding the underlying physics and improving the performance of these heat exchangers. More recently, researchers have been investigating the use of small hydraulic diameter tubes/channels and variable geometry designs as well as novel heat transfer surfaces in such heat exchangers. In order to design optimum heat exchangers for a given application, it is crucial to use a reliable thermal-hydraulic model to evaluate the performance of air-to-refrigerant heat exchangers. In the last two decades, significant strides have been made in modeling of tube-fin heat exchangers and microchannel heat exchangers. The modeling techniques include the use of performance maps, Logarithmic Mean Temperature Difference method (LMTD) and Effectiveness - Number of Transfer Unit method (ε -NTU) and fully discretized control volume approaches. The four main control volume based modeling approaches for heat exchangers are lumped, moving boundary, tube-by-tube and segment-by-segment approaches. The overall fidelity and computational time increases from lumped approach to segment-by-segment approach. This research aims at developing the state-of-the-art finite volume model of air-to-refrigerant heat exchangers and extend the boundaries of conventional heat exchanger modeling methods.

This dissertation starts with reviews on several topics including tube-fin heat exchanger circuitry optimization, microchannel heat exchanger pass arrangements

optimization, airflow maldistribution in air-to-refrigerant heat exchangers and finite volume heat exchanger modeling. Chapter 1 streamlines the research objectives and contributions. Chapter 2 presents a new Genetic Algorithm based tube-fin heat exchanger circuitry optimization algorithm. Chapter 3 presents three major applications of the proposed circuitry optimization algorithm: a new problem formulation for heat exchanger circuitry optimization under air flow maldistribution, a new problem formulation for heat exchanger circuitry optimization under frosting conditions and a multi-objective problem formulation for improved heat exchanger performance in reversible heat pumps. Chapter 4 extends the Integer Permutation based Genetic Algorithm to optimize microchannel heat exchanger pass arrangements. Chapter 5 details the derived modeling paradigms of the unified tube-fin heat exchanger model. Chapter 6 presents a computational fluid dynamics and heat exchanger co-simulation approach to capture the air flow maldistribution at the frontal face of heat exchanger and explore the effect of air flow maldistribution on heat exchanger performance. Chapter 7 concludes with a discussion of major contributions, paper publications and future work.

1.2 Literature Review

1.2.1 Review of tube-fin heat exchanger modeling

To the author's knowledge, the earliest simulations of a heat exchanger dates back to Hermann (1962) which developed an electronic analog computer flow chart to set up a steam generation process in a heat exchanger. The rapid development of electronic computers led the heat transfer community to realize the vast potential of computers in the study of heat transfer. Katz and Briggs (1965) outlined areas showing increasing use of computers at the time, including development of correlations, solving

fundamental equations and optimizing heat exchanger designs. In the recent decades, there have been several heat exchanger models and tools in the literature used to model both steady state and transient behavior of heat exchangers, which have been validated against experimental results. Rossi and Braun (1995) presented a heat exchanger model which is part of a vapor compression cycle simulation tool called ACMODEL developed by Shen *et al.* (2004). This heat exchanger model is based on the Effectiveness-Number of Transfer Units (ε-NTU) approach, and used correlations to obtain required coefficients for heat transfer, pressure drop, void fraction etc. Domanski (2003) presented a public-domain heat exchanger design and simulation tool called EVAP-COND. It followed a tube-by-tube control volume approach for modeling heat exchanger. EVAP-COND offers many features like refrigerant maldistribution through different circuits and one-dimensional airflow maldistribution. Jiang *et al.* (2002) and Jiang *et al.* (2006) presented a model based on segment-by-segment control volume approach. In this model, each tube is divided into many segments. This allows the user to model two-dimensional airflow maldistribution on coil face. Liu *et al.* (2004) developed a general steady state model for tube-fin heat exchangers based on graph theory. Their model accounts for refrigerant distribution through a flexible circuitry arrangement and accounts for heat conduction between tubes as well. Their approach is not based on the ε-NTU method. Rather, they apply energy conservation to a given control volume, starting with guessed outlet states for air and refrigerant as well as guessed wall temperatures. Liang *et al.* (2001) studied the effect of refrigerant circuitry on evaporator performance through numerical modeling. They developed a distributed simulation model for predicting the steady state operation of an R134a evaporator. Oliet

et al. (2007) carried out a numerical simulation of the dehumidification on tube-fin heat exchangers and suggested their modeling strategies, which aimed at accurately solving the dehumidification process. Lee and Domanski (1997) suggested a model to account for heat conduction through fins. This model is capable of accounting for tube-to-tube conduction. In this model, the heat transfer between air and refrigerant is calculated using the ε-NTU approach for every tube in the heat exchanger. Singh *et al.* (2009) proposed ε-NTU and energy balance-based models that can account for fin conduction as well as variable geometries. Recently Sarfraz and Bradshaw (2019) developed a tube-fin heat exchanger model which also considered tube-to-tube heat conduction.

A conventional tube-fin heat exchanger is shown in Figure 1-1 (a), and a variable geometry tube-fin heat exchanger is shown in Figure 1-1(b). The tubes are represented by black circles and the fin sheets are represented by gray rectangles. A dotted line represents a U-bend at the far end of the reader, while a solid line presents a U-bend at the near end of the reader. The variable geometry tube-fin heat exchanger (Figure 1-1 (b)) contains tubes with different diameters and irregular fin sheets.

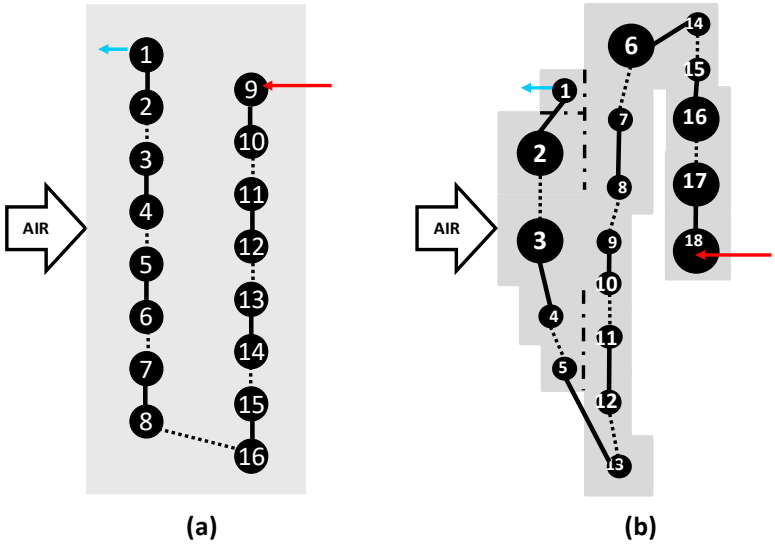

Figure 1-1: Tube-fin HX (a) Conventional geometry; (b) Variable geometry

1.2.2 Review of tube-fin heat exchanger circuitry optimization

Heat exchanger design optimization is the task where one really begins to appreciate the importance of a good model. The optimization algorithm generates different values for the inputs, for which the model is exercised and the resulting heat exchanger performance is reported back to the optimizer. This allows one to explore a practically infinite design space with relatively few (e.g., a few thousands) simulations. The use of optimization algorithms with heat exchanger model has been carried out for several decades. A summary of the different objectives and constraints used in heat exchanger optimization problems is given in Huang *et al.* (2015). Some of the key objectives used in optimization include: cost, capacity, entropy generation, entransy, etc. However, the holy grail of optimization in tube-fin heat exchangers (TFHXs) is the simultaneous geometry and refrigerant circuitry optimization.

Refrigerant circuitry, i.e., the configuration of tube connections that determine the refrigerant flow path, is proved to have a significant impact on heat exchanger performance (Chwalowski *et al.* (1989); Wang *et al.* (1999); Bigot *et al.* (2000); Liang *et al.* (2001)). For an existing tube-fin heat exchanger design, performing optimization on refrigerant circuitry is more convenient and cost saving than varying other structural parameters. Currently, design engineers usually choose refrigerant circuitry based on their experience or some benchmark result of a limited number of simulations for a few artificially designed circuitries. For instance, one of the most common circuitry design is the crossflow design in which refrigerant and moist air are flowing in opposite directions. However, there is no guarantee that such circuitry design is optimal design, especially for large HXs. The circuitry optimization problem is particularly challenging due to the high nonlinearity between the circuitry and TFHX performance as well as

the extremely large design space whose size increases exponentially with the increase of tube numbers. Taking a 10-tube TFHX as an example, just the 1-circuit design without merging or splitting has 10! (3,628,800) possibilities, not to mention taking multiple-circuit designs, merging and splitting types of U-bends into consideration.

In recent years, researchers used several different approaches to solve the TFHX circuitry design problem. The previous work can be classified into two categories, parametric analysis and design optimization. Early research in this field started out with parametric analysis which compared performance of pre-defined circuitries. Liang *et al.* (2000) and Liang *et al.* (2001) developed a HX model to evaluate performance of different circuitries based on exergy destruction. The study compared six different circuitry designs and found the best circuitry can reduce the HX material by about 5% meanwhile maintaining the same performance as the baseline. Zilio *et al.* (2007) experimentally tested two tube-fin heat exchangers with different circuitries working as CO_2 gas coolers and compared their performance, Figure 1-2(a) shows one of Zilio *et al.* (2007) tested circuitries. Aljuwayhel *et al.* (2007) developed a heat exchanger frost accumulation model to simulate the performance of counter-flow and parallel-flow circuitry evaporators under frosting conditions. Figure 1-2(b) and Figure 1-2(c) show the typical counter-flow and parallel-flow circuitries, given that air flows from left to right through the heat exchangers. They found that heat exchanger circuitry can influence the frost distribution across the evaporator as well as its transient capacity under frosting condition. They also found that parallel-flow circuitry is better than counter-flow circuitry under frosting condition. Joppolo *et al.* (2015) numerically compared 9 TFHXs with different circuitries using their condenser model and found

that with the same refrigerant pressure drop, good circuitry designs can improve heat exchanger capacity and reduce refrigerant charge. Bahman and Groll (2017) proposed an interleaved circuitry for evaporators operating under airflow maldistribution. Variations of interleaved circuitries have been used in the industry for over a decade. Figure 1-2(d) shows an example for interleaved circuitry. Their results show that compared with a baseline HX of which the circuitry is not interleaved, the interleaved circuitry designs can yield uniform superheat at the outlet of the individual circuits and can improve the cooling capacity and cycle COP by up to 16.6% and 12.4%, respectively. Cen *et al.* (2018) developed a method to automatically generate circuitry designs with the restriction that only adjacent tubes can be connected. They applied this circuitry enumeration method to generate 161 different circuitry designs for a 16-tube HX and found that the heat exchanger capacity of best circuitry is 2.1% larger than the worst circuitry. For all researches using parametric analysis, since they only evaluated a limited number of circuitry designs, their best circuitries are not necessarily the optimal designs.

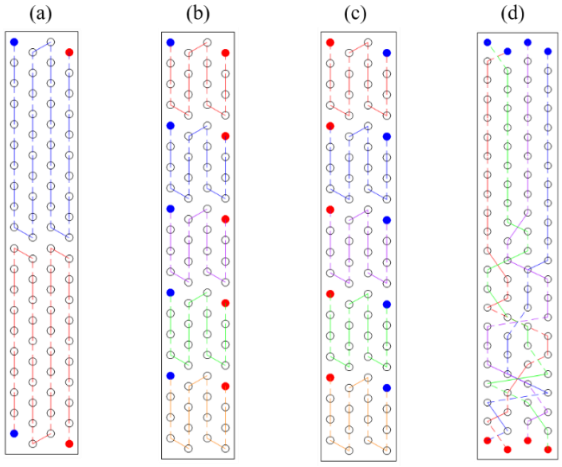

Figure 1-2: Examples of Circuitries: (a) One of CO2 Gas Cooler Circuitries from Zilio et al. (2007); (b) Counter-flow Circuitry; (c) Parallel-flow circuitry; (d) Interleaved circuitry

Besides parametric analysis, some researchers apply sophisticated optimization techniques such as heuristic algorithms to solve TFHX circuitry design problem. Domanski et al.(2004) developed an optimization tool called ISHED (Intelligent System of Heat Exchanger Design) that uses Evolutionary Learning and Symbolic Learning modules for circuitry optimization. They designed several domain knowledge based genetic operators. In their subsequent publications (Domanski *et al.*, 2005; Domanski and Yashar, 2007; Yashar *et al.*, 2010; Domanski *et al.*, 2011; Yashar *et al.*, 2012; Yashar *et al.*, 2015; Cho and Domanski, 2016), they applied this optimization scheme to condensers and evaporators under uniform and non-uniform airflow distributions, and experimentally validated the performance of the optimal circuitry on heat exchanger level and system level. Although their optimization scheme has capability to avoid non-manufacturable circuitry, in some cases the solutions will have undesirably long U-bends and U-bend crossings. In these cases, the authors suggest to revise the solutions manually to improve their manufacturability. As a result, their experimentally validated optimal circuitries offer superior heat exchanger capacity to that of manually designed circuitries. The maximum reported HX capacity improvement from optimization runs and experimental validation are 13% (Cho and Domanski, 2016) and 2.2% (Yashar *et al.*, 2015), respectively compared to their baseline circuitry. Wu *et al.*(2008a) and Wu *et al.*(2008b) developed another optimization approach, which switches between two optimization methods, i.e. knowledge-based Genetic Algorithm (GA) and Simulated Annealing. Moreover, the group created effective operators (greedy crossover and greedy mutation) to improve the convergence. The maximum predicted capacity improvement in their study is 7.4%.

Recently, Lee *et al.*(2016) proposed an analytical method to determine the optimal number of circuits for tube-fin condensers based on exergy destruction. Ploskas *et al.*(2017) represented circuitry using an adjacency matrix and constrained the hairpins to be on one side of the HX. By comparing five different derivative-free optimization algorithms, they concluded that TOMLAB/glcDirect and TOMLAB/glcSolve can efficiently find optimal or near-optimal circuitries. However, in their study, the performance improvement is not reported quantitatively.

The TFHX circuitry optimization problem has a large and discrete design space. This kind of problem is usually classified as combinatorial optimization problem (Gray *et al.*, 1997). Examples of combinatorial optimization problems include, but not limited to, Travelling Salesman Problem (TSP), Vehicle Routing Problem (VRP) and Minimum Spanning Tree Problem (MST). To solve such optmization problems, there are two groups of methods, classical methods (Deb (2012)) and evolutionary algorithms (Deb (2001)). The classical methods can be furthur classifed into two distinct groups: direct search methods and gradient-based methods. In direct search methods, the objective function and the constraint values are directly used to guide the search direction, whereas gradient-based methods use the derivatives of the objective function and/or constraints to guide the search process. Since derivatives are not used, the direct search methods are usually slow, requiring more function evaluations for convergence. On the other hand, gradient-based methods quickly converge near an optimal solution, but are not applicable in non-differentiable or discontinuous problems.

As a comparison, the evolutionary algorithms (EAs) simulate natural evolutionary processes and involve stochastic optimization techniques. For combinatorial problems, EAs often outperform classical methods (Gen *et al.*, 2008). Evolutionary algorithms such as Genetic Algorithms, Evolutionary Programming, Evolution Strategies, Genetic Programming, Learning Classifier Systems, Swarm Intelligence (including Ant Colony Optimization) and Particle Swarm Optimization have been extensively used to solve complex combinatorial problems (Gen *et al.*, 2008). Among them, Genetic Algorithms (Holland, 1992) mimic the principles of natural genetics and natural selection, and are extensively used in various problem domains due to their broad applicability, ease of use and global search feature (Goldberg, 1989).

1.2.3 Review of microchannel heat exchanger pass arrangements optimization

Very few studies in the open literature have aimed at understanding the principles behind optimizing the refrigerant flow path in single bank microchannel heat exchangers (MCHX), let alone multi-bank MCHX. Heun and Dunn (1996) examined the effects of microchannel port diameter and shape on MCHX pass arrangements. They conducted a theoretical heat exchanger analysis, which led them to conclude that smaller port sizes result in reduced heat exchanger internal volume and necessitate additional parallel refrigerant passages with reduced tube lengths. Port shape was shown to have a significant impact on heat exchanger volume and MCHX pass arrangements. In a companion paper, Heun and Dunn (1996) investigated the effect of refrigerant pressure drop on microchannel condenser performance. They found that for a given port diameter, the pressure drop variation caused an optimum relationship between the number of passes and the tube length. They conclude that an optimal

combination of the number of ports and the number of tubes minimizes the condenser volume for a given port diameter.

Ye *et al.* (2009) analyzed a microchannel condenser with multiple passes for automotive air-conditioning systems. They introduced a flow distributor in the condenser to enable parallel flow in adjacent passes. Through their MCHX design, the two-phase zone was effectively enlarged to enhance the condensation heat transfer and reduce the refrigerant pressure drop. Performance test results showed that the capacity of their condenser was up to 9.5% higher than the traditional microchannel condenser. Martínez-Ballester *et al.* (2013) presented a numerical model for microchannel condensers. Fin cuts was studied as a function of MCHX pass arrangements. Huang *et al.* (2015) explored the effect of variable geometry (fin depth, fin density, port size etc.) on air cooled microchannel condensers using a novel variable geometry microchannel heat exchanger model. Capacity was plotted as a function of material mass for variable geometry MCHX and conventional geometry MCHX. It showed that optimization of variable geometry MCHX is an effective way to improve HX performance and reduce material cost.

Mehendale (2013) employed the model developed by Schwentker *et al.* (2005) to simulate a single row refrigerant R410A microchannel condenser consisting of a fixed number of microchannel tubes. The number of MCHX tubes and refrigerant mass flow rate through the condensers were fixed, while the outlet subcooling was allowed to vary. The thermal-hydraulic performance of two-, three-, and four-pass configurations for MCHX was simulated. Based on the tradeoffs encountered between condenser capacity and refrigerant pressure drop, recommendations were provided to

aid HVACR practitioners to select the preferable pass arrangement for microchannel condensers. Mehendale (2013) showed that for a 54-tube microchannel heat exchanger, the 4-pass arrangement design with 20, 17, 11 and 6 tubes in each pass offers the best performance among all enumerated pass arrangements.

Recently, Li and Pega (2018) presented a parametric study on MCHX pass arrangement for condensers using their experimentally validated MCHX condenser model. The best pass arrangement among all 310 pass arrangements they enumerated offers 17.9% performance improvement compared to their baseline condenser. Since they only evaluated a small number of designs, their best pass arrangement design is not necessarily the optimal. It is thus clear that the principles governing the selection of the optimal pass arrangements for microchannel heat exchangers have not been explored in depth. Such studies on multi-bank microchannel heat exchangers are not founded in literature.

1.2.4 Review of robust optimization

For a large heat exchanger which consists of a number of tubes, the impact of changing a small number of tube connections should be considered in the optimization. The optimization with consideration of the uncertainty on the design parameters is referred as robust optimization in literature.

In many real-world engineering design problems, some design parameters have uncontrollable variations. A design can easily be nominally optimized without considering any parameter variation, however, this may lead to performance degradation of the optimal solutions and can even change the feasibility of the obtained solutions. The goal of robust optimization is to obtain optimal designs that are insensitive to parameter variations. There are two main types of robust optimization

methods: stochastic methods and deterministic methods. Stochastic methods (Hirokawa and Fujita (2008), Jin *et al.* (2003), Choi and Youn (2002), Lee and Lee (2001), Hughes (2001), Branke (2001), Du and Chen (2000), Yu and Ishii (1998), Tsutsui and Ghosh (1997) and Parkinson *et al.* (1993)) optimize designs based on statistical measures such as mean, variance and probability distribution functions of the design variables. The major disadvantage of these methods is that the determination of the statistical measures can be difficult or even impossible in real-world engineering design problems.

Taguchi (1978) is often considered the first person to study deterministic methods for robust optimization. After Taguchi, many researchers (Balling *et al.* (1986), Sundaresan *et al.* (1992), Sundaresan (1993), Zhu and Ting (2001), Lee and Park (2001), Renaud (1997), Badhrinath and Rao (1994) and Belegundu and Zhang (1992)) have studied deterministic methods using gradient information of the design parameters. One of the major limitations of deterministic methods is the requirement of continuous and differentiable objective functions. Gunawan and Azarm (2004) developed a new deterministic method for estimating the sensitivity of a design that does not require continuous or differentiable objective functions for single objective robust optimization problems. The robustness index developed by Gunawan and Azarm (2004) allows the decision maker to set the risk level which is useful when the feasible regions for a design are small and a perfectly robust solution for the given tolerance ranges may not exist. Decision makers can use this information to determine whether tolerances must be decreased or whether the maximum robustness index allowed under existing tolerance ranges is satisfactory. Li *et al.* (2006) extended the single-objective

deterministic method of Gunawan and Azarm (2004) to solve multi-objective problems. Later, Li *et al.* (2005) presents a Robust Multi-objective Genetic Algorithm (RMOGA) that optimizes two objectives: a fitness value and a robustness index.

Although the optimization studies conducted in this thesis does not involve robust optimization, The heat exchanger robust flow path optimization can be a good candidate for future work. For instance, one of the potential robust optimization research can be the circuitry optimization with consideration of the uncertainty on frontal air velocity field.

1.2.5 Review of heat exchanger airflow maldistribution

In real-world applications, due to the uneven airflow from a fan, there is almost always non-uniform airflow on the HX face. Majority of HX modeling works assume uniform air flow, but this assumption can lead to significant deviations of the predicted results. Previously, air velocity distribution at the frontal face of tube-fin heat exchangers, has been experimentally measured by Kirby *et al.* (1998) and Aganda *et al.* (2000) and CFD simulations were carried out by Yashar *et al.* (2014). Most tube-by-tube and segment-by-segment models are capable of accounting for air-flow maldistribution. In general, there are two methods used to account for air flow maldistribution. In the first method, the flow distribution is an input to the model in the form of air velocity value for each tube or for each control volume on the HX face. The distribution itself can be obtained by lab measurements or from detailed CFD analysis. The data from lab measurements, typically in the form of air-velocity as a function of height for a given fan-HX combination can be converted to a normalized polynomial and used in subsequent analyses. This is typically the easiest approach.

The second approach relies on a co-simulation between HX model and a detailed CFD package. The key to success in such simulations is to note that the finite volume models are based on a Cartesian grid, whereas CFD packages use a non-uniform and non-rectangular grid. When the detailed velocity output from the CFD package is mapped from this non-uniform grid to a uniform grid, there is a possibility of mass loss (leading to wrong air-side mass flow rate values). In order to avoid such issues, an appropriate spatial averaging technique must be utilized to ensure mass conservation. In this regard, some researchers have proposed multi-level approaches by coupling CFD with segmented HX model to account for the air flow maldistribution. Abdelaziz *et al.* (2008) coupled a segment-by-segment epsilon-NTU based coil model with CFD simulations to accurately account for the air flow distribution. They used 2D CFD models to calculate the velocity distribution and heat transfer coefficients. The tube pitch, row pitch and the coil angle were varied and compared against the baseline configuration. In a follow-up study, Singh *et al.* (2011) improved this approach by superimposing a CFD mesh on the heat exchanger model's geometric grid. The interpolated velocity profile from the method showed good air flow mass balance and after applying their 3D CFD simulation results to predict the heat exchanger performance, the capacity of a R410A condenser agreed within 4% of the experimental data.

In the attempt to simplify the calculation of complex heat exchanger geometries, the use of a momentum resistance model (or referred to as porous media model) has been investigated. The momentum resistance model originates from the Darcy's law of porous media where flow is assumed to be a creeping flow and has been expanded to

account for higher Reynolds number flow. Patankar and Spalding (1974) first introduced a distributed resistance approach for simplified shell side heat transfer and pressure drop modeling of a tubular heat exchanger and showed that the model could provide accurate results with much less computational time. Since then, such models have been used in deriving velocity and temperature solution in simple heat exchanger configurations. Kim and Kim (1999) obtained the analytical solutions for velocity and temperature in microchannel heat sinks using porous media model. They found that the analytical solutions agree well with the full conjugate heat transfer simulation and found the aspect ratio and effective thermal conductivity ratio as the variables of engineering importance. Subsequently, they extended their study to investigate finned-tube geometries (Kim *et al.* (2002), Do *et al.* (2007)) and proposed optimal angle of the circular sector and porosity for maximum thermal performance. Hooman and Gurgenci (2010) applied porous media transport approach to finned tube bundles problem and studied the correlation between the macroscopic properties of the porous media (permeability, form drag coefficient and the porosity). They concluded that the results are not very sensitive to the internal structure of the porous matrix as long as the macroscopic properties are accurate. Imke (2004) developed a tool using a porous media forced convection approach combined with empirical conventional closure correlations for normal-sized channel flow to estimate the performance of microchannel heat exchangers.

The momentum resistance model was applied in CFD to study the effect of air flow maldistribution in more complex geometrical configurations. Yashar and Domanski (2009) conducted particle image velocimetry (PIV) experiments for an A-

type coil heat exchanger running in both dry and wet-condition and validated their CFD simulation incorporating a momentum resistance model. Their results showed that the CFD air flow profile prediction matched well with the actual air velocity profile. Kritikos *et al.* (2010) investigated the thermal performance of a heat exchanger designed for aero engine applications using the exact geometry model and the porous medium model. They compared the Nusselt numbers and the temperature distributions to available experimental data and found that both approaches were in good agreement. Shi *et al.* (2010) proposed a semi-porous media approach where the tube bundle is simplified as a porous media while the half tubes on each side are modeled as exact. They compared results from the real tube model, the semi-porous media model and the conventional porous media model, and claimed that their approach has a better agreement with the experimental data in reasonable computational time. Rossetti *et al.* (2015) studied the effect of the air flow maldistribution in the channel of an open refrigerated display cabinet using CFD. They proposed a thermal resistance approach that allowed a reduction of computational effort by at least a factor of ten. These CFD studies, however, have focused on proving the efficiency and accuracy of the momentum resistance approach by validating the model with experimental data or full 3D simulations, and the parametric studies have been limited to a few variables and short ranges. The literature review shows that the heat exchanger optimization researches by the means of integrating momentum resistance CFD model with heat exchanger numerical model are very scarce.

1.3 Research Objectives

The presented work in this thesis concerns itself as cutting-edge refrigerant flow path optimization and steady state modeling of air-to-refrigerant tube-fin heat exchangers.

(i) The first part of the thesis focuses on the development and applications of a novel Integer Permutation based Genetic Algorithm (IPGA) for refrigerant flow path optimization in heat exchangers with generalized geometries. The research aims to:

- Develop a complete algorithm to optimize tube-fin HX circuitries and microchannel HX pass arrangements
- Develop effective chromosome representation and GA operators to map genotype to phenotype (circuitry for TFHX or pass arrangement for MCHX)
- Develop hybrid initialization approaches to maintain diversity and feasibility of initial individuals and to facilitate convergence
- Handle manufacturability constraints such that the optimal design can be manufactured in a cost-effective manner
- Handle operating constraints such that refrigerant pressure drop, outlet saturation delta T and sensible heat ratio can be limited to acceptable ranges
- Implement new problem formulations to obtain optimal circuitry designs which can compensate for performance degradation due to air flow maldistribution
- Implement a new problem formulation to obtain superior HX performance under frosting conditions
- Implement a new problem formulation to obtain circuitry designs with improved performance under both cooling and heating operating modes in reversible heat pumps

(ii) The second part of the thesis presents a first-principle based model to simulate variable geometry tube-fin heat exchanger with the most design flexibility and comprehensive consideration of thermal and hydraulic phenomenon. The proposed model is developed based on a previous existing heat exchanger model which can simulate variable geometry heat exchangers. Comprehensive improvements are made to distinguish the proposed heat exchanger model as the most advanced air-to-refrigerant heat exchanger simulation tool available for novel heat exchangers with generalized geometries. This heat exchanger model aims at providing the following capabilities:

• Allows modeling variable geometric parameters including topology optimized tube shape, different tube size and irregular fin dimensions

• Supports multiple fluid groups in the same heat exchanger

• Improves the pressure drop prediction by calculating air and refrigerant gravitational and momentum pressure drop in addition to friction pressure drop

• Capable of modeling next generation heat exchanger and accelerated air heat exchanger

• Enhances numerical stability by implementing correlation smoothing with user-defined boundaries.

2 TUBE-FIN HEAT EXCHANGER CIRCUITRY OPTIMIZATION USING INTEGER PERMUTATION BASED GENETIC ALGORITHM

In this chapter, an Integer Permutation based Genetic Algorithm is developed solve tube-fin heat exchanger circuitry optimization problem. The primary contribution of this chapter is to present the details of this new algorithm.

2.1 Integer Permutation based Genetic Algorithm

2.1.1 Representation of heat exchanger circuitry

To conduct optimization using Genetic Algorithm, the first step is the effective mathematical representation of the circuitry. A good individual (chromosome) representation can not only reduce the search-space, but can also simulate the nature of the problem (Deb (2012)). It has been shown that a meaningful and appropriate chromosomal representation of the problem can speed up Genetic Algorithm to converge to a global optimal (Kargupta *et al.* (1992)). For tube-fin heat exchanger circuitry optimization problem, the proposed optimization algorithm represents refrigerant flow-path along tubes as a sequence of integers, wherein each integer represents a uniquely identifiable tube in a heat exchanger. The optimization technique is independent of the actual numbering of the tubes. For an integer permutation, each integer (i.e., tube number) appears exactly once, thus, any chromosome generated by the Genetic Algorithm can be mapped to a valid circuitry and the size of the search space is dramatically reduced by the elimination of redundant designs.

Two different chromosome representations are developed and implemented in the new optimization framework. Consider a 15-tube, 4-circuit HX as an example (shown in Figure 2-1(a)). The red circle indicates the inlet tubes and blue circle

indicates the outlet tubes. A solid line represents a U-bend on the front end, while a dotted line represents a U-bend on the far end of the heat exchanger.

The first type of chromosome is called a "Two-Part Chromosome" as shown in Figure 2-1(b), in which the first part of the chromosome denotes tube sequences, the second part denotes the number of tubes in each circuit. This type of chromosome works well when optimal number of circuits can be determined before conducting the optimization using preliminary analysis such as the one presented in (Lee *et al.* (2016)) or using rules of thumb or application of specific knowledge.

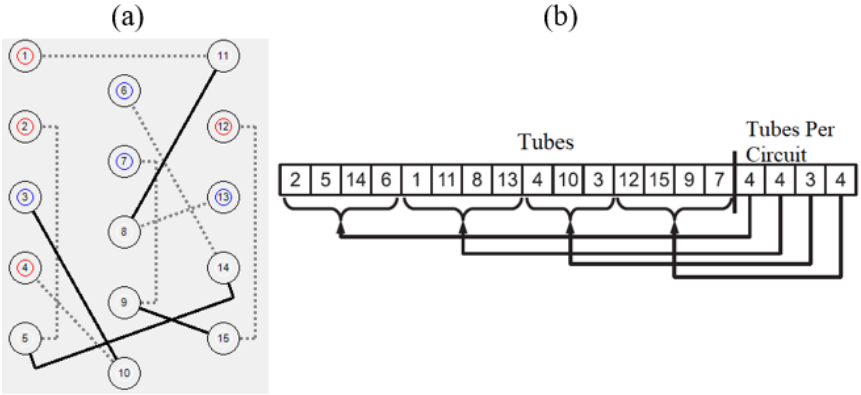

Figure 2-1: Chromosome Representation: (a) 15-tube heat exchanger example; (b) Corresponding two-part chromosome

However, in majority of the applications, especially for new product design, the optimal number of circuits cannot be easily derived and it is common to have splitting and merging tubes in a tube-fin heat exchanger as shown in Figure 2-2(a). So a more general chromosome representation is desired. Therefore, the 'Split Branch Chromosome', as shown in Figure 2-2(b), is proposed. The Split Branch Chromosome uses the concept of jagged arrays, with each element of this array representing a branch of tubes. Each branch contains 3 parts. The 1st part of the branch represents the tube sequence. The 2nd part of the branch represents the upstream tube. The 3rd part of the

branch represents the downstream tube. Dummy tube number '0' is used as the place holder in the 2nd part if the 1st tube of the branch is an inlet tube of a circuit. And dummy tube number '-1' is used as the place holder in the 3rd part if the last tube of the branch is an outlet tube of a circuit. Figure 2-2(b) shows the chromosome representation of the 24-tube heat exchanger in Figure 2-2(a). This sample heat exchanger has one splitting tube (tube # 3) and one merging tube (tube #20). With the Split Branch Chromosome, number of circuits is flexible, i.e., the optimal number of circuits is also an output from optimization. Intuitively, Split Branch Chromosome represents a refrigerant circuitry in a more realistic manner because it "physically" separates different branches from each other.

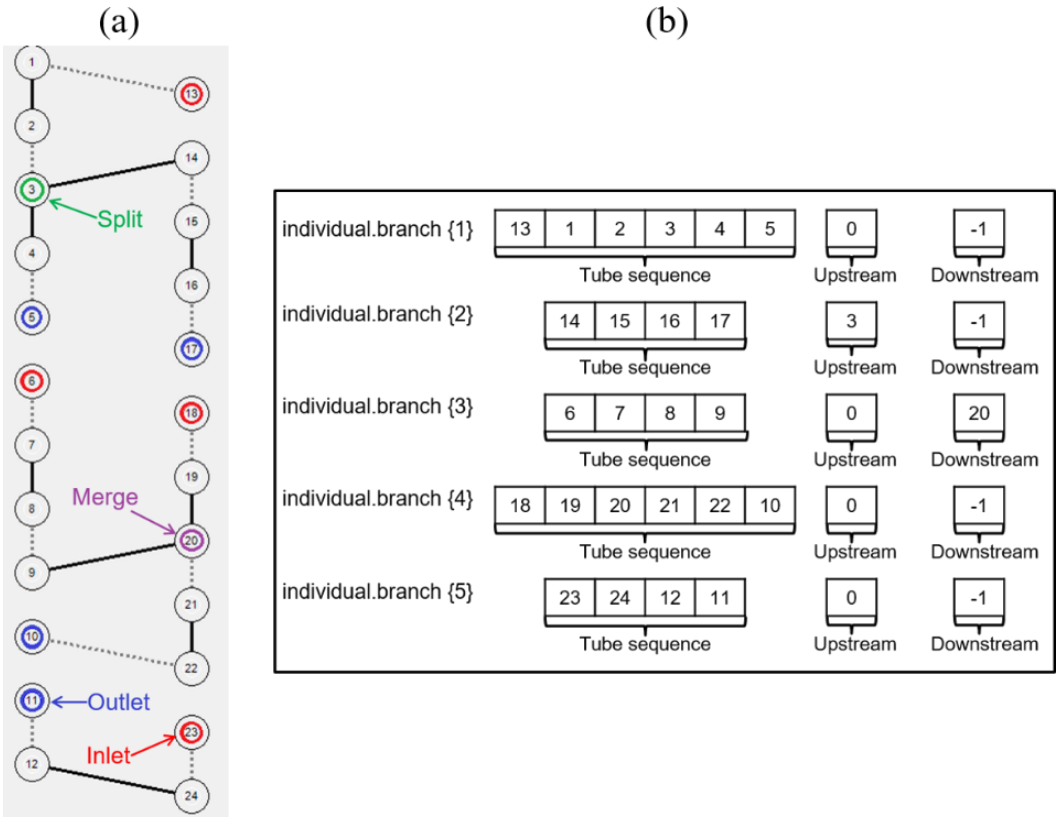

Figure 2-2: Chromosome Representation: (a) 24-tube heat exchanger sample; (b) Split branch chromosome

2.1.2 Selection

The selection operator, selects superior individuals in a population and forms a mating pool. The common selection methods from Genetic Algorithm literature are tournament selection, proportionate selection (i.e. Roulette wheel selection) and ranking selection (Goldberg (1989)). All these selection operators essentially pick the above-average individuals from the current population and insert duplicates of those elite individuals in the mating pool in a probabilistic manner. In this research, a tournament selection operator with tournament size 2 is used along with an efficient constraint handling method which will be explained in section 2.2.2. Goldberg (1989) has shown that the tournament selection has better and equivalent convergence and computational time complexity properties compared with other selection operators in the literature.

2.1.3 GA operators

The selection operator selects good individuals, while the creation of new individuals relies on the genetic operators. Conventional Genetic Algorithm uses crossover and mutation operators. There exist a number of crossover and mutation operators (Spears and Jong (1998)). For the conventional crossover operator, two individuals are randomly picked from the mating pool and some portion of their chromosomes are exchanged to create two new individuals. Since each chromosome represents one heat exchanger and the chromosomal representation of heat exchanger circuitry has the characteristic that each integer appears exactly once, it is obvious that exchanging genes among two individuals will undermine the structure of integer permutation and potentially generate many infeasible individuals. Coit and Smith (1996) has shown that constraint handling method such as penalty method cannot

efficiently avoid the infeasible individual if Genetic Algorithm generates too many infeasible individuals than feasible ones and the optimization process will remain stagnant. For these reasons, new genetic operators are required to ensure feasibility and convergence of the proposed method.

In this study, eight novel genetic operators are developed. By transforming the selected individual to a new individual with potentially better fitness, these genetic operators direct the search and drive the optimization process. The 'gene sequence inversion' operator as shown in Figure 2-3(a) chooses a random subsection of a branch and inverts the order of the tubes inside it. The 'gene insertion' operator as shown in Figure 2-3(b) puts a randomly selected tube into a random position.

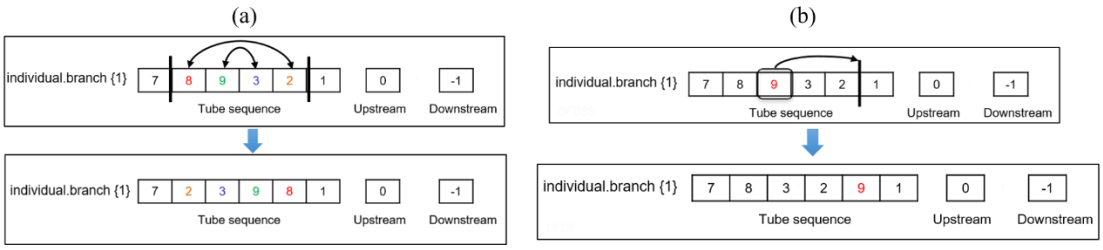

Figure 2-3: (a) Gene sequence inversion; (b) Gene insertion

The 'in-branch transposition' operator in Figure 2-4(a) transposes two randomly chosen tubes inside a branch, while the 'cross-branch transposition' operator in Figure 2-4(b) transposes two randomly selected tubes between 2 different branches.

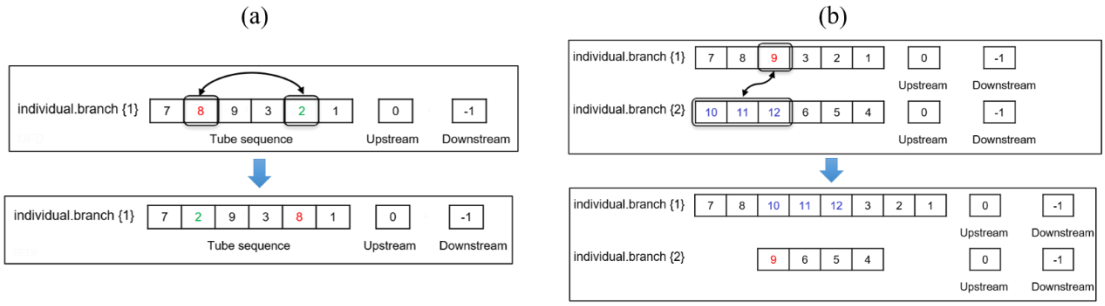

Figure 2-4: (a) In-branch transposition; (b) Cross-branch transposition

The ‘branch detachment’ operator as shown in Figure 2-5(a) splits a randomly selected branch into two branches. The ‘branch union’ operator as shown in Figure 2-5(b) chooses two branches and unites them into one branch. It is obvious that branch union operator and branch detachment operator offer the capability to vary the number of circuits such that the number of circuits can be optimized in a generic fashion.

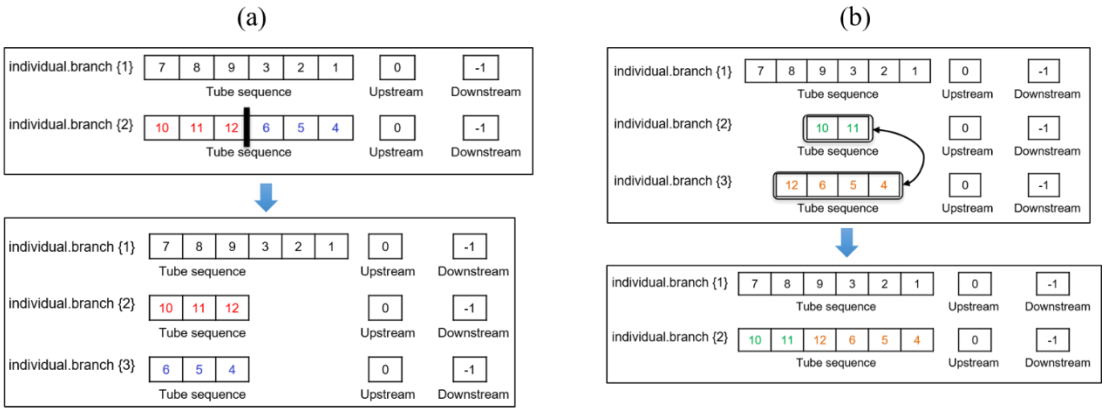

Figure 2-5: (a) Branch detachment; (b) Branch union

In order to generate splitting tubes, the split operator as shown in Figure 2-6(a) is developed to randomly determine one tube as the splitting tube and make a sub-section of tubes to form a new branch, thus creates a split. Figure 2-6(b) illustrates the effect of the split operator.

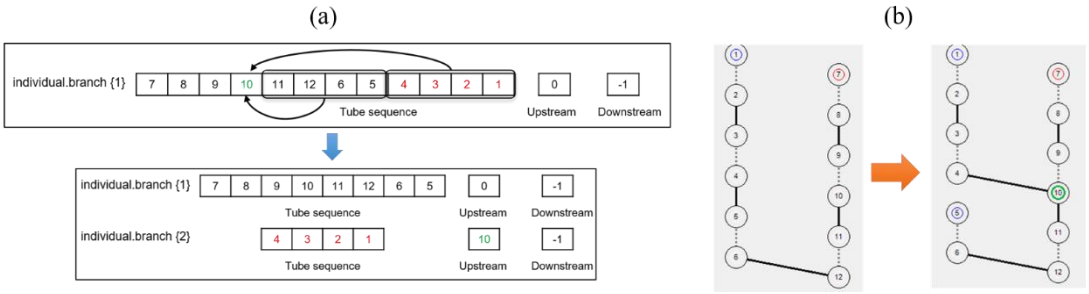

Figure 2-6: (a) Split operator; (b) Effect of split operator

Lastly, the merge operator as shown in Figure 2-7(a) randomly determines one tube as the merging tube and makes a sub-section of tubes to form a new branch, thus creates a merge. Figure 2-7(b) illustrates the effect of the merge operator.

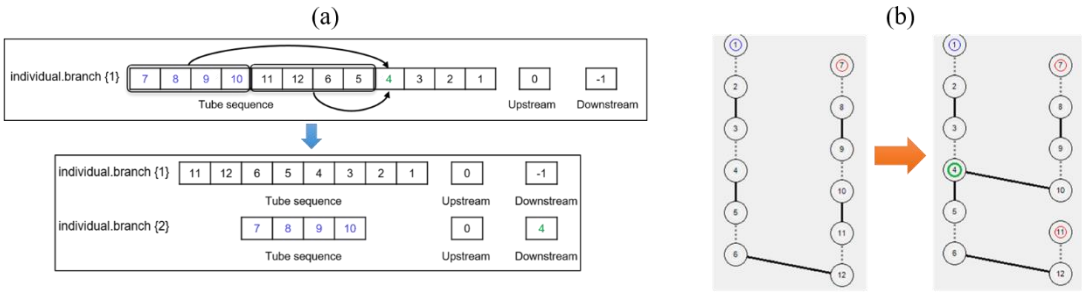

Figure 2-7: (a) Merge operator; (b) Effect of merge operator

2.2 Constraint Handling

For an optimization problem, constraints can be set on any inputs (design variables) and/or any outputs including the objective values. For tube-fin circuitry optimization problem, it is crucial to have options to add manufacturability constraints and guarantee that the optimal designs can be manufactured in a cost-effective manner.

2.2.1 Manufacturability Constraints

Four manufacturability (mfg.) constraints are incorporated in the new method. These constraints are typically set by the user at the beginning of optimization.

1. Inlets and outlets on the same side of HX: Figure 2-8(a) shows a design, of which inlets and outlets are on the same side of HX. Figure 2-8(b) shows an undesirable circuitry in which inlets and outlets are located on opposite sides.

2. Limit or avoid long U-bends: In this constraint, U-bend is not allowed to span across more than two tube rows/banks. In Figure 2-8 (c), the tube connection highlighted in green ellipse spans across the maximum allowed distance, while the two

long U-bends highlighted in red ellipses are not allowed according to the maximum allowed distance of 'long U-bend' set by the user of this algorithm.

3. Limit or avoid U-bend crossovers: There are three different types of U-bends crossovers. As shown in Figure 2-8(d), 'full overlap' in yellow caption indicates two collinear U-bends, in which one U-bend is located above the other. 'Partial overlap' in red caption indicates two collinear U-bends which are partially overlapped. 'U-bend crossing' in blue caption indicates two intersected U-bends. Among the three kinds of U-bend crossovers, partially overlapped collinear U-bends may be the least preferred type from manufacturer point of view.

4. Limit the number of tubes splitting or merging from a single tube: Figure 2-8(e) illustrates a heat exchanger design where the refrigerant from four tubes (tube #5, #6, #13 and #14) merges into tube #9. While the refrigerant at tube #12 splits into two tubes (tube #8 and #16). The proposed algorithm provides the option for the user to set maximum number of tubes splitting or merging from a single tube.

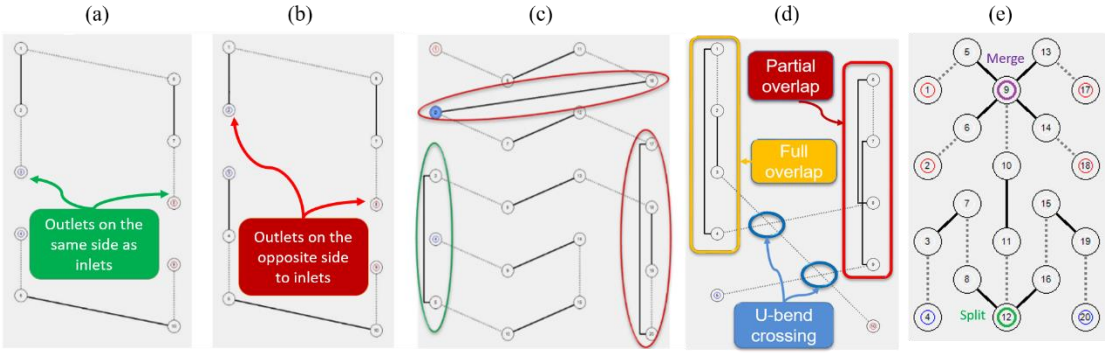

Figure 2-8: Manufacturability Constraints: (a) Inlet & Outlet on the same side; (b) Inlet & outlet on the opposite side; (c) Long U-bends; (d) U-bend crossings; (e) Tubes splitting or merging from a single tube

2.2.2 Constraint Handling Method

The proposed algorithm uses an efficient constraint handling technique which is called constraint dominated sorting (Deb (2000)). This constraint handling method

shows superior performance than the conventional penalty method in two aspects. Firstly, the efficiency of penalty method depends on the premise that the penalty parameter must maintain the same order of magnitude as the objective value which is not practical in various optimization problems. Secondly, it can lead to artificial optima, because the penalty term changes the formula of the objective function (Deb (2012)). The advantages of constraint dominated sorting avoids the use of any artificial penalty parameter, and it accounts for the degree of infeasibility (i.e. the extent of constraint violations). In the fitness assignment stage, constraint dominated sorting follows these principles (Deb (2000)):

1. In a given population, any feasible individual is preferred over infeasible one.

2. Between two feasible individuals, the one with better objective value is preferred.

3. Between two infeasible individuals, the one having lower constraint violation is preferred.

According to above arguments, Deb (2000) developed the fitness function in Equation (1-1), where infeasible solutions are compared based on their constraint violation:

$$F(x) = \begin{cases} f(x) & \text{if } g_j(x) \geq 0, \quad \forall\ j = 1,2,...,m \\ f_{\max} + \sum_{j=1}^{m} g_j(x) & \text{otherwise} \end{cases} \qquad (1\text{-}1)$$

Where $F(x)$ is the fitness value, $f(x)$ is the objective value, f_{max} is the objective value of the worst feasible solution in the population and $g_j(x)$ is constraint violations. Thus, the fitness of an infeasible solution depends on the amount of constraint violation and the population of solutions at hand and no penalty parameter is used.

2.3 Hybrid Initialization Approaches

Coit and Smith (1996) has shown that the efficiency of optimization methods is significantly influenced by the feasibility of initial individuals. To increase the feasibility of initial individuals and speed up the convergence of Genetic Algorithm, a hybrid initialization approach using three different strategies is developed. These strategies are discussed in the following sub-sections.

2.3.1 Predefined circuitry patterns

The first initialization approach is to generate predefined circuitry patterns, which consist of user-defined patterns and auto-generated recurring patterns. User-defined patterns are those that are manually designed by the user based on rule of thumb, heuristics and including the baseline circuitry. Recurring patterns means that a predefined algorithm will generate a regular circuitry pattern and repeat this pattern to assemble the entire heat exchanger. Some examples of the recurring patterns for a 4 bank, 88 tubes HX are shown in Figure 2-9. The circuitry generation algorithm has been designed in such a way that both parallel flow and counter flow HXs are included, the cases that inlet tube at the top of the circuit or inlet tube at the bottom of the circuit are also included, and the number of circuits can be varied from one to number of tube per bank.

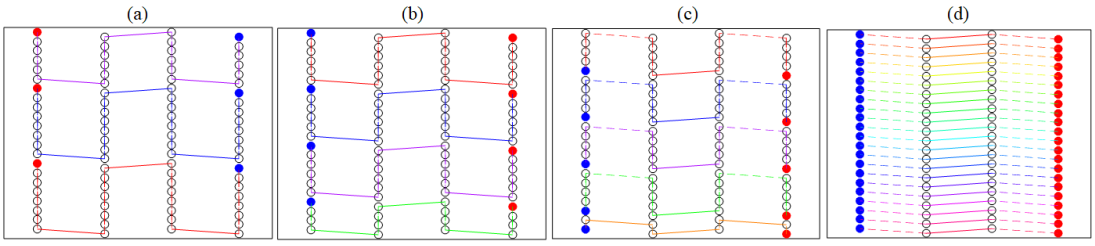

Figure 2-9: Illustration for Recurring Circuitry Patterns: (a) 4-circuit, parallel flow, inlet tube at top; (b) 4-circuit, counter flow, inlet tube at top; (c) 5-circuit, inlet tube at bottom; (c) 22-circuit, counter flow

2.3.2 Integer permutation sampling

The second initialization approach is generating circuitries by integer permutation sampling, which consists of two sub-methods: random permutation sampling and Latin Hypercube sampling. The user can use one of these two integer permutation sampling methods or use both methods to generate portions of initial population.

Consider a 9-tube HX as an example, Figure 2-10 illustrates nine possible initial individuals that the random permutation sampling can generate. As can be seen from Figure 2-10(a), individual-8 and individual-9 are very similar. Moreover, individual-3 and individual-4 are the same. This means that using the random number generator, it is possible to generate similar or exactly similar individuals, even though this likelihood is low. As a comparison, Figure 2-10(b) illustrates nine initial individuals that the Latin Hypercube sampling generates. As can be seen from Figure 2-10(b), each tube appears only once in each row of the table, which means that Latin Hypercube sampling can avoid similar individuals and increase diversity of initial population.

(a)

Individual-1	9	2	5	6	3	1	8	4	7
Individual-2	6	1	8	5	7	4	2	9	3
Individual-3	3	7	4	9	8	2	5	6	1
Individual-4	7	4	9	8	2	6	1	3	5
Individual-5	3	7	4	9	8	2	5	6	1
Individual-6	1	6	3	7	9	5	4	8	2
Individual-7	2	8	7	3	5	9	6	1	4
Individual-8	4	9	1	2	6	7	3	5	8
Individual-9	4	6	7	2	9	1	3	5	8

(b)

Individual-1	9	2	5	6	3	1	8	4	7
Individual-2	6	1	8	5	7	4	2	9	3
Individual-3	3	7	4	9	8	2	5	6	1
Individual-4	7	4	9	8	2	6	1	3	5
Individual-5	8	5	2	4	1	3	9	7	6
Individual-6	1	6	3	7	9	5	4	8	2
Individual-7	2	8	7	3	5	9	6	1	4
Individual-8	4	9	1	2	6	7	3	5	8
Individual-9	5	3	6	1	4	8	7	2	9

Figure 2-10: Examples of Initial Individuals Generated by Integer Permutation Sampling: (a) Random permutation; (b) Latin Hypercube sampling

2.3.3 Optimal solutions from sub-problem optimization

The third initialization method is generating circuitries by running sub-problem optimization. Before running the core circuitry optimization problem targeting at maximizing HX capacity, a sub-optimization problem with the goal of attaining short U-bends is performed beforehand. This can significantly increase the feasibility of initial designs when the manufacturability constraints are enabled in the core optimization problem. In other words, this initialization method can generate circuitries which satisfy the manufacturability constraints first, regardless of their thermo-hydraulic performance.

The sub-problem optimization is performed either on a small section of heat exchanger or on the original heat exchanger with the objective of minimizing the number of long U-bends. The computational burden of evaluating the performance of a given circuitry is directly proportional to the number of tubes in a heat exchanger. Thus using a small-section (i.e., lower number of tubes) for sub-problem optimization is expected to be computationally more efficient. If the sub-problem optimization is performed on a small sectional heat exchanger, the resulting small heat exchanger circuitry will be repeated to assemble the entire heat exchanger. It is preferable to perform sub-problem optimization on the sectional heat exchanger with a small number of tubes instead of the original heat exchanger with a large number of tubes, because the computational effort is much smaller due to the significantly reduced design space. Figure 2-11(a) shows an example generated by optimizing the small sectional heat exchanger. However, if there air maldistribution exists, then the optimization on the entire heat exchanger with a large number of tubes is required in order to avoid circuitry

design with recurring patterns (Li et al., 2018). Figure 2-11(b) shows an initial design generated by optimizing the entire heat exchanger.

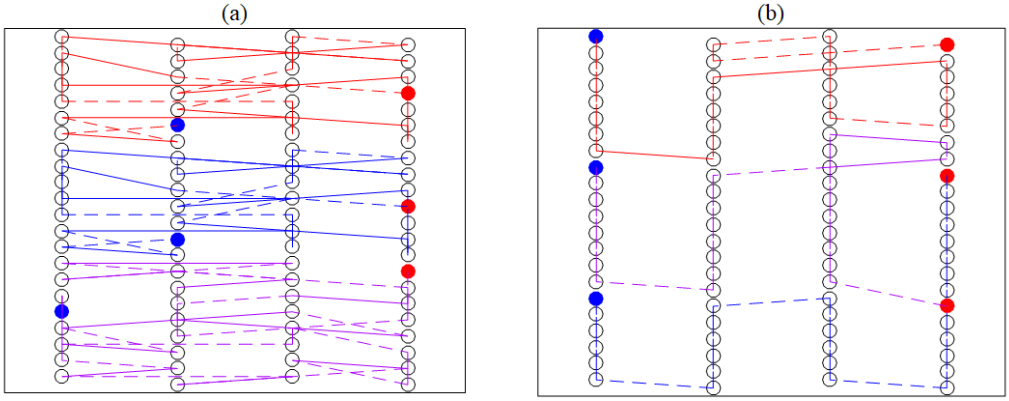

Figure 2-11: Sample Solutions from Sub-problem Optimization: (a) Optimize the small sectional HX and repeat its pattern; (b) Optimize the entire HX

2.4 Case Study

2.4.1 Baseline heat exchanger

This section represents a case study to demonstrate the efficacy of the proposed optimization algorithm. An evaporator from an A-type indoor unit (Alabdulkarem *et al.* (2015)) is used as the baseline for circuitry optimization. Table 2-1 shows the structural parameters and operating conditions for the baseline evaporator.

Table 2-2 lists the empirical correlations used for local heat transfer and pressure drop calculations during the performance simulation of this evaporator.

Table 2-1: Structural Parameters and Operating Conditions of Baseline Evaporator

Structural Parameters	**Value**	**Operating Conditions**	**Value**
Tube Outer Diameter	9.5 mm	Refrigerant	R410A
Fins Per Inch	15 FPI	Refrigerant Inlet Pressure	1154.5 kPa
Fin Type	Wavy Louver	Refrigerant Inlet Quality	0.22
Tube Length	0.503 m	Refrigerant Mass Flow Rate	0.0312 kg/s
Vertical Spacing	20.0 mm	Air Volume Flow Rate (Uniformly Distributed)	600 ft^3/min
Horizontal Spacing	25.0 mm	Air Pressure	101.325 kPa
Number of Tube Banks	4	Air Temperature	26.42 °C
Number of Tubes Per Bank	22	Air Relative Humidity	50.97 %

Table 2-2: Correlations Adopted in HX Simulation

Operating Mode	**Heat Transfer Correlations**	**Pressure Drop Correlations**
Refrigerant - Liquid Phase	Dittus and Boelter (1985)	Blasius (1907)
Refrigerant - Two Phase	Jung *et al.* (1989)	Jung and Radermacher (1989)
Refrigerant - Vapor Phase	Dittus and Boelter (1985)	Blasius (1907)
Air	Wang *et al.* (1998)	Wang *et al.* (1998)

The baseline as shown in Figure 2-12(a) has 4 circuits in each slab denoted in different colors. The majority of U-bends connect adjacent tubes in vertical direction, while there are 2 long U-bends in the middle of this HX, with both long U-bends spanning across 3 tube rows. There are also two U-bend crossings. Once, Jiang *et al.*

(2006)'s model was used to simulate the performance of this heat exchanger under different operating conditions. Jiang *et al.* (2006)'s model was validated with measured data (Alabdulkarem *et al.* (2015)) and the deviation in cooling capacity between simulations and experiments are below 5% as shown in Figure 2-12(b). In this case study, the airflow distribution is assumed uniform. In next chapter, circuitry optimization with the consideration of HX air flow maldistribution will be presented.

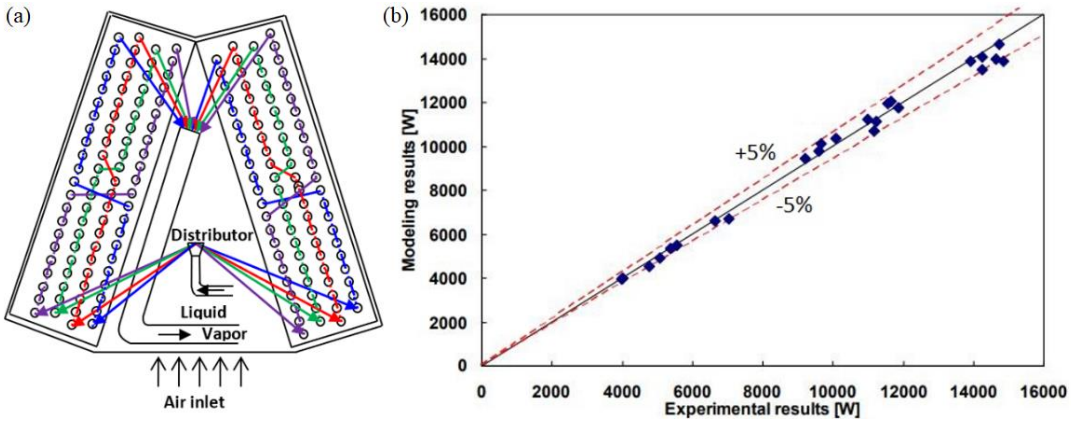

Figure 2-12: (a) Baseline Circuitry; (b) Experiment Tests vs Simulations

2.4.2 Objectives

As discussed in Huang *et al.* (2015), various performance metrics have been used as objectives and constraints in heat exchanger optimization formulations. In the context of tube-fin heat exchanger circuitry optimization, three types of objective have been used by previous investigators, as follows:

1.Maximize HX capacity (Domanski *et al.* (2004); Wu *et al.* (2008a); Ploskas *et al.* (2018)).

2.Minimize the total length of U-bends (Wu *et al.* (2008b)).

3.Maximize the ratio of capacity to refrigerant pressure drop (Ploskas *et al.* (2018)).

The proposed optimization method supports various objective functions including the three aforementioned ones. In this case study, the capacity is maximized to demonstrate the efficacy of the proposed method.

2.4.3 Unconstrained optimization

The first study performed is an unconstrained optimization, a trivial problem, with the goal of maximizing HX capacity. For all the optimizations presented in this section, the population size is 200 and the number of generations is 500. The GA replacement rate is set as 0.2. This is based on a parametric analysis that was conducted to examine the impact of the GA replacement rate on the optimization results. This analysis will be described later in section 2.5. Figure 2-13(a) shows the GA progress. Figure 2-13(b) shows the optimal circuitry. In the first 39 generations, the cooling capacity dramatically increases, as the number of circuits quickly drops to 1. Figure 2-13(c) shows a histogram of the number of circuits for all the designs evaluated in this optimization. Amongst a total of 100,000 evaluations, over 96% runs are successful. As can be observed from Figure 2-13(c), the algorithm evaluates a wide range of number of circuits (from 1- to 22-circuits), where 22 is the number of tubes per bank. It is obvious that without the penalty on pressure drop, the coils with fewer circuits outperform the coils with more circuits, and therefore, GA tends to converge to 1-circuit design. It should be noted that branch union operator (section 2.1.3) can unite 2-circuit design into 1-circuit design, while branch detachment operator can modify 1-circuit design to be 2-circuit design. Therefore, in later stage of this optimization run, the best individual in one generation has either 1 circuit or 2 circuits.

From Figure 2-13(a), the unconstrained optimization yields an optimal circuitry with a capacity increase from 5094 W to 6065 W or 14.6%. While the refrigerant

pressure drop increases from 11.8 kPa to 972.5 kPa or by 8800% due to the increase in mass flux and total refrigerant flow path length. In addition to the undesirably high pressure drop, the optimal circuitry has several long U-bends and U-bend crossovers, which make it very challenging and expensive to manufacture.

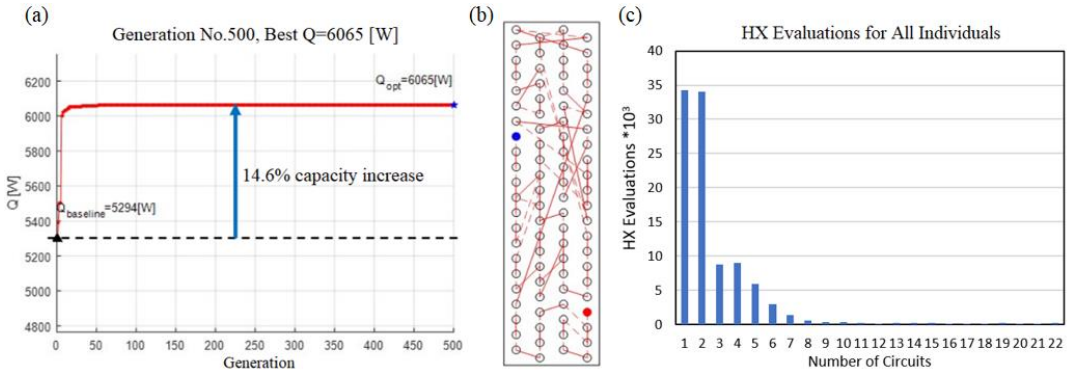

Figure 2-13: (a) Optimal circuitry; (b) GA optimization progress; (c) Histogram of number of circuits

2.4.4 Constrained optimization

In order to address the aforementioned concerns, different combinations of constraints are enforced on this optimization problem. Figure 2-14 shows the optimal solutions from three constrained optimization runs and Table 2-3 presents a detailed analysis of those optimal designs. In Table 2-3 U-bends L1' and 'U-bends L2' denote the number of U-bends which span across 1 tube row and 2 tube rows, respectively. 'U-bends ≥ L3' denotes the number of long U-bends which span more than 2 tube rows.

Case (c) in Table 2-3 is a loosely constrained optimization run. In this case, manufacturability constraints, i.e. inlets and outlets on the same side, preventing long U-bends and preventing partial collinear U-bends crossovers, are enforced. Figure 2-14(c) shows its optimal solution. It results in 13.8% capacity improvement. The

optimal solution has 2 circuits, which still results in 12 times higher pressure drop than the baseline. Nevertheless, the circuitry can be readily manufactured.

Case (d) in Table 2-3 is another constrained optimization run, in which only the refrigerant pressure drop constraint is enforced. This constraint restricts the design to have equal or less refrigerant pressure drop than the baseline. Figure 2-14(d) shows its optimal solution which has 4 circuits, the same as the baseline. And the optimal presents 4% increase of capacity than the baseline, and slightly lower pressure drop than the baseline. It is worthwhile to mention that some existing methods (Domanski *et al.* (2004) and Ploskas *et al.* (2018)) do not demonstrate the option to provide pressure drop constraints.

Case (e) in Table 2-3 shows the optimal design from a constrained optimization run, in which both manufacturability constraints and the operating constraint are applied. Figure 2-14(e) shows its optimal solution which achieves 2.5% capacity increase and 26.5% less refrigerant pressure drop than the baseline. The circuitry has acceptable manufacturability without any long U-bends or collinear U-bend crossing. Compared with other cases, the optimal solution from case (e) has desired thermal, hydraulic and manufacturability performance. And it can be noticed that the optimal evaporators in case (d) and (e) provide similar amount of latent cooling as baseline, because these two evaporators have similar sensible heat ratio (SHR) as the baseline.

Table 2-3: Evaporator Optimization Results with Different Constraints

Case	Baseline (a)	(b)	(c)	(d)	(e)
Constraints	-	No constraints	Mfg. constraints	Refrigerant DP constraint	Mfg. constraints and DP constraint
Capacity [W]	5294	6065(14.6%↑)	6027(13.8%↑)	5497 (3.8%↑)	5424 (2.5%↑)
Ref. DP [kPa]	11.8	972.5 (81x↑)	160.5 (12x↑)	11.4 (3.6%↓)	8.6 (26.5%↓)
SHR	79.6%	67.6%	72.5%	79.8%	80.1%
HX Model Runs	-	20,160	17,693	20,160	20,160
U-bends L1	82	61	51	17	43
U-bends L2	0	4	35	9	40
U-bends ≥ L3	2	2	0	58	0
Collinear U-bends	0	3	0	43	0

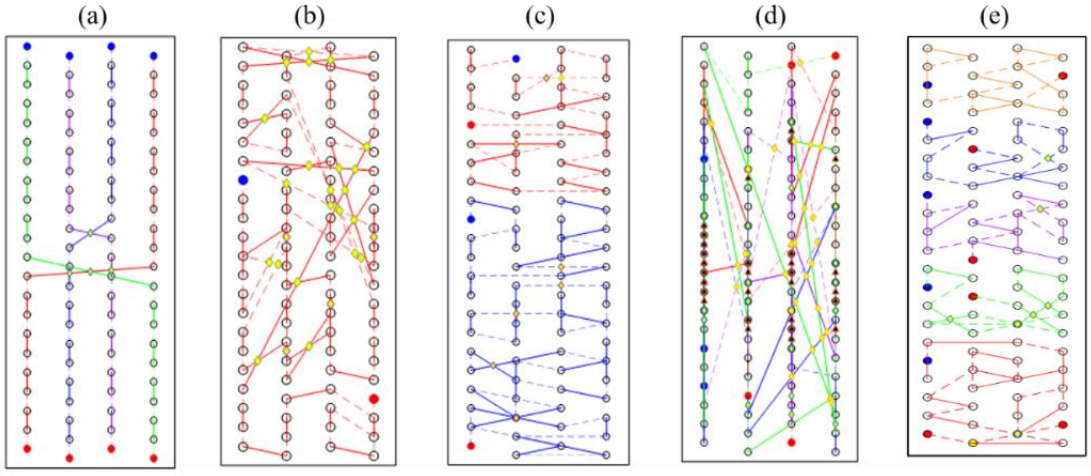

Figure 2-14: Optimal Circuitry Designs (a) Baseline; (b) Unconstrained; (c) With mfg. constraints; (d) With refrigerant DP constraint; (e) With mfg. and DP constraints

2.5 Stability Test

Since GA is a stochastic optimization algorithm, different runs have the possibility to converge to different solutions. In order to access the stability of proposed optimization algorithm, the optimization case study with four different constraint combinations (case (b) to case (e) in Table 2-3) in last section are repeated 15 times per each case. For all optimization runs, the population size is 200 and the number of generations is 500. The parametric analysis is conducted by varying the GA replacement rate. And this analysis found that when using 0.2 as the GA replacement rate, there are more optimization runs which converge to better heat exchanger performance, because the elitism is preserved with small replacement rate. Therefore, in this section, the demonstrated optimization runs adopt 0.2 as the GA replacement rate. Figure 2-15, Figure 2-16 and Figure 2-17 illustrate the distributions of the optimal designs obtained from all the 60 independent runs in terms of HX capacity, refrigerant pressure drop and sensible heat ratio, respectively. The small variations of results between multiple optimization runs for each case indicates that the proposed algorithm has good stability.

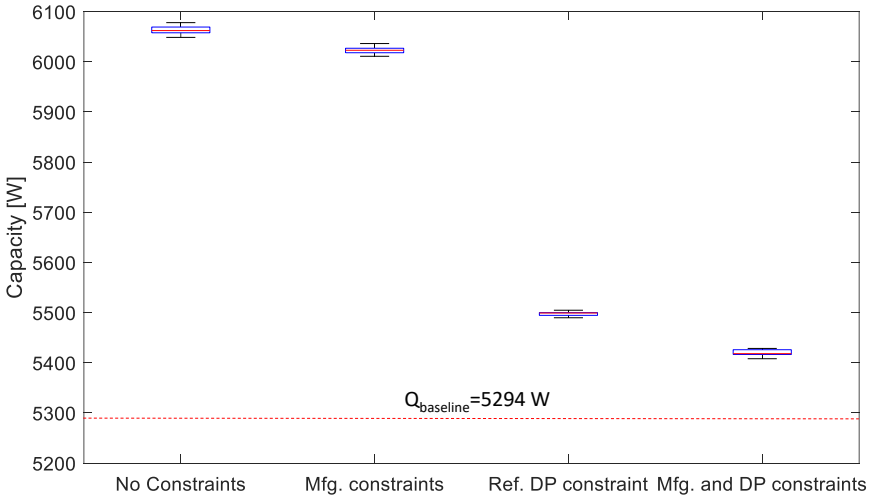

Figure 2-15: Capacity Distribution of Optimal Designs under Different Constraints for 60 runs.

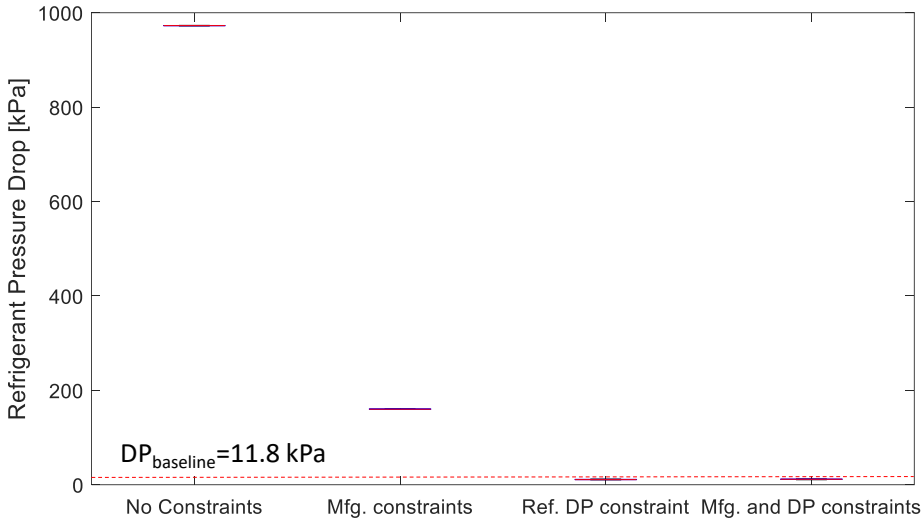

Figure 2-16: Refrigerant Pressure Drop Distribution of Optimal Designs under Different Constraints

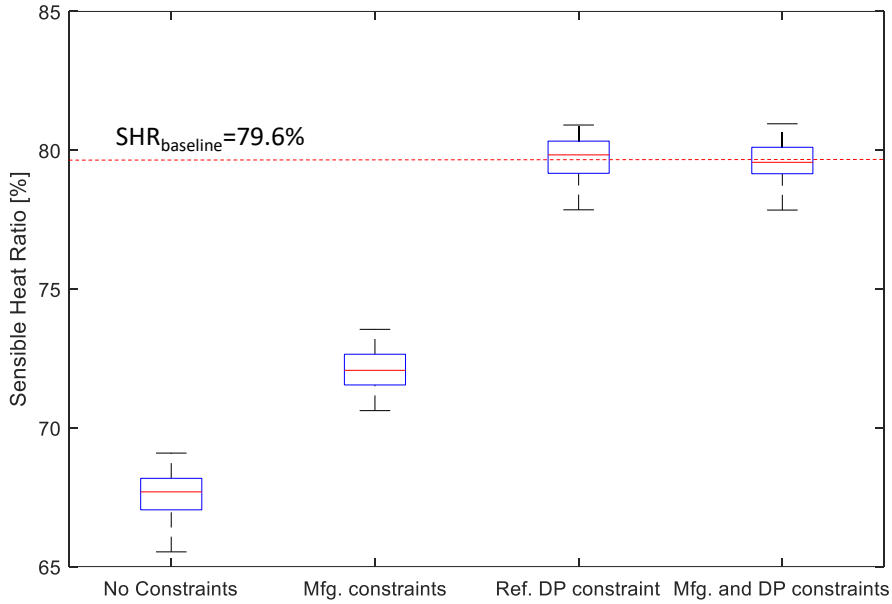

Figure 2-17: Sensible Heat Ratio Distribution of Optimal Designs under Different Constraints

2.6 Comparison with Methods from Literature

Domanski *et al.* (2004) and Wu *et al.* (2008a) applied their methods to optimize the same 36-tube R22 evaporator as shown in Figure 2-18(a) under uniform airflow distribution. In this section, the proposed algorithm is benchmarked against the previous two methods by optimizing the same heat exchanger. The population size for

this optimization run were set to be the same as those in the previous study: population size is 15 and number of generation is 200. The boundary condition to simulate this evaporator is specified evaporator outlet condition. According to Domanski *et al.* (2004), the evaporator outlet pressure is fixed at a saturation pressure corresponding to 7.2°C saturation temperature, while the outlet superheat is 5°C. The evaporator inlet enthalpy is determined based on the outlet enthalpy of a condenser. which is corresponding to 40°C condensation temperature and 5°C subcooling. The HX structural parameters, operating conditions and correlations are provided in Domanski *et al.* (2004).

Figure 2-18(b) shows the optimal solution as reported in Domanski *et al.* (2004). It achieves 4.2% capacity increase, accompanied by 27.7% refrigerant pressure drop increase. There is one partial overlap U-bend crossover highlighted in red rectangular and the author suggested to manually modify the circuitry to improve its manufacturability. Figure 2-18(c) shows the optimal solution from Wu *et al.* (2008a). The capacity increase is 4.1%, and the manufacturability is better than the former counterpart since there is no long U-bend or partial overlapped collinear U-bends. However, the refrigerant pressure drop also increases by 26.0%. Figure 2-18(d) shows the optimal solution from the proposed algorithm. The optimal design has 1 splitting tube (the solid black circle). In this optimization run, the manufacturability constraints and the refrigerant pressure drop constraint are enforced. As a result, the capacity improvement is 6.2% compared to the baseline, which is the largest among the three methods.

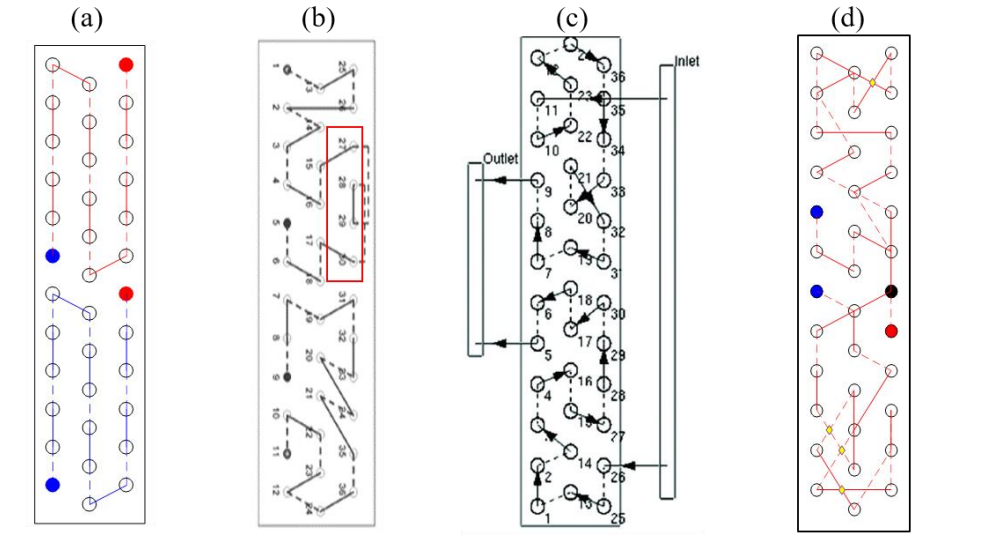

Figure 2-18: HX Circuitry Designs: (a) Baseline; (b) Domanski *et al.* (2004); (c) Wu *et al.* (2008a); (d) Proposed algorithm

Table 2-4 shows a detailed comparison between proposed circuitry optimization method with the optimization methods developed by Domanski et al. (2004) and Wu et al. (2008a). The highlights and advantages of the proposed method are as follows:

1. The number of circuits does not need to be presumed before running the optimization. This is attributed to the new chromosome representation and the GA operators.
2. In terms of manufactuability constraints, in addition to providing the user with the option to prevent long U-bends as the other two counterparts, IPGA also provides the option to prevent undesirable U-bends crossing and the option to set the maximum number of tubes splitting or merging from a single tube.
3. In terms of operating constraints, in addition to providing the option to set constraint on refrigerant pressure drop as Wu *et al.* (2008a), options to set constraints on outlet saturation ΔT and sensible heat ratio are demonstrated.

Table 2-4: Comparison of Tube-fin Heat Exchanger Circuitry Optimization Methods

Investigator	Implemented Algorithms	Number of Circuits	Mfg. Constraints			Operating Constraints	
			Prevent Long U-bends	Prevent U-bends Crossing	Limit Splits / Merges	Pressure Drop	Outlet ΔT & SHR
Domanski *et al.* (2004)	Evolutionary Learning & Symbolic Learning	Fixed before Optimization Run	✓	✗	✓	✗	✗
Wu *et al.* (2008a)	Genetic Algorithm & Simulated Annealing	Fixed before Optimization Run	✓	✗	✗	✓	✗
IPGA (Proposed method)	Genetic Algorithm	Flexible and optimizable	✓	✓	✓	✓	✓

2.7 Exhaustive Search Verification

As explained in section 2.2.2, IPGA uses an efficient constraint handling technique: constraint dominated sorting (Deb (2000)). To get more insights into the performance of different constraint handling methods, an exhaustive search is performed on a 10-tube, 2-bank water radiator. At first, all the 58,941,091 possible designs in design space are enumerated and simulated, and then they are classified as feasible or infeasible designs based on whether the circuitry satisfies manufacturability (Mfg.) constraints. Finally, the feasible designs are sorted in descending order of HX

capacity, i.e. the top feasible circuitry design in the sorted list has the largest heat capacity and satisfies Mfg. constraints, and therefore, it is the global optimal.

IPGA with two different constraint handling methods are applied on a constrained optimization problem. The Mfg. constraint is to prevent long U-bends which span across 2 tube rows. The first version of IPGA adopts penalty method to handle constraints, and the penalty parameter is set to be 1000 such that the penalty term has the same order of magnitude as the capacity of the baseline HX. The 2nd version of IPGA uses constraint dominated sorting to handle constraints. The numerical experiments are performed by running two versions of IPGA consecutively for 30 times. In all runs, population size is fixed as 100 and number of generation is fixed as 200. Those numbers are relatively low for conventional optimization practice in order to test the capability of IPGA to find global optimal in relatively small computational effort. The verification results are summarized in Table 2-5. Among the 30 runs of IPGA combined with penalty method, 3 runs (out of 30) find a top-10 capacity design, while among the 30 runs of IPGA combined with constraint dominated sorting 8 runs (out of 30) successfully find a top-10 capacity design. The penalty method only has 4 runs that finally converge to a top-100 capacity design, however, constraint dominated sorting has 23 runs to find a top-100 capacity design. It can be noticed that constraint dominated sorting can guarantee all optimal solutions that are within the top 10,000 designs. Last but not the least, 11 penalty method runs find infeasible solutions, while all the solutions using constraint dominated sorting are feasible. This verification confirms that constraint dominated sorting is more effective and efficient than penalty

method and IPGA with constraint dominated sorting is capable of finding globally optimal or near optimal designs with a relatively low computational effort.

Table 2-5: Exhaustive Search Verification Results

GA Runs / Method	Top 1-10	Top 1-10^2	Top 1-10^3	Top 1-10^4	Below Top 10^4	Infeasible solutions
Penalty Method R=1000	3	4	9	14	5	11
Constraint Dominated Sorting	8	23	28	30	0	0

2.8 Summary

A novel Integer Permutation based Genetic Algorithm is developed to solve the tube-fin heat exchanger circuitry optimization problem. Six genetic operators are designed to generate circuitry with potentially better performance. The manufacturability aspect is handled using an efficient constraint-dominated sorting method. The case studies on an experimentally validated evaporator show that the proposed optimization algorithm can generate circuitry designs with capacities superior to manually designed circuitries, while guaranteeing manufacturability. Hybrid initialization techniques are developed to improve the feasibility of initial individuals. Exhaustive search on small heat exchanger proved that the proposed Integer Permutation-based GA can find optimal or near-optimal refrigerant circuitry designs using relatively low population size and iteration number. Overall, 2.4-14.6% capacity increase compared to the baseline circuitry is observed under different operating and manufacturing constraints.

3 APPLICATIONS OF INTEGER PERMUTATION BASED GENETIC ALGORITHM

3.1 Heat Exchanger Circuitry Optimization for Improved Performance under Air Flow Maldistribution

In packaged fan-coil units, air flow paths are highly constrained which induces severe air flow maldistribution at the frontal face of heat exchangers. Bahman and Groll (2016) have shown that the air flow maldistribution can significantly degrade HX performance especially for evaporators. Lab tests (Payne and Domanski (2003), Gong *et al.* (2008)) and numerical simulations (Lee and Domanski (1997), Kærn *et al.* (2011)) have been conducted to explore the air flow maldistribution effect on HX performances. Aganda *et al.* (2000) and Domanski (1991) showed that the air maldistribution can degrade HX capacity by 35% and 75% respectively under different operating conditions and air maldistribution profiles compared to HX performance under uniform air flow distribution. Because mal-distributed airflow can result in different air-side heat transfer characteristics and uneven refrigerant flow distribution in refrigerant side, circuitry of tube-fin HX has significant influence on HX performance especially under the operating conditions with air flow maldistribution. Kærn and Tiedemann (2012) and Kærn *et al.* (2013) compared the performance of several different refrigerant circuitries and showed that the degradation is associated with non-uniform superheat at the outlet of each circuit and a good circuitry can effectively improve HX performance under air maldistribution. Studies (Casson *et al.* (2002), Domanski *et al.* (2005), Wu *et al.* (2008a)) have indicated that circuitry optimization is a more convenient and economic way to address air flow maldistribution as compared with other approaches, such as controlling the refrigerant mass flow rates in each circuit.

Currently, all reported HX circuitry optimization are performed under specific air velocity profiles. That is to say, the optimal circuitry for a specific velocity profile does not necessarily have desirable performance under other profiles. This brings inconvenience for HX design engineers, because they need to obtain the air velocity profiles for different fan-coil geometry and run circuitry optimization tool repetitively. This necessitates a new circuitry optimization problem formulation which can result in optimal designs with preferable performance under various airflow distributions.

3.1.1 Methodology

To account for the refrigerant maldistribution induced by the air maldistribution, heat exchanger performance is evaluated using a finite volume, mass flow based tube-fin heat exchanger model (Jiang *et al.* (2006)). The refrigerant flow distribution in each circuit is solved in an iterative fashion based on the pressure residual at the outlet of each circuit.

In order to achieve optimal circuitry with improved and stable performance under various air flow distributions, new problem formulations are implemented and will be described in detail in next section. In the objective function evaluation stage, a finite number of air velocity profiles are imposed on the HX model. For each individual (i.e. each circuitry design), HX performance under all velocity profiles will be evaluated, and an objective value will be assigned based on the overall performance for the given circuitry under all air distribution profiles.

17 typical airflow distribution profiles are digitalized from literature. These profiles are all realistic air velocity distributions from experimental measurements collected from different sources (Yashar and Domanski (2010); Yashar and Cho (2007); Yashar *et al.* (2008); Yashar and Domanski (2009); Bahman and Groll (2017)). After

these 17 velocity profiles are collected, profiles with similar trends which are measured from fan-coil unit with similar geometry are eliminated, this can reduce HX model runs in the objective value evaluation stage. Figure 3-1 shows six representative velocity profiles used in the finite search. Except Figure 3-1(a) which is an artificially uniform distribution, the remaining 5 profiles are realistic profiles. Figure 3-1(b) and Figure 3-1(e) are measured from the top slab of A-coil. Figure 3-1(c) is measured from an inclined single coil, the inclination angle to the duct wall is 65°. Figure 3-1(d) is the frontal air distribution for the bottom slab of an A-coil. Figure 3-1(e) is air distribution from a packaged environmental control unit (ECU). In the optimization practices conducted in this thesis, all profiles are scaled to offer 600 CFM air volume flow rate and imposed on the tested HX.

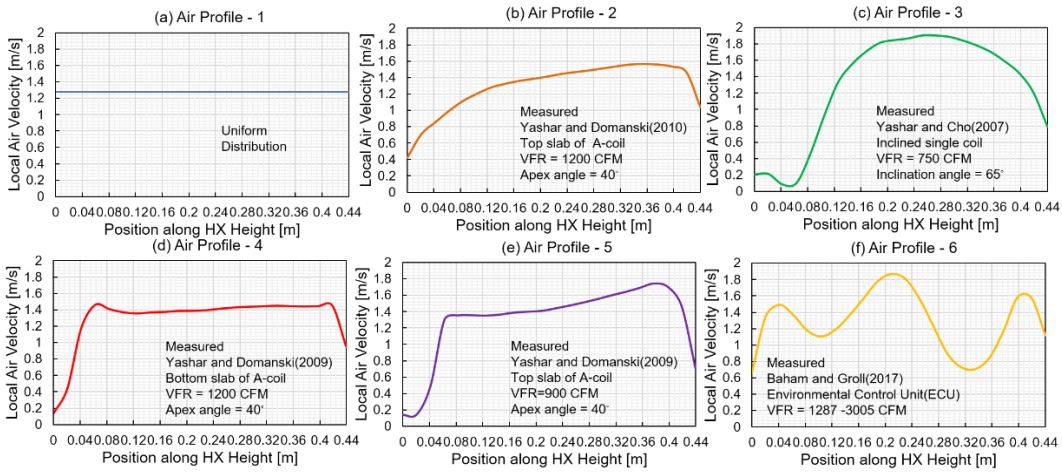

Figure 3-1: Air Velocity Distribution Profiles Collected from Lab Measurements

3.1.2 Problem Formulations

One goal of this study is to find a good metric to assess the overall performance of circuitry under the variation of air distributions. Thus, three different criteria are used to measure the overall performance. Each of this criterion leads to one optimization problem formulation.

Equation (3-1) shows the 1st problem formulation, in which the objective is to maximize the minimum capacity among all velocity profiles. In other words, for a given circuitry the optimizer tries to improve the worst case capacity among all airflow profiles. Meanwhile three constraints are added in IPGA. The first constraint limits the optimal circuitry to have equal or less refrigerant pressure drop than the baseline circuitry. The 2nd constraint limits the capacity of the optimal circuitry to be larger than that of the baseline. The 3rd and 4th constraints limit outlet saturation temperature and sensible heat ratio to acceptable range. The last two constraints are mfg. constraints to make the inlet and the outlet tubes on the same side of HX, and to avoid long U-bends spanning across more than 3 tube rows.

$$
\begin{aligned}
&\text{Objective-1: } \mathit{Maximize}(\mathit{Min.}(Q)) \\
&\text{Subject to:} \\
&\Delta P_{refrigerant} \le \Delta P_{refrigerant,\,baseline} \\
&Q \ge Q_{baseline} \\
&|\,\Delta Tsat_{outlet} - \Delta Tsat_{baseline,outlet}\,| \le 1.5K \\
&|\,SHR - SHR_{baseline}\,| \le 2\% \\
&\text{Inlets and outlets on the same side of HX} \\
&\text{No long U-bend across 3 tube rows}
\end{aligned}
\tag{1-2}
$$

Another criterion to measure the performance of a circuitry can be the average capacities among all profiles. Thus, the 2nd objective function examined is shown in Equation (1-3) . The 3rd criterion is to use the standard deviation (STD) of capacities among all profiles. Therefore, the objective function is to minimize the STD as shown in Equation (3-3). The constraints are the same as those in Equation (3-1).

$$\text{Objective-2: } \mathit{Maximize}(\mathit{Avg.}(Q)) \tag{1-3}$$

$$\text{Objective-3: } \mathit{Minimize}(\mathit{Std.}(Q)) \tag{1-4}$$

3.1.3 Results

In this session, case studies using the three problem formulations are analyzed aiming at finding the best problem formulation. The same baseline R410A evaporator as described in section 2.4.1 is used. In all optimization runs performed in this chapter, the number of generations used in IPGA is 200 and the population size is 100. These two numbers are relatively low for GA runs, therefore this chapter also demonstrate the capability of IPGA to optimize circuitry under air maldistribution with low computational cost.

3.1.3.1 Maximizing worst-case capacity

Figure 3-2 shows the results for the 1st problem formulation with the goal of maximizing the worst-case capacity. The GA progress plot as in Figure 3-2(a) indicates the optimal circuitry in Figure 3-2(b) can offer 5401W cooling capacity. The optimal circuitry brings a 3.4% capacity increase compared to the baseline. Figure 3-2(c) shows a radar plot, where the six spokes are capacities under six air profiles from Figure 3-1. It is obvious, the optimal coil (blue) can offer larger capacity under all air velocity profiles than the baseline HX (yellow). This indicates that the 1st problem formulation in Equation 3-1 is effective to obtain desirable circuity.

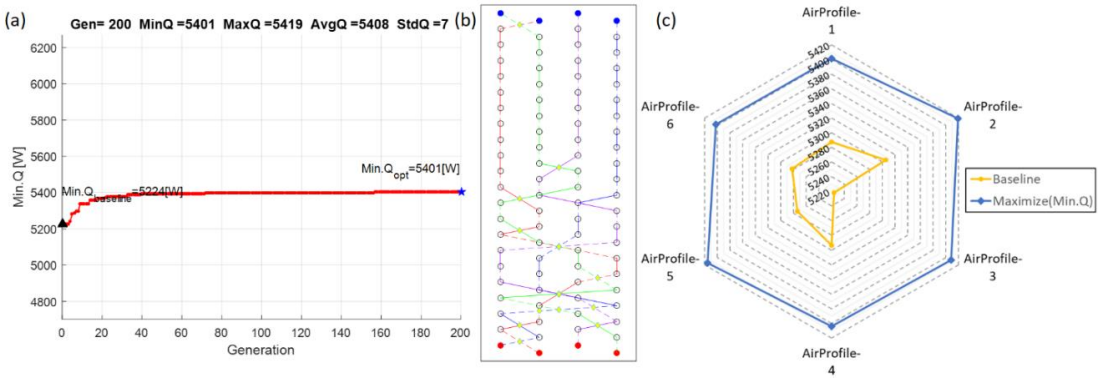

Figure 3-2: Optimization results from Max (Min.Q): (a) GA Progress; (b) Optimal Circuitry; (c) Optimal vs Baseline

3.1.3.2 Maximize average capacity

Figure 3-3 shows the results for the 2nd problem formulation in Equation (3-2). The optimal circuitry (Figure 3-3(b)) shows 2.4% increase in the average capacity. Although there is no constraint on the minimum capacity, the optimal coil still offers a minimum of 5399W cooling capacity as compared with a minimum 5223W of the baseline, which is a 3.4% increase. Figure 3-3 (c) demonstrates that the optimal from Max (Avg.Q) also shows improved performance under all air distribution profiles.

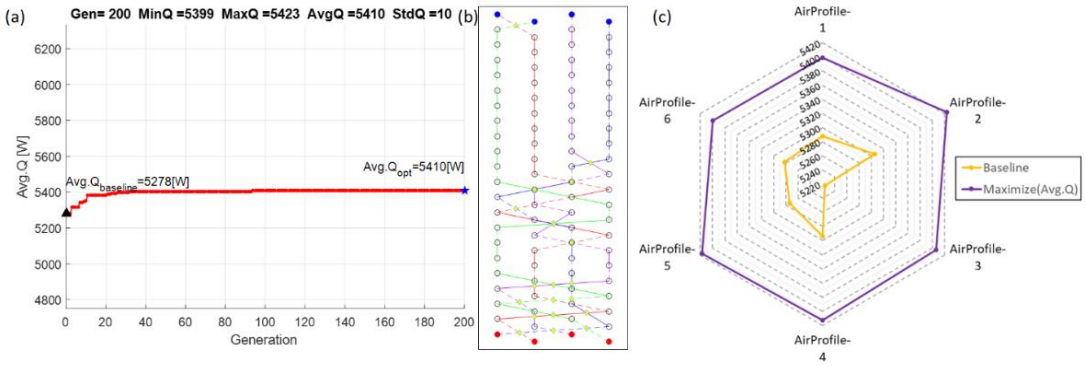

Figure 3-3: Optimization Results from Max(Avg.Q): (a) GA progress; (b) Optimal circuitry; (c) Optimal vs baseline

3.1.3.3 Minimize standard deviation of capacities

The third optimization is performed with the goal of minimizing the standard deviation (STD) of capacities across the different maldistribution profiles. Figure 3-4 (a) shows that IPGA can effectively minimize the STD of capacities from 29W to 1W. Figure 3-4(b) shows the optimal circuitry, which is a fully interleaved pattern. As shown in Figure 3-4(c), the capacities of optimal circuitry under the six profiles are 5321W, 5323W, 5321W, 5322W, 5323W, 5321W with only 1W standard deviation. This indicates that the optimal design (green) is very resilient and can withstand the variation of different air flow distributions. But this optimal only offers an average capacity of 5305W, which is almost 100W lower than the previous two solutions.

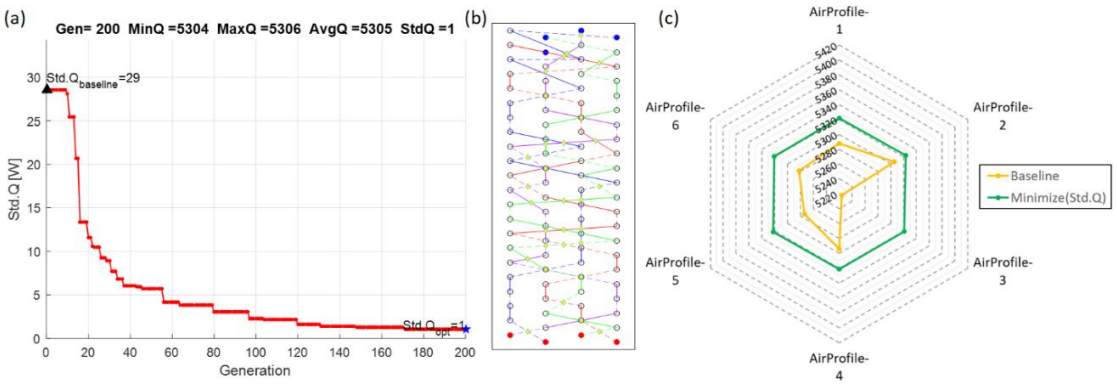

Figure 3-4: Optimization Results from Min(Std.Q): (a) GA progress; (b) Optimal circuitry; (c) Optimal vs baseline

3.1.3.4 Comparison of results

A comparison of the three optimal designs obtained from previous three problem formulations are summarized in Figure 3-5. The red line refers to the performance of an optimal solution obtained under single uniform air distribution profile with the same operating and mfg. constraints. Its circuitry arrangement can be found in Figure 3-7(d).

As shown in Figure 3-5, the optimal designs from Max(Min.Q) and Max(Avg.Q) are both preferable because their average capacity values are the highest, these two optimal circuitries show very similar performance as the blue and purple lines coincide. In terms of stability, the solution from Min(Std.Q) is the best, as it has only 1W difference in capacities under all profiles, followed by the solutions from Max(Min.Q) and Max(Avg.Q), whose STD are 7.2W and 9.7W respectively. However, the performance of the optimal circuitry from single uniform air distribution profile (red) has obvious shortcoming under air profile-3, and it also shows lower performance when subjected to profile-#2, #4, #5, #6. Actually, it only has superior performance under uniform air (profile-1). Its ability to resist air maldistribution is worse than the baseline. This example illustrates that an optimal design obtained under one specific air distribution cannot guarantee good performance under other airflow distributions.

Furthermore, using the optimal circuitry obtained from uniform air assumption in a real fan-coil unit may result in reduced performance in the scenario of air flow maldistribution.

In following section, for the ease of discussion the optimal coil obtained under uniform air distribution is referred as conventional optimal design. Since the solutions from Max(Min.Q) and Max(Avg.Q) show good overall performance (large Avg.Q) and stability (small Std.Q), they are referred as new optimal designs considering they are obtained from new problem formulations proposed in this chapter.

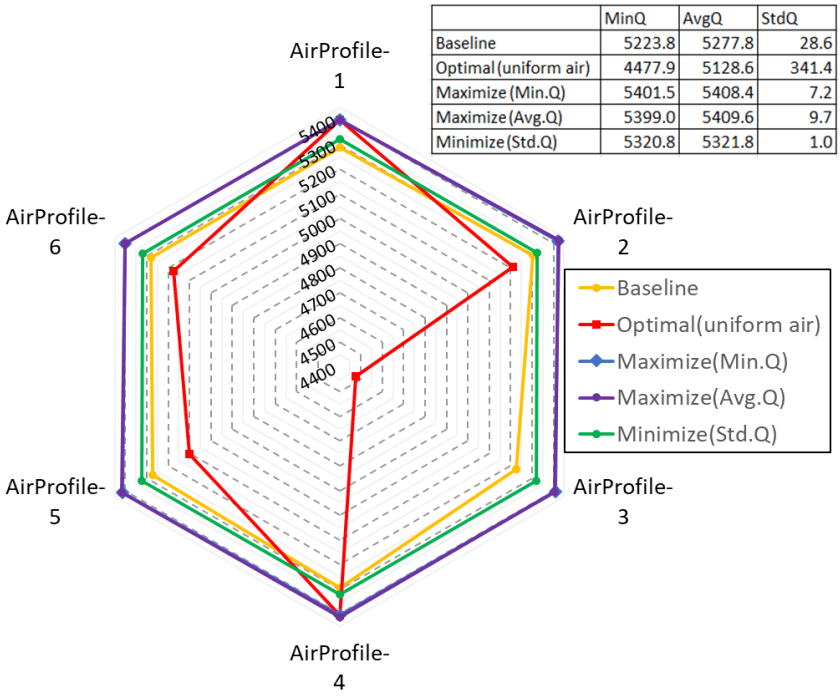

	MinQ	AvgQ	StdQ
Baseline	5223.8	5277.8	28.6
Optimal (uniform air)	4477.9	5128.6	341.4
Maximize (Min.Q)	5401.5	5408.4	7.2
Maximize (Avg.Q)	5399.0	5409.6	9.7
Minimize (Std.Q)	5320.8	5321.8	1.0

Figure 3-5: Comparison of Conventional Optimal, New Optimal and Baseline

3.1.4 Performance of Optimal Circuitries

Since the new optimal designs are obtained from a finite search on the six representative air velocity profiles, it is likely that the new optimal designs only perform well under those six profiles. It is of great significance to see whether they still

show stable performance under other maldistribution profiles which are not included in the previous six-profile database. Moreover, during the heat exchanger operation as part of an air conditioner, the air flow distribution changes continuously, especially when the fan speed changes during startup and shutdown cycles. In this session, the performance of the new optimal design during fan ramp-up and ramp-down is examined.

An OpenFOAM® based CFD model (Chapter 6) particularly developed for simulating air velocity field for A-type indoor unit is used to obtain representative air velocity profiles under different air flow rates and heat exchanger orientations. In order to simulate the fan startup or shutdown process, the CFD simulations are performed under different air volume flow rate (AFR) ranging from 300 CFM to 900 CFM. Figure 3-6(a) shows the three air velocity profiles for different air volume flow rate, the apex is located at the right end, where more air tends to accumulate due to contraction. The performance of the five designs mentioned in last section are compared under the three air maldistribution profiles. As shown in Figure 3-6(b), the baseline and the conventional optimal design have the lowest capacities under the three profiles, while the new optimal designs from Max(Min.Q) and Max(Avg.Q) are the best, followed by the new optimal design from Min(Std.Q). This study verifies that the circuitry optimization problem formulations can effectively generate designs which are resilient to air maldistribution during fan startup or shutdown.

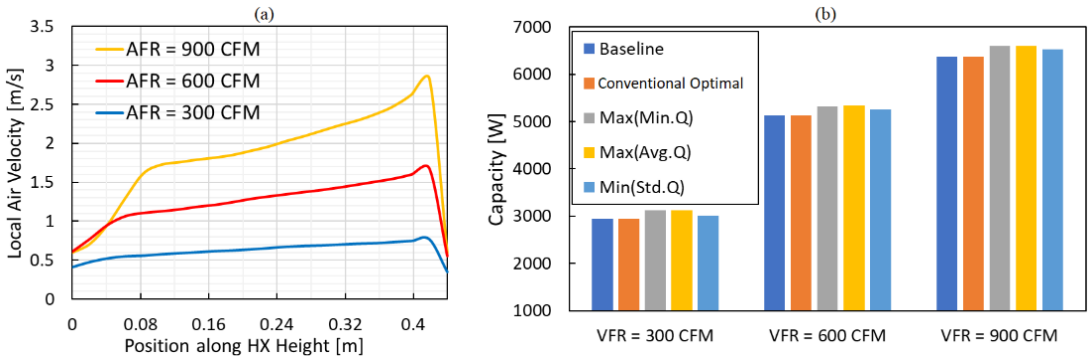

Figure 3-6: (a) A-coil Airflow Profiles for Different Air Flow Rate; (b) Performance Comparison of Circuitry Designs

3.1.5 Analysis of Optimal Designs

To understand the underlying reason which distinguishes the new optimal design from the conventional optimal design and the baseline, the new optimal design from Max(Min.Q), conventional optimal and the baseline are simulated under Profile-3. Recall that the capacity of new optimal is the best (5407W), the baseline is intermediate (5223W), the conventional optimal offers the least capacity (4477W).

Figure 3-7(a) shows the uneven refrigerant mass flow rate distribution in each circuit of the three HXs. The new optimal design has the most uniform refrigerant distribution than the other two designs, the standard deviation for mass flow rates is 38% of that for conventional optimal. Figure 3-7(b) shows the superheat at the outlets of each circuit. It is obvious that the new optimal design has the most uniform outlet superheat. Figure 3-7(c) shows the heat load offered by each circuit. It can be seen the 1st circuit in the conventional optimal design contributes a very small amount of capacity, causing the capacity distribution in conventional optimal very unbalanced.

To understand the reason, the conventional optimal circuitry pattern is shown in Figure 3-7(d), it can be recognized that it has the characteristic that each of its circuit is separated “physically” in 4 blocks from left to right. Figure 3-7(d) also shows the air

volume flow rate distribution on these 4 blocks. As can be seen, the 1st circuit shares a very small amount of air, while the 3rd circuit shares the most amount of air. Thus, if we view each circuit as a small HX, the 1st small HX takes insufficient air, and thus has very poor performance. Looking at the new optimal design in Figure 3-2(b), it does not separate each circuit physically, because its four circuits are fully interlaced. Therefore, the amount of air flowing through each circuit is well balanced.

In conclusion, the new optimal design results in more uniform refrigerant mass flow rate, outlet superheat and capacity distribution through each circuit. Furthermore, a good circuitry should be designed as interleaved circuitry, in which circuits are interlaced multiple times as the one show in Figure 3-2(b). The circuitry pattern which isolates circuits along HX height direction should be avoided. This finding is consistent with Bahman and Groll (2017).

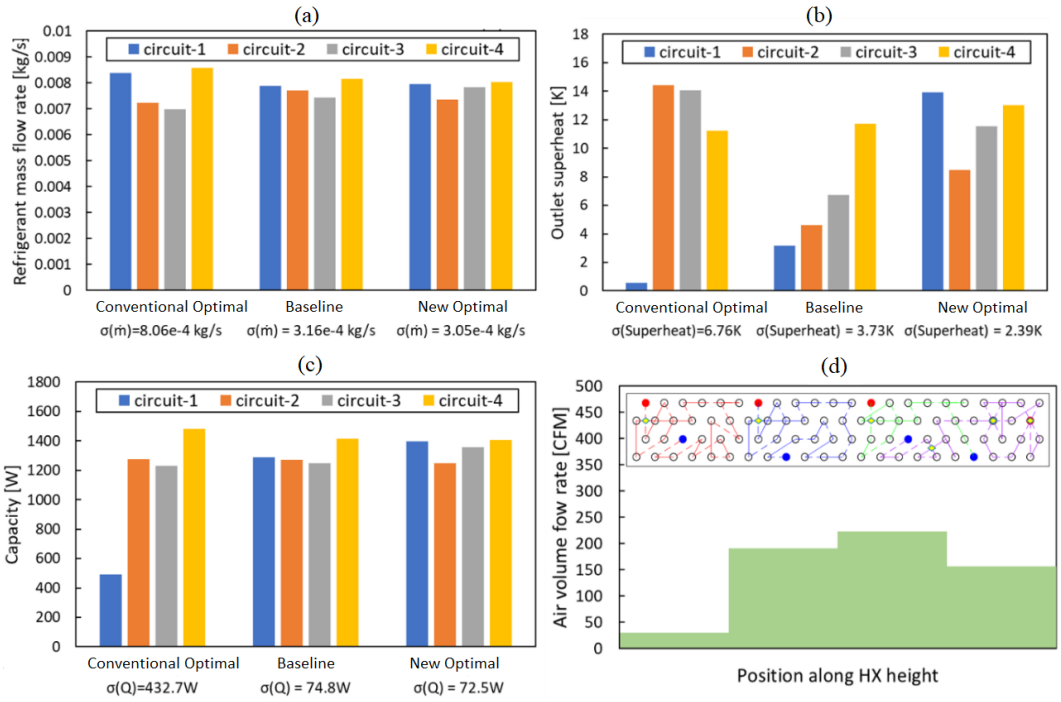

Figure 3-7: Comparison of Conventional Optimal, New Optimal and Baseline: (a) Refrigerant mass flow distribution in each circuit; (b) Superheat at the outlets of each circuit; (c) Capacity offered by each circuit; (d) Air flow rate distribution

3.1.6 Performance of Optimal Heat Exchanger Designs in a System

In this section, we investigate the performance of conventional optimal, new optimal and baseline design in a complete system, also referred to as a cycle, since the system is based on a vapor compression cycle. A component-based vapor compression simulation tool -VapCyc® (Winkler *et al.* (2006)) is used. This is a realistic cycle which has been validated in Alabdulkarem *et al.* (2015) by adopting the baseline circuitry in section 2.4 as its evaporator. Figure 3-8(a) shows the cycle schematic. The detailed information about other components of this cycle can be found in Alabdulkarem *et al.* (2015). The operating condition is the AHRI Standard 210/240 Test-A condition (AHRI (2008)) .

The A-type coil is first simulated in OpenFOAM® based CFD model (Chapter 8), then the air maldistribution profile is imposed on the air side of the A-type unit. As shown in Figure 3-8(b), the new optimal design leads to a COP improvement from 3.54 to 3.71, or 4.8% compared to the baseline cycle. While the conventional optimal obtained from uniform air distribution causes a degradation of COP from 3.54 to 3.46 by 2.3%. The cooling capacity of the entire A-type unit (2 slabs of coils) is improved from 9944W to 10452W by 5.1%, in contrast, the conventional optimal results in a capacity degradation from 9944W to 9701W by 2.4%, because this optimal design is a solution from uniform airflow assumption, it is not able to account for air maldistribution due to no interleaving. It can be seen from P-h diagram, the new optimal (red) has higher evaporating temperature than other two cycles. It has smaller temperature difference between refrigerant and air while offering more cooling capacity.

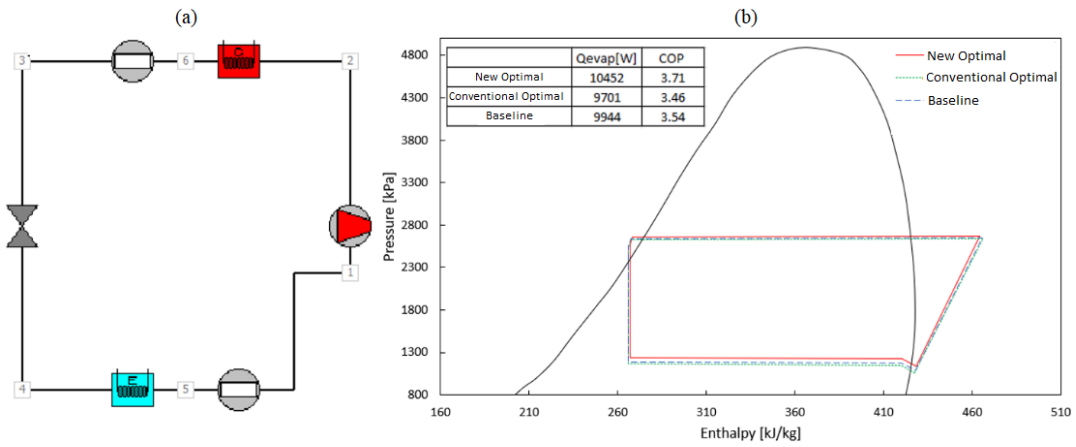

Figure 3-8: Performance Comparison of New Optimal, Conventional Optimal and Baseline in a Cycle: (a) Simulated cycle in VapCyc®; (b) R410A P-h diagram using three HX designs

3.1.7 Summary

The new circuitry optimization problem formulations implemented in this section guarantee that the optimal circuitry offers an acceptable minimum performance regardless of the variation of airflow distribution. The results show that the optimal designs obtained from the new problem formulations are significantly more resilient to multiple airflow maldistribution profiles than the conventional optimal design obtained under solely uniform air distribution. After conducting optimization with the new problem formulation on a real vapor compression cycle, the new optimal circuitry leads to a predicted 4.8% COP improvement and a 5.1% cooling capacity improvement. Although the actual improvement from the new optimal design needs further validation by manufacturing and testing the circuitry in lab, the results demonstrate great potential for the proposed problem formulation to improve heat exchanger performance in real-world application.

3.2 New Heat Exchanger Circuitry Optimization Problem Formulation for Improved Performance Under Frosting Conditions

3.2.1 Background

In this chapter, the application of IPGA to improve heat exchanger performance under frosting conditions is discussed. One of the major concerns for the refrigeration and heat pump engineers is frost formation on outdoor unit since it can lead to significant reduction in heat exchanger capacity and cycle efficiency.

Frost will accumulate on the surfaces of evaporator when the coil surface temperature is below the dew point temperature of incoming air and meanwhile the air dry bulb temperature is below 0 °C. The process of frost formation on the surface of an evaporator is a result of two mechanisms: the buildup of small ice particles that exist in the free air stream and accumulate by impaction or interception when they contact the evaporator coil surfaces (Malhammar (1988)) and the diffusion of water vapor onto cold surfaces due to the water vapor concentration difference between the air stream and the frost layer surface (Sanders (1974)).

Formation of frost on a heat exchanger surface results in reduction in heat transfer rate due to fouling characteristics of frost development and blockage of air free flow passages through the heat exchanger. Several techniques have been proposed to reduce the frost accumulation rate thereby increasing the evaporator operation time between defrost operations. For example, Ogawa *et al.* (1993) suggested to use variable geometry tube-fin heat exchangers with different fin geometries on different tube banks to reduce the heat and mass transfer rates at the first few banks exposed to incoming air. However, this geometry modification may be difficult to realize without adding substantial complexity in manufacturing process. Aljuwayhel *et al.* (2007) developed

a heat exchanger frost accumulation model to simulate the performance of counter-flow and parallel-flow circuitry evaporators under frosting conditions. They validated the model by testing an evaporator with counter-flow circuitry. They found that heat exchanger circuitry can influence the frost distribution across the evaporator as well as its transient capacity under frosting conditions. Their study shows that good circuitry design is a convenient and economic way to reduce the effect of frost accumulation and can provide longer evaporator operation time before defrosting.

3.2.2 Problem Formulation

Usually, the dynamic simulation of HX performance under frosting conditions is computationally expensive, which means the computational time for a single simulation can take from a few minutes to several hours. Assuming one HX evaluation takes a few minutes to complete, as there will be at least thousands of HX evaluations in one optimization run, using dynamic HX model to evaluate HXs generated by the optimizer is not feasible in the interest of time. This study strives to tackle this problem by exploring an effective problem formulation used in steady state HX optimization in order to generate circuitry designs with desirable dynamic performance under frosting conditions. One goal of this study is to explore a HX performance index which can serve as a metric for its dynamic performance under frosting conditions. Qiao *et al.* (2017) observed that the tubes on which the frost is the least likely to deposit are those tubes where the refrigerant is superheated for an evaporator.

Based on this insight, the problem formulation shown in Equation (1-5) is proposed, which aims to maximize the total length of superheat section in an evaporator . Five constraints are enforced on this problem. The 1st constraint guarantees that the optimal design has equal or larger capacity than the baseline. The

2nd constraint limits that the optimal circuitry has less refrigerant pressure drop than the baseline. The 3rd constraint confines the outlet superheat of the entire coil to be similar to that of the baseline within ±1 K variation. The last two constraints are manufacturability constraints. The 4th constraint makes the inlet and the outlet tubes on the same side of HX. The 5th constraint avoids long U-bends spanning across 2 or more tube banks.

$$
\begin{aligned}
&\text{Objective: Maximize(total superheat tube length)} \\
&\textit{Subject to}: \\
&\quad Q \geq Q_{baseline} \\
&\quad \Delta P_{refrigerant} \leq \Delta P_{refrigerant,baseline} \\
&\quad \Delta Tsat - 1\,K \leq \Delta Tsat \leq \Delta Tsat + 1\,K \\
&\quad \text{Inlets and outlets on the same side of HX} \\
&\quad \text{No long U-bend across more than 2 tube rows}
\end{aligned}
\tag{1-5}
$$

3.2.3 Baseline Outdoor Heat Exchanger

An outdoor heat exchanger (Figure 3-9) from a flash tank vapor injection cycle (FTVI) is used as the baseline for circuitry optimization. The steady state heat exchanger model was validated with measured data for this coil in previous research under different operating conditions (Xu et al, 2013). Figure 3-10 shows that the heat exchanger capacity deviations between model (Jiang *et al.* (2006)) and experiments are within 6%.

Figure 3-9: Outdoor unit from FTVI

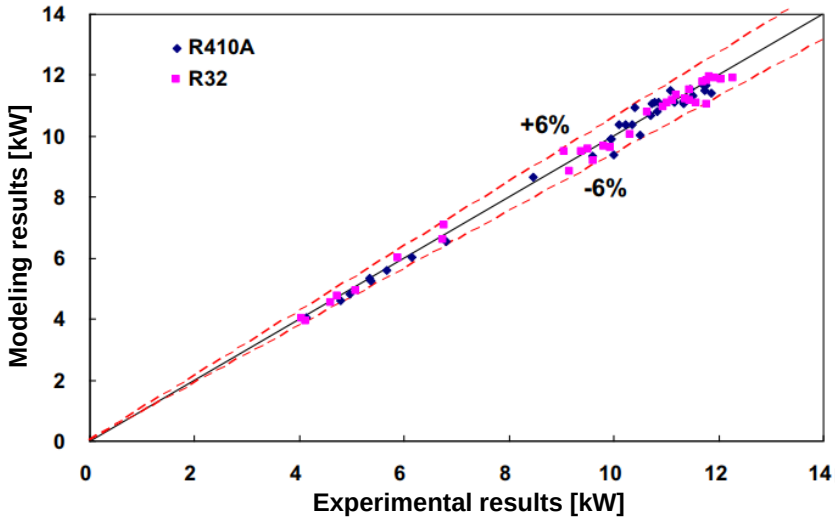

Figure 3-10: Experimental tests vs simulations

Table 3-1 lists the structural parameters of the baseline HX. Table 3-2 shows the operating conditions used in the steady state HX simulation. The air side condition is adopted from (ASHRAE, 2010) frost accumulation test. Table 3-3 lists the empirical correlations used for the local heat transfer and pressure drop calculations.

Table 3-1: Structural Parameters of Baseline Evaporator

Structural Parameters	*Value*
Tube Outer Diameter	7.9 mm
Fins per inch	22 FPI
Fin Type	Wavy Herringbone
Tube Length	2.565 m
Vertical Spacing	24.1 mm
Horizontal Spacing	20.9 mm
Number of Tube Banks	2
Number of Tubes Per Bank	32

Table 3-2: Operating Conditions of Baseline Evaporator

Operating Conditions	*Value*
Refrigerant	R410A
Refrigerant Inlet Pressure	636.3 kPa
Refrigerant Inlet Quality	0.19
Refrigerant Mass Flow Rate	0.035 kg/s
Air Volume Flow Rate (Uniformly Distributed)	2267 ft^3/min
Air Pressure	101.325 kPa
Air Temperature	1.7 °C
Air Relative Humidity	82 %

Table 3-3: Correlations Adopted in HX Simulation

Operating Mode	*Heat Transfer*	*Pressure Drop*
Refrigerant Liquid Phase	Gnielinski (1976)	Blasius (1907)
Refrigerant Two Phase	Shah (2017)	Müller-Steinhagen and Heck (1986)
Refrigerant Vapor Phase	Gnielinski (1976)	Blasius (1907)
Air	Kim *et al.* (1997)	Kim *et al.* (1997)

3.2.4 Circuitry Optimization Results

For the optimization conducted in this case study, the GA population size is 200 and the number of generations is 500. The GA progress plot (Figure 3-11) indicates that after 500 generations, the optimal circuitry yields an increase in total superheated tube length from 59.69% to 70.63% of the entire HX tube length. Figure 3-12 shows the optimal circuitry design after 500 generations.

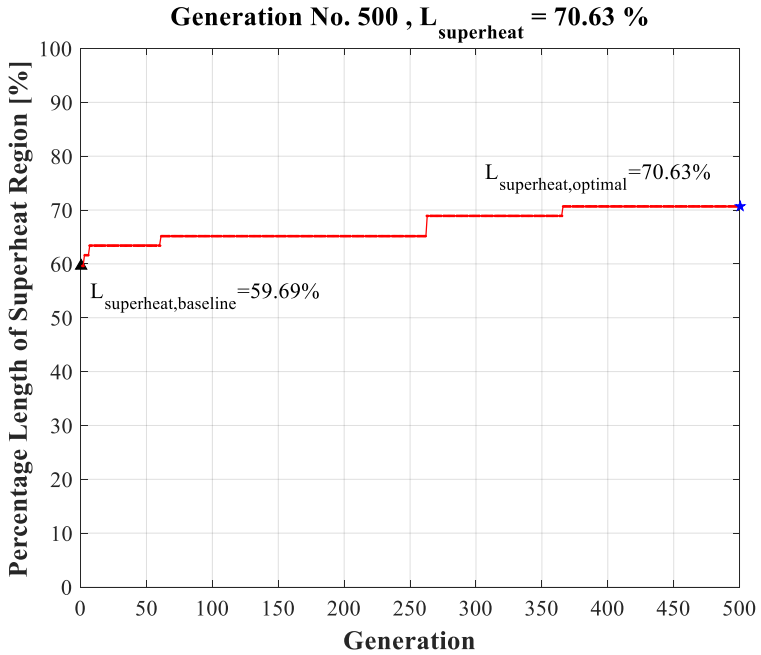

Figure 3-11: IPGA optimization progress

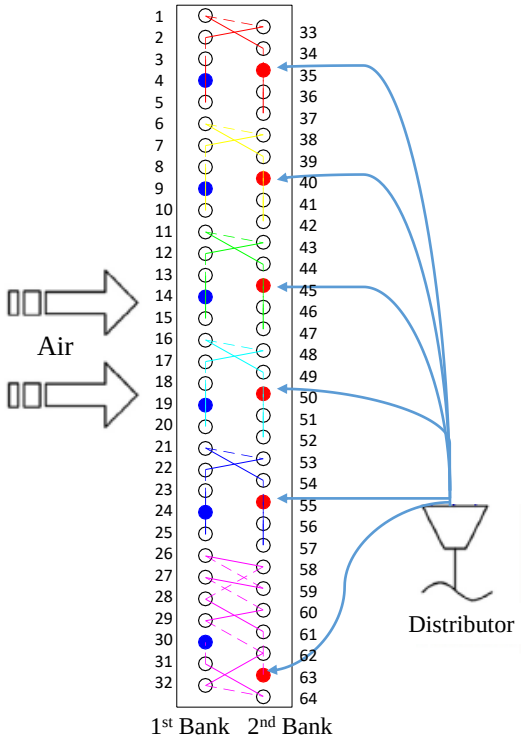

Figure 3-12: Optimal heat exchanger circuitry

Table 3-4 compares the steady state performance of the baseline and the optimal design. The optimal design has almost the same capacity as the baseline, while the refrigerant pressure drop yields a decrease from 59.6 kPa to 55.8 kPa by 6.3%. This is because the optimal circuitry in Figure 3-12 has 6 circuits without merging U-bends. However, the baseline (Figure 3-9) has six inlets and three outlets, so in each circuit two streams merge into one. The high refrigerant pressure drop in baseline is induced by the large refrigerant mass flux at the downstream of each circuit. Despite the significant increase of superheated tube length, the total outlet superheat of the baseline and the optimal design only varies within 1 K, which is essential in avoiding the refrigerant flooding in compressor.

Table 3-4: Comparison of Baseline VS Optimal Design

Case	*Baseline*	*Optimal*
Capacity [W]	7502	7514
Refrigerant DP [kPa]	59.6	55.8
Outlet Superheat [K]	10.4	11.3
Superheat length [%]	59.7	70.6
U-bends L1	55	40
U-bends L2	6	18
U-bends ≥ L3	0	0

3.2.5 Heat Exchanger Simulation under Frosting Conditions

3.2.5.1 Dynamic heat exchanger model with non-uniform frost growth prediction

In order to evaluate the HX performance under frosting conditions, a distributed-parameter heat exchanger model Qiao *et al.* (2015) implemented using Modelica language on Dymola 4.7 (Dassault Systemes, 2014) is used. This dynamic heat exchanger model is integrated with a detailed frost growth prediction model (Qiao *et al.* (2017)) to account for non-uniform frost accumulation on a fan-supplied coil. The air flow redistribution is solved by linearizing a system of non-linear air pressure drop equalization equations. Readers are referred to Qiao *et al.* (2015) for details of the dynamic HX model and the frost growth model.

It is worth mentioning that this HX model as well as the frosting growth model were validated with measured data for the flash tank vapor injection heat pump cycle. Figure 3-13 (reproduced from Qiao et al., 2017), shows the comparison between the dynamic simulation results and experimental data for this FTVI system in terms of HX

capacity, power consumption and cycle COP. The HX frost growth model can predict the transients of this system with reasonable accuracy under frosting conditions.

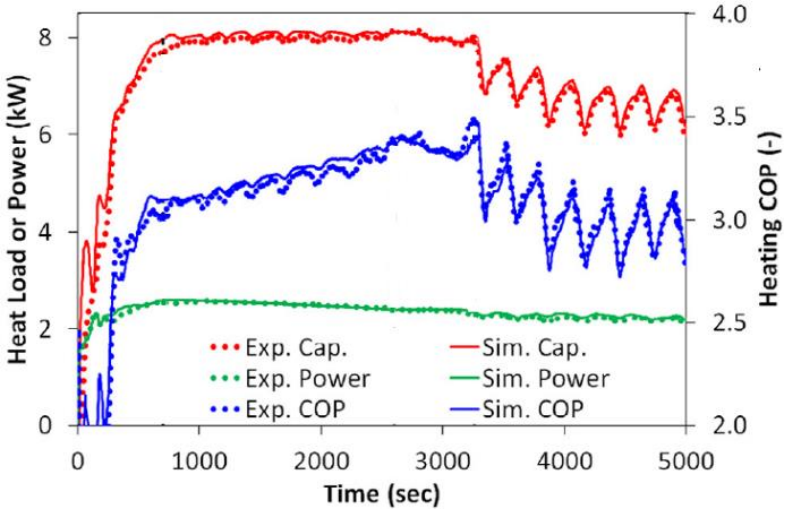

Figure 3-13: Frosting experiment tests vs simulations (Qiao et al, 2017)

3.2.5.2 Transient simulation results and discussion

In this section, the baseline and optimal circuitry designs are simulated for 6000 seconds frost test. The adopted operating conditions is the same as those in Table 3-2 (ASHRAE, 2010). Figure 6 compares the HX capacity between the baseline and optimal design. Both capacities decrease as frost accumulates on HX surface. However, the capacity of the baseline decreases faster than the optimal design, which ultimately yields a 11.6% capacity difference at the end of 6000s frosting test.

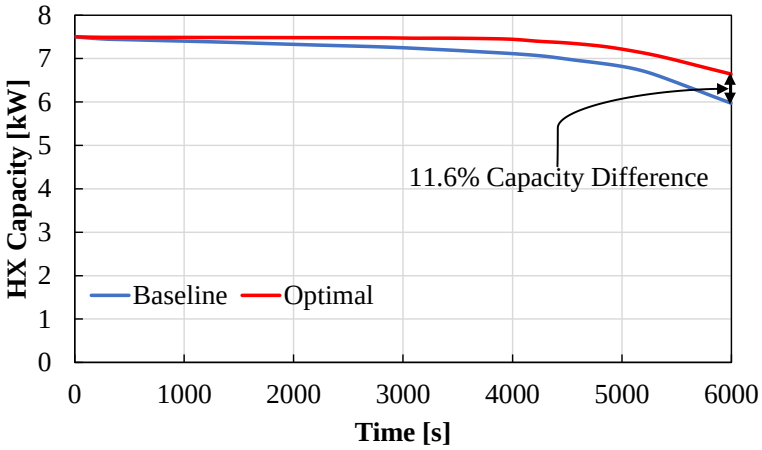

Figure 3-14: Evaporator capacity transients

Figure 3-15 shows the transients of the total frost mass accumulation on HX surface. At the early stage of the frosting test, the frost mass on the two HXs are very close. The frost mass starts to show noticeable difference after 3300s and the difference ends up to be 5.1% at 6000s (4.12 kg frost on the baseline and 3.91 kg frost on the optimal design).

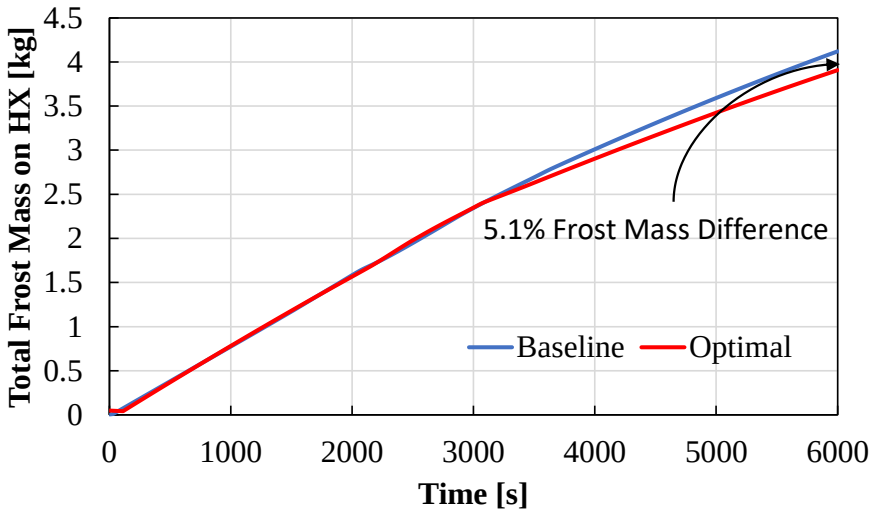

Figure 3-15: Frost mass transients

Figure 3-16 presents the frost mass distribution on each tube bank of the two HXs. It is evident that the 1st tube bank of the baseline has much faster frost accumulation rate. Although the frost growth rate for the 2nd bank of the baseline is less than the frost growth rate of the 2nd bank of the optimal design, it doesn't provide much benefit for the baseline, because the large amount of frost on the 1st bank tends to dominate the air flow resistance of the entire coil. In fact, the slow frost growth on the 2nd bank attributes to the insufficient air which can flow through the 1st bank to reach the 2nd bank.

In other words, despite the total frost growth rate on the two HXs are similar (Figure 3-15), the bank-wise frost distribution on the optimal circuitry is more uniform than that of the baseline (Figure 3-16).

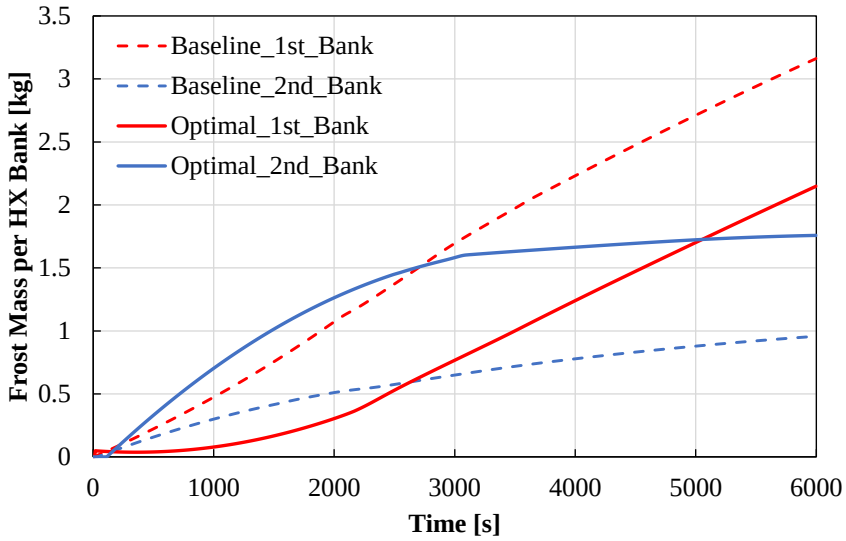

Figure 3-16: Frost distribution on different banks

Figure 3-17 and Figure 3-18 perform an in-depth observation on the frost distribution by presenting the time evolution of the frost thickness on each tube for the two HXs. It is prominent that the frost thickness on the tubes at the 1st bank of optimal design (Figure 3-18, tube #1 to #32) are much less than that of the baseline (Figure 3-17, tube #1 to #32). This indicates that in addition to the uniform bank-wise frost distribution, the optimal design also yields more uniform frost distribution on each tube. As listed in Figure 3-17 and Figure 3-18, at the end of the test (6000s), the standard deviation of frost thickness among all tubes is 0.22 mm for the baseline, while that for the optimal is only 0.13 mm. This result implies that the proposed circuitry optimization problem formulation can generate circuitry design with more uniform frost distribution.

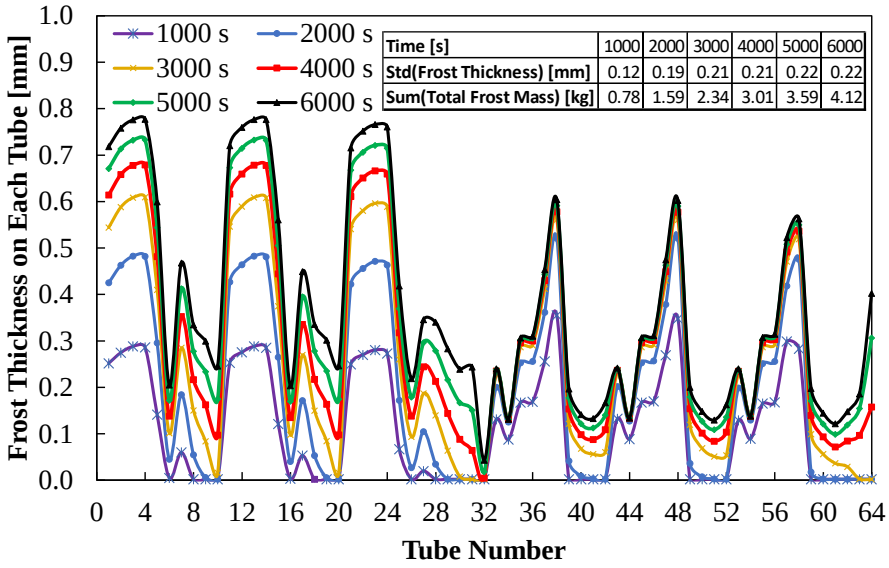

Figure 3-17: Tube-wise evolution of frost thickness (baseline)

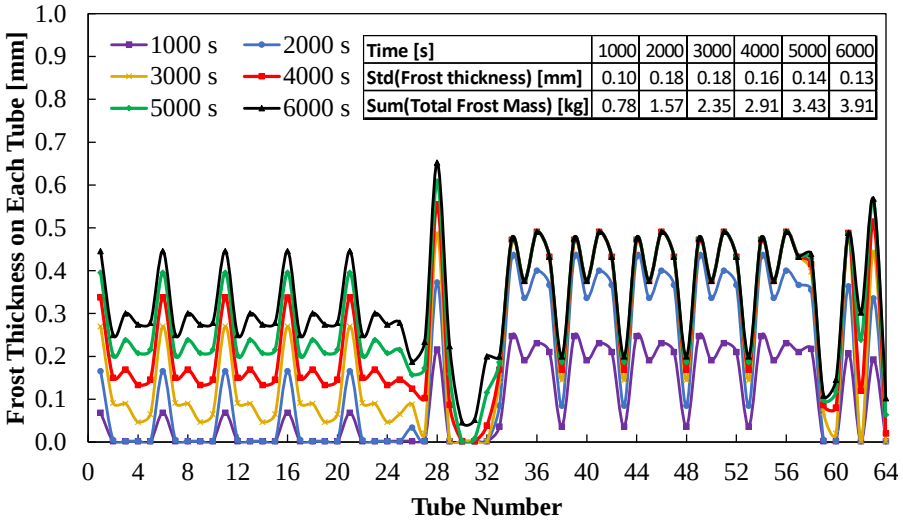

Figure 3-18: Tube-wise evolution of frost thickness (optimal circuitry)

Figure 3-19 shows the transients of the air volume flow rate during the frost buildup process. It can be seen that the air flow rate reduction of the baseline coil is substantially higher than that of the optimal design. The non-uniform frost distribution results in 16.7% air flow rate difference at the end of the frosting test. This reinforces the previous finding that the capacity merit of the optimal design attributes to the superior characteristics of the frost accumulation and the associated effect on the air side pressure drop.

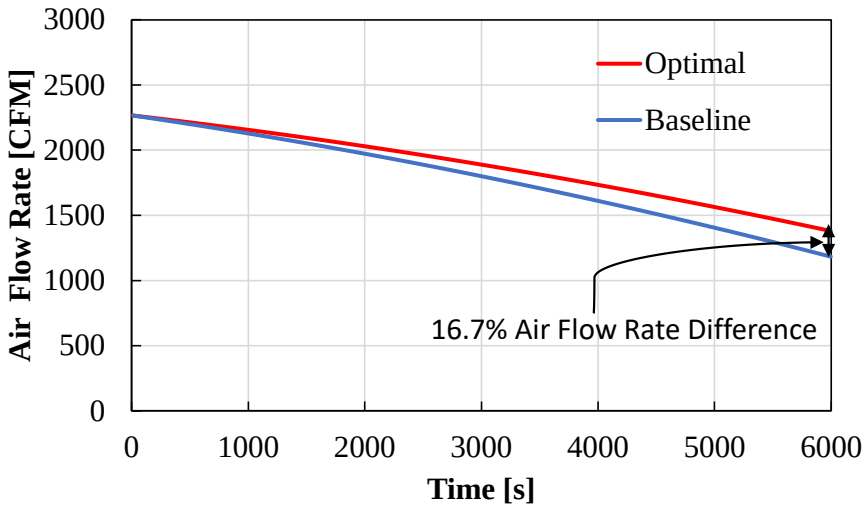

Figure 3-19: Transients of air flow rate

3.2.6 Summary

This chapter presents a new tube-fin heat exchanger circuitry optimization problem formulation to obtain HX designs with improved performance under frosting conditions. In order to verify the efficacy of this new problem formulation, a dynamic HX model integrated with frost growth model is used to evaluate the performance of baseline and optimal circuitry designs. The results show that the optimal circuitry leads to a predicted 11.6% HX capacity improvement and 5.1% frost mass reduction at the end of the 6000 seconds frosting test. Although the actual improvement from the optimal circuitry design needs to be further validated by manufacturing and testing the HX, these results demonstrate that the proposed problem formulation has potential to generate circuitry designs with larger HX capacity, more uniform frost distribution and therefore longer evaporator operation time between defrost operations.

3.3 New Heat Exchanger Circuitry Optimization Problem Formulation for Improved Performance in Reversible Heat Pump Applications

3.3.1 Introduction

The HX circuitry optimization studies published in the previous literature are conducted under a specific operating condition, i.e., the HX either works as a condenser or an evaporator in a system. However, the optimal circuitry obtained under the air conditioning (AC) mode cannot guarantee preferable performance if it is used in the heat pump (HP) mode. Taking an indoor unit as an example, the optimal circuitry obtained by optimizing the HX as an evaporator in AC mode does not necessarily guarantee desirable performance when the refrigerant flow is reversed, and it operates as a condenser under HP mode. It is thus clear that circuitry optimization for HX in reversible heat pump application has not been explored. This necessitates a new problem formulation to obtain optimal designs with improved performance in both AC and HP modes. This chapter implements a bi-objective problem formulation for tube-fin heat exchanger circuitry optimization.

3.3.2 Problem Formulation

In order to obtain the optimal circuitry for tube-fin heat exchanger in reversible heat pump applications, the problem is formulated as a bi-objective optimization problem. Equation (1-6) shows the problem formulation. The first 3 constraints are operating constraints, while the last 3 constraints are mfg. constraints. The 1st objective is to maximize the HX capacity under AC mode and the 2nd objective is to maximize the HX capacity under HP mode. Six constraints are enforced on this problem. The 1st and 2nd constraints limit that the optimal circuitry has less refrigerant pressure drop than the baseline under AC and HP modes, respectively. The 3rd constraint confines

the outlet saturation ΔT (i.e. outlet superheat for evaporator, outlet subcooling for condenser) to be similar with that of the baseline within ±1.5 K variation. The other three constraints are manufacturability constraints. The 4th constraint makes the inlet and the outlet tubes on the same side of HX. The 5th constraint avoids long U-bends spanning more than 2 tube rows. The last constraint avoids partially overlapped U-bends crossing.

$$
\begin{aligned}
&\text{Objective-1: Maximize}(Q_{\text{AC mode}})\\
&\text{Objective-2: Maximize}(Q_{\text{HP mode}})\\
&\textit{Subject to}:\\
&\quad \Delta P_{\text{refrigerant, AC mode}} \le 1.1\times \Delta P_{\text{baseline, refrigerant, AC mode}}\\
&\quad \Delta P_{\text{refrigerant, HP mode}} \le 1.1\times \Delta P_{\text{baseline, refrigerant, HP mode}}\\
&\quad \Delta T\text{sat}_{\text{outlet}} \le \Delta T\text{sat}_{\text{baseline,outlet}} \pm 1.5\ K\\
&\quad \text{Inlets and outlets on the same side of HX}\\
&\quad \text{No long U-bend spans more than 2 tube rows}\\
&\quad \text{No partially overlapped U-bends crossing}
\end{aligned}
\tag{1-6}
$$

It is worthwhile to mention that in order to evaluate the performance of the HX under both operating modes, the HX performance under AC mode is first evaluated, then the refrigerant flow direction is reversed (i.e. the inlets and outlets tubes are swapped), and the HX performance under HP mode is evaluated. In addition to the reversion of refrigerant flow direction, the air and refrigerant inlet conditions and the empirical correlations to predict in-tube heat transfer coefficient and pressure drop are also changed to accommodate the operating condition change between AC mode and HP mode.

3.3.3 Bi-objective Optimization

Throughout this chapter, the baseline used in this case study is the same A-type indoor unit as used in Chapter 2 and Chapter 3. The Pareto front as shown in Figure 3-20(a) has 15 optimal designs. The X-axis and Y-axis are the HX capacities under AC mode and HP mode, respectively. Given the very narrow spread of the Pareto set, we conclude that for this particular problem, there are not very many circuitry options that yield significant performance gains. The geometry would have to change to achieve additional performance gains. Furthermore, it is important to note that for any optimization formulation with a fixed mass-flow rate (i.e., without system simulation involved), the Pareto-set will have a narrow spread due to underlying cycle energy balance. Among the 15 optimal designs, the one (highlighted in green circle in Figure 3-20(a)) whose capacities rank at the median of the 15 designs is sampled for further analysis, since it has the most balanced performance under both AC and HP modes. Figure 3-20(b) shows the circuitry of this design as an evaporator (AC mode), and Figure 3-20(c) shows its circuitry as a condenser (HP mode). In the circuitry plots, a solid line represents a U-bend on the front end of the heat exchanger, while a dotted line represents a U-bend on the farther end. Different color represents different circuits. The red tubes are the inlets, while the blue ones are outlets. It can be seen that the optimal circuitry has acceptable manufacturability without long U-bends or partially overlapping U-bend.

Table 4 presents the detail of this optimal design. Compared with the baseline, the bi-objective optimal design yields the capacity increase from 5294 W to 5401 W by 2.0% when it is used as an evaporator under AC mode. When this HX operates as a condenser under HP mode, it yields the capacity increase from 5744 W to 5872 W by

2.2%. This indicates the bi-objective optimal design is resilient to variation in operating conditions.

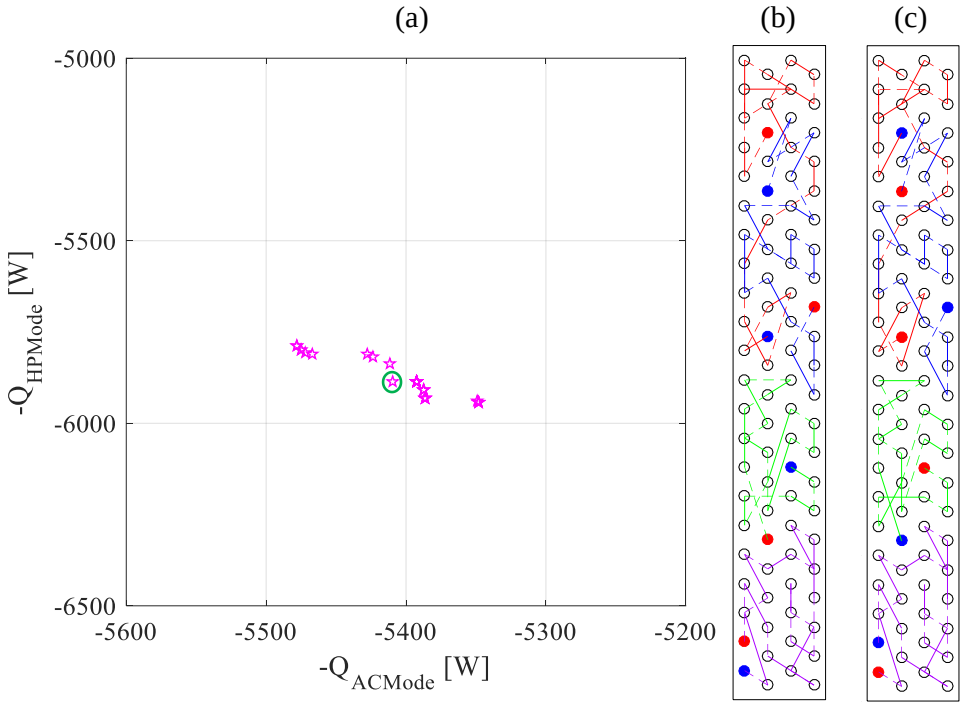

Figure 3-20: (a) Pareto Front of Bi-objective HX Optimization; (b) Optimal Design with Medium Performance as Evaporator; (c) Optimal Design with Medium Performance as Condenser

3.3.4 Single Objective Optimization

In this section, the same baseline heat exchanger is optimized solely under air-conditioning mode. The refrigerant pressure drop constraint, the outlet superheat constraint and the three manufacturability constraints are kept the same as those in Equation (1-6). The GA settings (the population size, the number of generations and population replacement ratio) are also the same as in the previous practice.

Figure 3-21(a) shows the optimal evaporator from this single objective optimization. The circuitry arrangement of this optimal evaporator is shown in Figure 3-21(b). After swapping its inlets and outlets tubes, Figure 3-21(c) shows the reversed circuitry when it is used as a condenser. According to Table 5-1, the optimal circuitry

(Figure 3-21(b)) yields 2.4% capacity increase from 5294 W to 5421 W under AC mode. However, if this HX (Figure 3-21(c)) is used as a condenser in a reversible heat pump, the capacity degrades from 5744 W to 5177 W by 9.9% compared with the baseline in HP mode. These results indicate that HX circuitry optimization under a specific operating condition cannot guarantee desirable HX performance under the other operating mode.

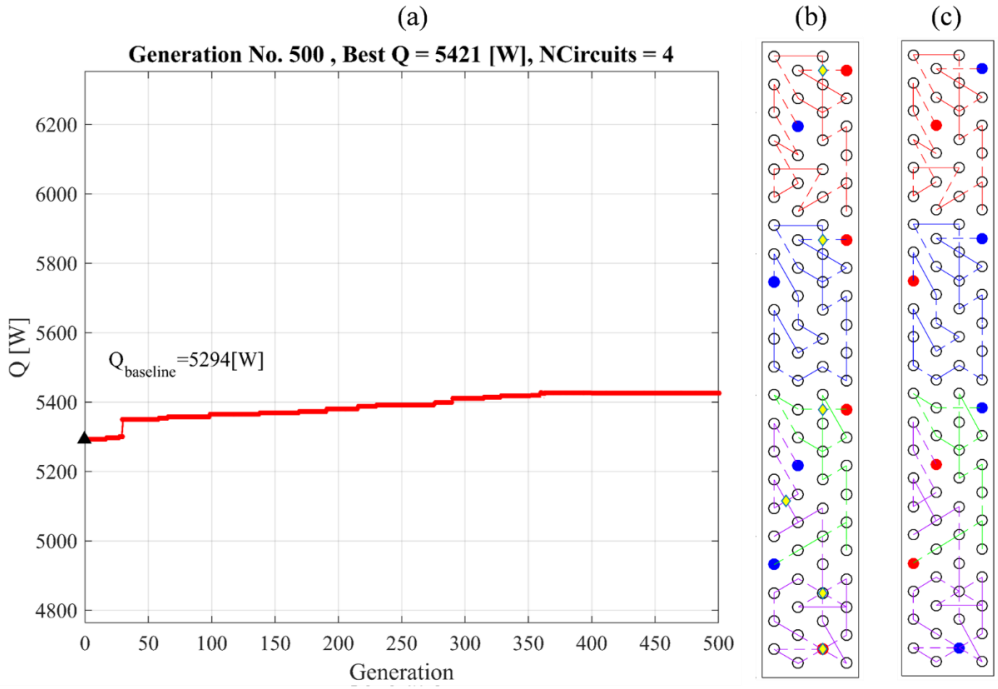

Figure 3-21: (a) GA Progress from Single Objective Optimization; (b) Optimal Circuitry from Optimization under AC mode; (c) Reversed Circuitry as a Condenser under HP mode

Table 5-1 compares the performance of the baseline, the bi-objective optimal design and the AC-mode single objective optimal design. It can be seen that the bi-objective optimal design yields more than 100 W capacity increase under both AC and HP mode than the baseline, meanwhile its refrigerant pressure drop (as shown in Table 3-5) is always less than that of the baseline under the same operating condition. In contrast, the optimal design from single optimization under AC mode obtains 2.4% capacity increase as an evaporator, but its performance under HP mode degrades

significantly. Moreover, its refrigerant pressure drop increases by 5.4% (Table 3-5). These results demonstrate the necessity of the proposed problem formulation to improve the performance of HX under different operating conditions.

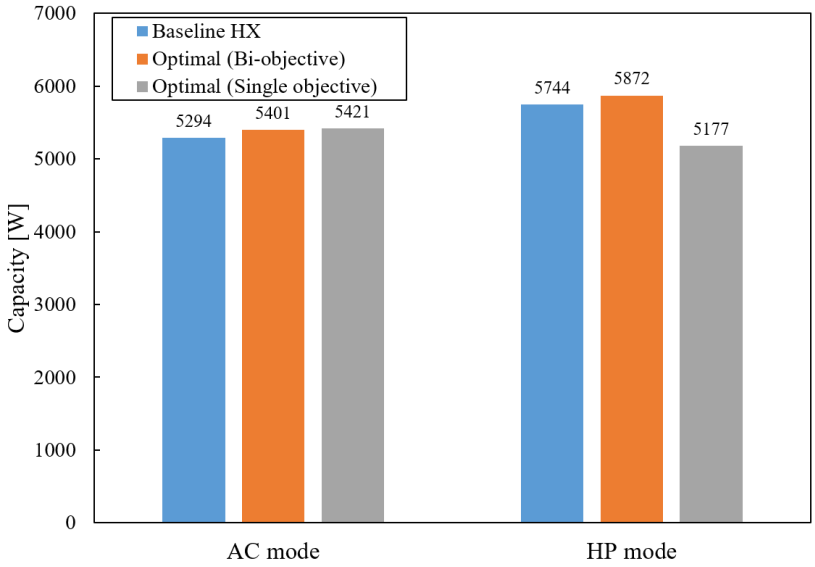

Figure 3-22: Comparison of Bi-objective Optimal vs Single Objective Optimal

Table 3-5: Summary of Optimization Results

Case	**Baseline**		**Optimal from Bi-objective Optimization**		**Optimal from Single Objective Optimization**	
Mode	AC	HP	AC	HP	AC	HP
Capacity [W]	5294	5744	5401 (2.0%↑)	5872 (2.2%↑)	5421 (2.4%↑)	5177 (9.9%↓)
Ref. DP [kPa]	11.8	7.4	11.4 (3.6%↓)	7.3 (1.4%↓)	11.7 (1.0%↓)	7.8 (5.4%↑)
Sensible Heat Ratio	79.6%	100%	79.8%	100%	80.6%	100%
Outlet Saturation ΔT [K] (+ superheat, - subcooling, 0 two-phase)	+8.6	-9.48	+9.7	-8.13	+10.1	0.0
Refrigerant Charge [g]	182.5	877.7	165.4 (↓)	935.2 (↑)	158.9 (↓)	828.5 (↓)

3.3.5 Summary

This chapter implements a bi-objective problem formulation to optimize HX circuitry, the new problem formulation aims at obtaining optimal circuitries with improved performance under both air conditioning and heat pump modes for reversible heat pump system. After implementing the new problem formulation to an A-type indoor heat exchanger unit from a real reversible heat pump system, the new optimal circuitry leads to 2.0% capacity improvement when it is used as an evaporator under AC mode and 2.2% capacity improvement when it is used as a condenser under HP mode. As a comparison to the bi-objective optimization, the capacity of the optimal from single objective optimization obtained under air condition mode results in 10% (527 W) capacity degradation when it is used in heat pump mode. Use of this bi-objective problem formulation to optimize circuitry in early design stages can help assure a certain minimum acceptable performance of heat exchangers in heat pumps during both cooling and heating mode usage.

4 MULTI-BANK MICROCHANNEL HEAT EXCHANGER PASS CONFIGURATION OPTIMIZATION USING INTEGER PERMUTATION BASED GENETIC ALGORITHM

4.1 Introduction

Microchannel heat exchangers (MCHX) have been increasingly applied in air-conditioning and heat pumps because they offer greater compactness, significant charge reduction, lower refrigerant pressure drop and lower air-side fan power consumption compared to tube-fin heat exchangers (Mehendale *et al.* (2016)). Typically, for the given envelope volume and operating condition, the system designer has the freedom to choose a suitable geometry for optimization of MCHX performance.

Design engineers usually choose MCHX pass arrangement based on their experience or the benchmark result of a limited number of simulations for a few artificially designed pass arrangements. For instance, one of the most common pass arrangement for MCHX has multiple passes, which starts from the top and ends at the bottom. There is no guarantee that manually designed pass arrangements are optimal designs, especially for large HXs. The pass arrangement optimization for multi-bank MCHX is particularly challenging due to the extremely large design space whose size increases exponentially with the increase of tube numbers. To the authors' knowledge, there is no optimization algorithm which has appeared in the literature to optimize MCHX pass configurations.

4.2 Chromosome Design for Microchannel Heat Exchanger Pass Arrangements

For microchannel heat exchanger pass optimization problem, the proposed algorithm represents tubes in one pass as an array of integers. The optimization technique is independent of the actual numbering of the tubes. This is similar to the

chromosome representation for the circuitry of tube-fin heat exchanger as described in section 2.2.1. For an integer permutation, each integer (i.e., tube number) appears exactly once, thus, any chromosome generated by the Genetic Algorithm can be mapped to a valid MCHX pass arrangement design and the size of the search space is dramatically reduced by the elimination of redundant designs.

Consider a 20-tube, 2-bank MCHX as an example (shown in Figure 4-1(a)). There are 2 circuits (i.e. 2 refrigerant streams). One circuit has 4 passes and the other circuit has 3 passes. The 2 red arrows indicate the refrigerant inlets and the 2 blue arrows indicates the refrigerant outlets. The refrigerant streams flowing through the headers are represented by black arrows. A novel chromosome (Figure 4-1(b)) is developed to represent MCHX pass arrangement. It also uses the concept of jagged arrays, where each element of this array stores the pass arrangement in each circuit (i.e. refrigerant stream). Each circuit contains a sequence of integer arrays, and each of these arrays represents the tube numbers in each pass. By using this chromosome, number of circuits, number of passes in each circuit and number of tubes in each pass are all flexible and can be varied by the optimizer.

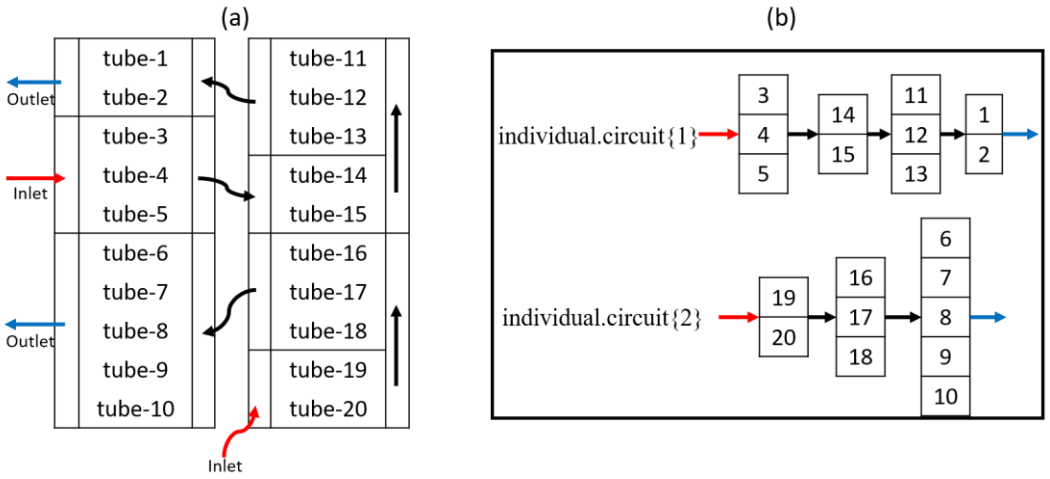

Figure 4-1: Pass Arrangement Representation: (a) 20-tube MCHX; (b) Chromosome

4.3 Selection Operator and Constraint Handling

The selection operator is the same as that mentioned in Section 2.1.2 and the constraint handling method (Deb (2000)) is the same as that detailed in Section 2.2.2. In Chapter 2, it has been shown that this selection operator and constraint handling technique can solve tube-fin heat exchanger circuitry optimization problem efficiently.

According to Deb (2001), the most efficient constraint handling approach is to incorporate constraint inside the working principles of the GA operators, such that all generated designs are feasible designs. In the MCHX pass arrangement optimization problem, since there is usually an upper limit of refrigerant mass flux in individual tubes to avoid large pressure drop, design engineers have the demand to set 'minimum number of tubes per pass' as a manufacturability constraint. Different from the way manufacturability constraints are handled for tube-fin heat exchanger circuitry optimization in Chapter 2, the IPGA for MCHX pass arrangement optimization implements new genetic operators that incorporate manufacturability constraints in an intrinsic manner.

4.4 GA Operators

The creation of new individuals relies on the genetic operators. In this study, six novel genetic operators are developed. As shown in Figure 4-2(a), 'circuit union' operator merges 2 randomly selected circuits into 1 circuit. 'Circuit split' operator (Figure 4-2(b)) split 1 circuit from a randomly selected location into 2 circuit. Because 'circuit union' and 'circuit split' can vary number of circuits, these two operators impose the most prominent change on MCHX design. 'Pass union' operator (Figure 4-2(c)) selects two adjacent passes in the same bank and merge them into 1 pass.

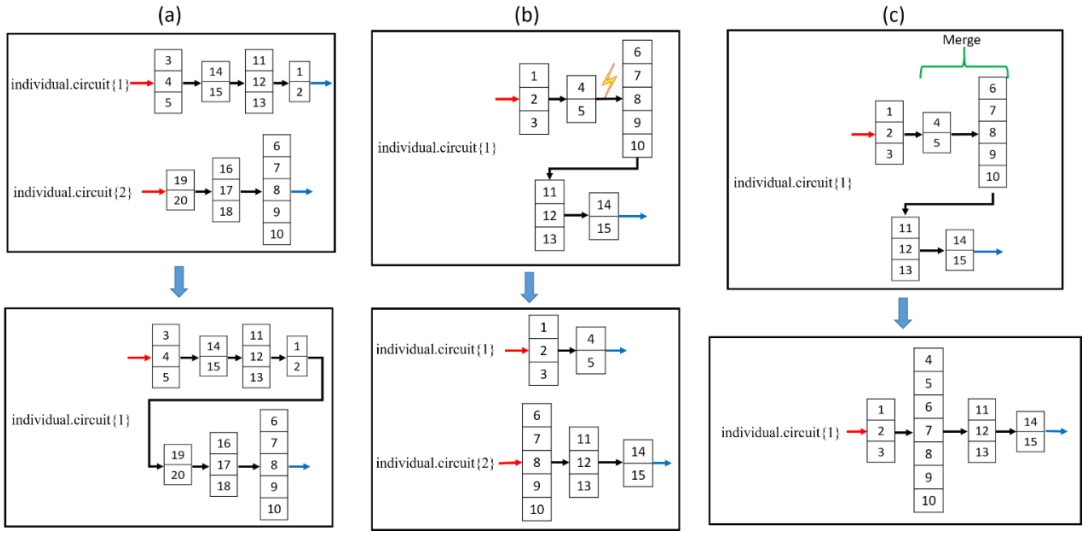

Figure 4-2: GA Operators: (a) Circuit union; (b) Circuit split; (c) Pass union

In addition, 'pass split' operator (Figure 4-3(a)) selects 1 pass and split it into 2 passes. It needs to be mentioned that 'pass split' operator will only select those passes whose total number of tubes are more than 2 times of 'minimum allowed number of tubes in each pass' to perform splitting operation. And the splitting location, although randomly determined, can guarantee that each of 2 generated passes after splitting satisfies the 'minimum number of tubes in one pass' constraint. 'Pass sequence inversion' operator (Figure 4-3(b)) will randomly select one circuit and reverse its pass sequence (reverse the refrigerant flow direction). As shown in Figure 4-3(c), 'tube redistribution operator' reallocates tubes into different passes while maintaining the total number of passes the same. It needs to be mentioned that when redistributing tubes, different tubes are only relocated to adjacent passes in the same bank. Despite the fact that the group of tubes to be relocated are selected randomly, the algorithm is implemented in such a way that it will guarantee there are enough tubes left after the tubes are removed. In this way, manufacturability constraint is implemented as the intrinsic working principle of the GA operators.

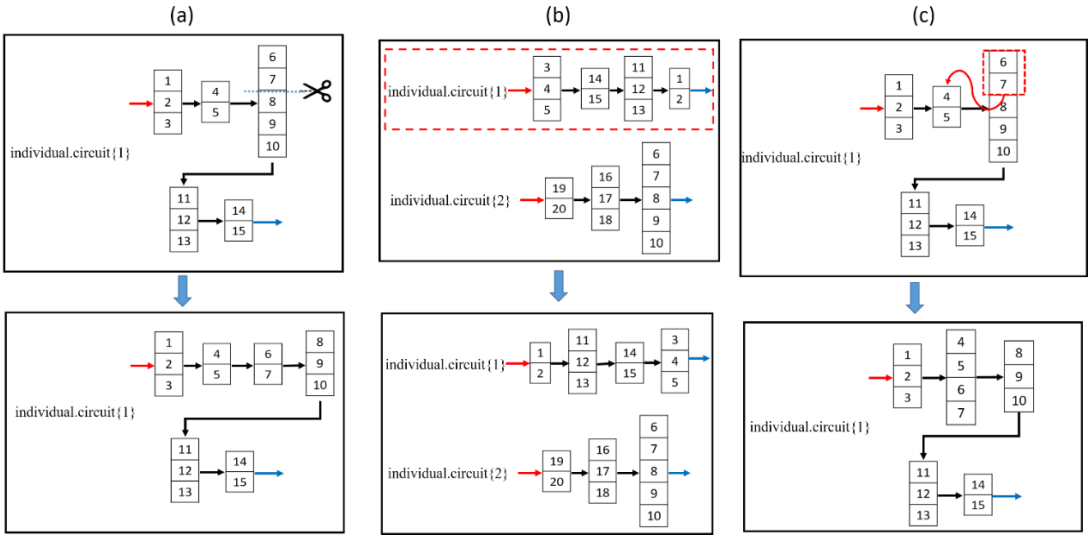

Figure 4-3: GA Operators: (a) Pass split; (b) Pass sequence inversion; (c) Tubes redistribution

4.5 Case Study

4.5.1 Baseline heat exchanger

This section presents two case studies to demonstrate the efficacy of the Integer Permutation based Genetic Algorithm for optimization of MCHX pass configuration. In order to compare the optimal design obtained from the proposed algorithm with the best design obtained from previous research (Mehendale *et al.* (2016)). The 1st case study uses a single-bank MCHX evaporator from Mehendale *et al.* (2016) as the baseline. It has 36 tubes and 12-12-12 pass arrangement from top to bottom. The 2nd case study uses a 2-bank MCHX evaporator to illustrate the capability of the proposed algorithm to handle multi-bank MCHX. Its tube and fin dimensions are similar to those MCHXs typically applied in commercial heat pump applications.

The air side operating conditions are adopted from AHRI (2008). In order to conduct a fair comparison with the finite search results obtained from Mehendale *et al.* (2016), the evaporator outlet superheat is fixed at 5°C and the evaporator inlet conditions as well as the R410A mass flow rate are iteratively solved using an existing

validated model (Schwentker *et al.* (2005)). Table 4-1 summarizes the structural parameters of the two baseline MCHXs and the operating conditions under which all simulations are performed. In both case studies, the airflow distribution is assumed to be uniform. The empirical correlations used for local heat transfer and pressure drop calculations during the performance simulation of the MCHX evaporators can be found in Mehendale *et al.* (2016).

Table 4-1: Structural Parameters and Operating Conditions of Baseline MCHXs

Parameters	MCHX 1 (single bank)	MCHX 2 (multi-bank)
Total number of tubes	36	58
Number of banks	1	2
Number of tubes per bank	36	29
Number of passes	3	4
Pass arrangement	12-12-12	13-13-16-16
Tube Length (m)	0.562	0.252
Tube Height (m)	0.0018	0.0018
Tube Width (m)	0.0254	0.02
Tube Vertical Spacing (m)	0.01641	0.0078
Bank Horizontal Spacing (m)	0.01905	0.022
Port shape	circular	rectangular
Port size (m)	0.001 (diameter)	0.00091 (width) * 0.00132 (height)
Number of ports per tube	18	17
Fin density (fins per inch)	20	18

Air inlet dry bulb (°C)	8.33
Air relative humidity	72.7%
Average air velocity (m/s)	2.0, uniform distribution
R410A Inlet State	Keep the enthalpy as inlet of the expansion valve (40 °C saturation temperature, 5 K subcooling)
Target outlet superheat (°C)	5

4.5.2 Objectives and Constraints

The proposed optimization algorithm supports various objective functions. In this case study, the MCHX capacity is maximized to demonstrate the capability of the proposed method. There are 5 constraints imposed on this problem. The 1st constraint limits the optimal design has equal or less refrigerant pressure drop than 1.2 times the refrigerant pressure drop of the baseline, where 1.2 accounts for a 20% relaxation of pressure drop constraint (20% chosen for example purposes). The 2nd constraint limits the optimal design offers larger capacity than the baseline. The 3rd and the 4th constraint limit the outlet saturation temperature and the sensible heat ratio of MCHX evaporator in acceptable ranges. The last constraint is mfg. constraint. The required minimum number of tubes per pass is set as 3 in order to prevent large refrigerant pressure drop.

$$
\begin{aligned}
&\text{Objective: } \textit{Maximize}(Q) \\
&\text{Subject to:} \\
&\Delta P_{refrigerant} \le 1.2 \times \Delta P_{refrigerant,baseline} \\
&\mathrm{Q} \ge \mathrm{Q}_{baseline} \\
&|\, \Delta Tsat_{outlet} - \Delta Tsat_{baseline,outlet} \,| \le 1.5K \\
&|\, SHR - SHR_{baseline} \,| \le 2\% \text{ (for evaporator only)} \\
&\text{Minimum number of tubes per pass = 3}
\end{aligned}
\tag{2-1}
$$

4.5.3 Case study I: single-bank MCHX

The first optimization is performed on the single-bank 36 tube MCHX evaporator. The population size is 200 and the number of generations is 500 and the GA replacement rate is 0.2. Figure 4-4(a) shows the GA progress. Figure 4-4(b) shows the optimal pass arrangement. From Figure 4-4(a), the optimization yields an optimal design with a capacity increase from 4088 W to 4510 W, or by 10.3%. As expected, there is no pass which has less than 3 tubes. The pass arrangement of the baseline is 12-12-12, while the pass arrangement of the optimal design (Figure 4-4(b)) is 5-9-22. The advantage of 5-9-22 pass arrangement can be explained like this. In an evaporator the density of the refrigerant progressively decreases as it flows through the MCHX, thus, it necessitates successively larger inner volumes in the refrigerant flow direction considering the relationship between fluid velocity and refrigerant pressure drop.

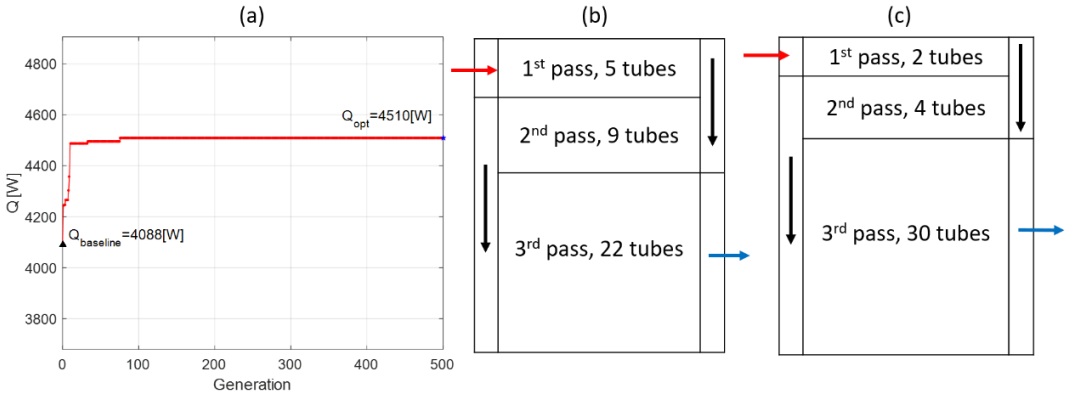

Figure 4-4: 1-bank MCHX (a) GA progress; (b) Optimal; (c) Best design in Mehendale et al. (2016)

Mehendale *et al.* (2016) also investigated the influence of refrigerant pass arrangement for the same evaporator under the same operating condition. Their parametric study explored all possible two-, three-, and four-pass MCHX configurations. In their analysis, 54 two-pass, 374 three-pass, and 1554 four-pass designs were simulated and the best performing design in terms of capacity has 2-4-30

pass arrangement (Figure 4-4(c)). Table 4-2 presents a detailed comparison of the baseline, the optimal design obtained from this proposed algorithm and best design found in Mehendale *et al.* (2016). It can be observed that although the best design from parametric study yields 12.7% capacity improvement, which is larger than 10.3% capacity improvement of the optimal design, however, its refrigerant pressure drop is 2.8 times that of the baseline. This is due to the small number of tubes in the 1st and 2nd passes. Table 4-2 also lists the solved R410A inlet state and mass flow rates for each design since they are iteratively calculated to reach target outlet condition.

Table 4-2: Single Bank MCHX Optimization Results

Case	Baseline	Optimal Design	Best design (Mehendale *et al.* (2016)
Capacity (W)	4088	4510 (10.3%↑)	4607 (12.7%↑)
Ref. DP (kPa)	8.1	9.7 (19.8%↑)	22.7 (2.8x)
Pass Arrangement	12-12-12	5-9-22	2-4-30
Outlet Superheat (°C)	4.98	5.01	4.97
Refrigerant Mass Flow Rate (kg/s)	0.0249	0.0268	0.0276
R410A Inlet Tsat (°C)	2.30	2.97	2.33
R410A Inlet Quality	0.240	0.237	0.240

4.5.4 Case study II: multi-bank MCHX

In order to assess the efficacy of the proposed approach to optimize multi-bank MCHX. A 2-bank, 58-tube MCHX evaporator describe in section 3.1 is used as the baseline. The population size, the number of generations and GA replacement rate are the same as previous case study. The problem formulation is the same as Equation (2-1). Figure 4-5(a) shows the GA iteration progress, Figure 4-5(b) and Figure 4-5(c) shows the pass arrangements of the baseline and the optimal design, respectively. It can be seen that the baseline has 4 passes, while the optimal design has 5 passes. Table 4-3 shows that the optimal design yields a capacity increase of 8.1% (i.e., from 6005 W to 6493 W), while the pressure drop increases from 9.4 kPa to 11.2 kPa by 19.1%. This pressure drop increase is acceptable, given that the relaxation parameter is set as 1.2.

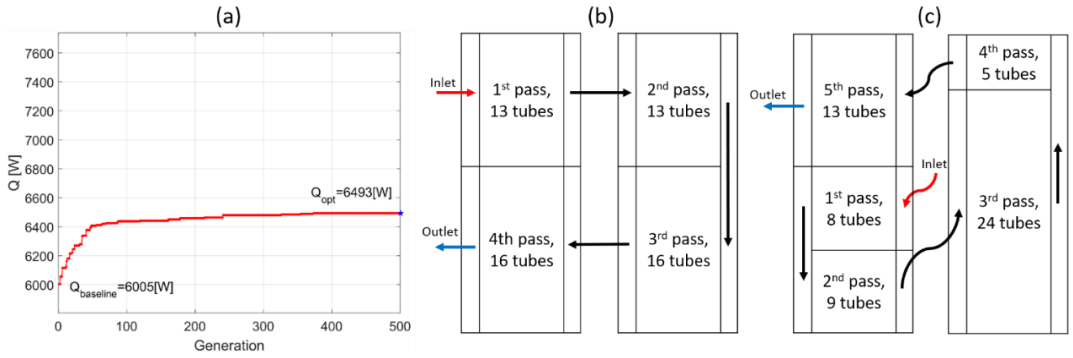

Figure 4-5: 2-bank MCHX (a) GA progress; (b) Baseline; (c) Optimal design

Table 4-3: Multi-bank MCHX Optimization Results

Case	Baseline	Optimal Design
Capacity (W)	6005	6493 (8.1%↑)
Ref. DP (kPa)	9.4	11.2 (19.1%↑)
Pass arrangement	13-13-16-16	8-9-24-5-13

Outlet Superheat (°C)	4.97	5.00
Refrigerant mass flow rate (kg/s)	0.035	0.038
R410A inlet Tsat (°C)	2.35	2.56
R410A inlet quality	0.240	0.238

4.6 Summary

Microchannel heat exchangers are increasingly applied in heat pump applications. Their performance is strongly influenced by the pass arrangement. For multi-bank MCHX, pass optimization is particularly challenging since the number of candidate designs is exponentially large. So far, very few studies on MCHX pass arrangements have appeared in the literature, and no study presents an optimization algorithm to solve this problem. In this chapter, a novel integer permutation-based GA algorithm is presented to solve the microchannel heat exchanger pass optimization problem. Six genetic operators are designed to generate pass arrangement with potentially better performance. The manufacturability constraint is handled inside the generic operators, such that all resulting designs generated by those operators are feasible in terms of manufacturability constraints. Two case studies on a single bank MCHX evaporator and a multi-bank MCHX evaporator show that the proposed optimization algorithm can generate pass arrangement designs with predicted capacities superior to pass arrangements designed manually, meanwhile guarantee good manufacturability. As a result, the proposed algorithm yields MCHX designs which have 8.1-10.3% capacity improvement than non-optimized MCHX pass arrangements.

5 MODELING OF VARIABLE GEOMETRY TUBE-FIN HEAT EXCHANGER

5.1 Concept of Variable Geometry

Most existing fin-and-tube heat exchangers have standard tube layout like inline or staggered with uniform tube sizes, tube pitches, tube locations and a rectangular footprint, as shown in Figure 5-1(a).

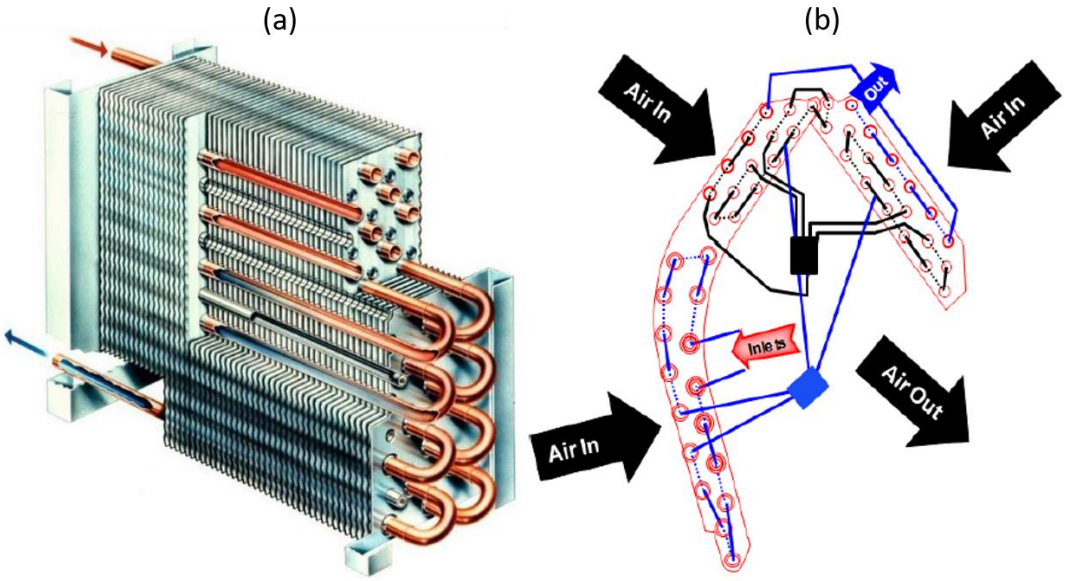

Figure 5-1: (a) Tube-fin heat exchanger with staggered tube configuration; (b) Tube-fin heat exchanger with arbitrary tube layout

The popularity of standard tube configuration is dictated by several aspects, which include ease of manufacturing and familiarity with the design process. However, restricting the design to such uniformity does not push the limits of what can be achieved in terms of performance by adapting the coil design to flow conditions of refrigerant and air side as well as envelope constraints. There are several degrees of freedom which can be exploited to improve the design of a tube-fin heat exchanger such as:

1. Tube size: studies have led to a better understanding of the dependence of refrigerant flow regimes during evaporation or condensation on heat transfer coefficients and pressure drop (Cheng, et al.,2008). These flow regimes have a strong correlation with the refrigerant mass flux through a tube. Extensive experimental studies of in-tube heat transfer and pressure drop along with the developed correlations can result in a better understanding of the tube design. In most applications, there are multiple circuitries. In such way, the refrigerant mass flux varies in different circuits. This knowledge empowers engineers to incorporate different tube sizes to maximize heat transfer coefficients while minimizing pressure drop.

2. Tube shape: conventional tubes are typically limited to round, elliptical or flat shapes which result in particular limitation on thermal-hydraulic characteristics. These limitations can be addressed by employing alternate shapes. Min and Webb (2004) studied tube shapes (round, oval, and flat) with tube diameters above 6.0 mm. They showed that flat and oval could have as low as 50% of the pressure drop compared to round tube, while reducing thermal performance by 10%–20%. Bacellar *et al.* (2017) presents a proof-of-concept design with small finless tubes and a novel shape that can outperform a microchannel heat exchanger. Thus, a heat exchanger model with capability to account for novel tube shapes is in demand.

3. Tube pitch: air flowing into a heat exchanger can have significant maldistribution due to several factors like location of fan or conditions downstream of the heat exchanger. This maldistribution implies that tube pitches and locations inside a heat exchanger need to be designed so as to maximize the air side performance, i.e.,

increase overall UA while maintaining the air side pressure drop within acceptable limits.

These are only a few opportunities available in terms of optimizing the design of a tube-fin heat exchanger. For instance, Waltrich *et al.* (2011) presented an alternative evaporator design, the so-called 'accelerated flow evaporator' as shown in Figure 5-2. The air-side cross-section area decreases with the distance from the air flow inlet, accelerating the air as it flows across the tubes and hence improving the air-side local heat transfer. Ultimately, the basis of such increased design flexibility is to provide optimum conditions for heat transfer, while minimizing pressure drop.

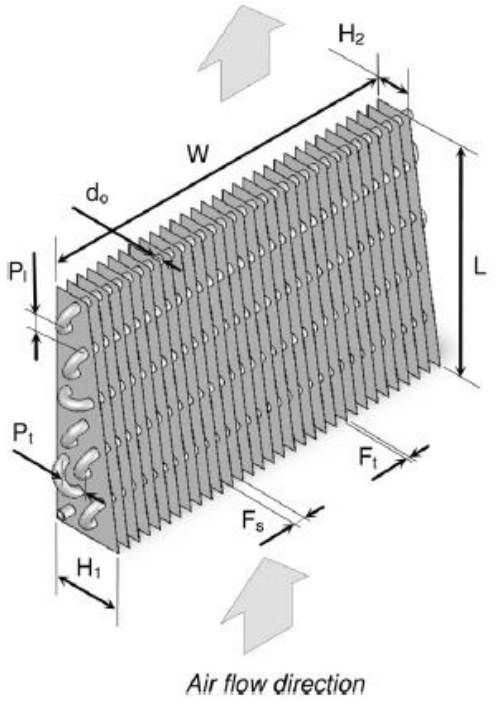

Figure 5-2: Accelerated air evaporator from Waltrich et al. (2011)

To facilitate the design process, it is imperative to have a design-simulation tool which can model a heat exchanger with arbitrary tube shapes, sizes and fin dimensions. Such a model should have the capability of modeling a fin-and-tube heat exchanger with, all or some, of the above characteristics.

5.2 Modeling Assumptions

The assumptions of the model are as follows:

- Steady state model
- Segment can be sub-divided to track the exact flow pattern change point
- Thermally and hydraulic fully developed flow
- The thermo-physical properties and heat transfer coefficients are evaluated based on the inlet of each segment/sub-divided segment
- If header is used, refrigerant is well-mixed in the intermediate header
- Air is assumed to propagate perpendicularly through the heat exchanger
- As air propagates through a coil, it mixes thoroughly in a fin-and-tube control volume before heat transfer occurs
- Air side heat transfer coefficients and pressure drop values are obtained through existing correlations which are applied on a segment-by-segment basis

5.3 Tube Connections

The tube connections for conventional tube-fin heat exchanger is restricted to 'U-bend'. To enlarge the design space for novel heat exchanger, this new heat exchanger model supports U-bends and headers in the same HX. As shown in Figure 5-3, the tubes of the next generation heat exchangers are connected by headers similar to MCHXs, instead of U-bends for conventional TFHX. The new heat exchanger model aims at handling those new HXs with improved prediction capabilities.

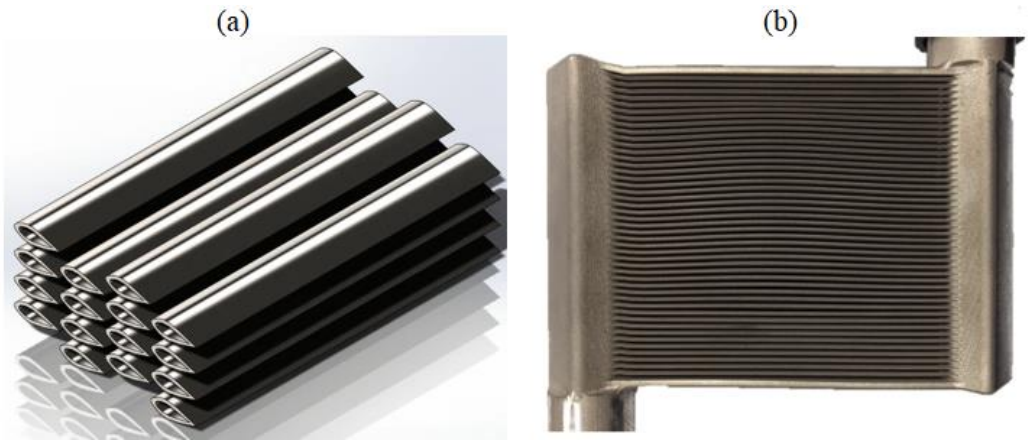

Figure 5-3: (a) Next generation heat exchanger with novel tube shapes; (b) Next generation heat exchanger made by additive manufacturing

The U-bend length calculation is improved based on Jiang *et al.* (2006), Figure 5-4(a) is a schematic to show how Jiang *et al.* (2006)'s model handle long U-bends. In Jiang *et al.* (2006)'s model, the radius of the U-bend is half of the tube distance, this will produce extraordinary long U-bend in the model if the tube distance is large. Figure 5-4(b) shows the improved U-bend length calculation, when long U-bend is encountered, the bend radius is restricted to half of the tube vertical spacing, then the two bends are connected by a straight tube. The new U-bend length calculation is more realistic compared to how hairpins are actually manufactured. Because the U-bend pressure drop is based on U-bend length, with the improved U-bend length model, the U-bend pressure drop prediction is also improved. Meanwhile, refrigerant charge prediction inside U-bends is added compared to Jiang *et al.* (2006) model.

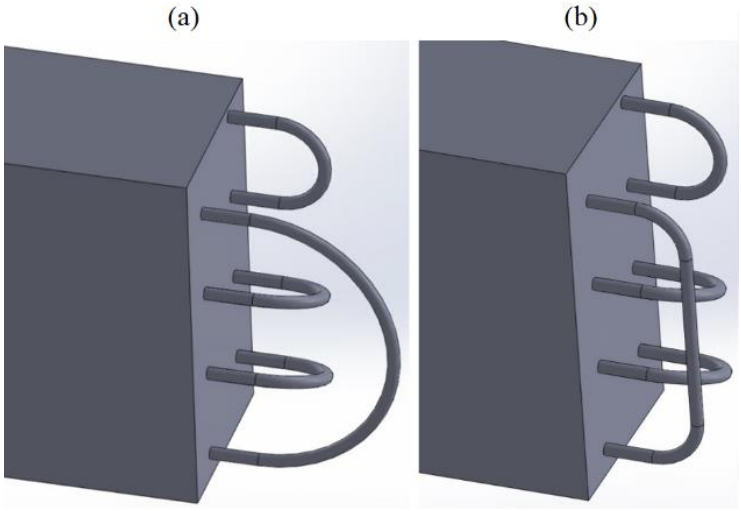

Figure 5-4: (a)U-bend length calculation in Jiang et al. (2006); (b) Improved U-bend length calculation

5.4 Basic Solving Methodology

The proposed model is improved based on the solution methodology implemented by Jiang *et al.* (2006), a segmented heat exchanger modeling tool.

This model was developed to provide the greatest generality and flexibility in designing and simulating air-to-refrigerant heat exchangers. It is based on a detailed numerical model of thermal and fluid flow phenomena integrated with comprehensive working fluid libraries, correlations for heat transfer, pressure drop etc. and optimized numerical libraries. The graphical interface offers ease of circuitry design, input and output of data, choice of fin types and refrigerants, parametric study and optimization capability. Jiang *et al.* (2006)'s modeling approach is introduced here. The primary focus of current research is to introduce a model for variable geometry air-to-refrigerant heat exchanger. Therefore, the reader is referred to the original publication for further detail about Jiang *et al.* (2006)'s model.

To allow generalized circuitry, Jiang *et al.* (2006) utilize a junction-tube connectivity matrix. Such a matrix allows for the tracking of refrigerant flow from

inlet(s) of the coil to the outlet(s). This allows multiple circuits within a heat exchanger with merging and splitting of circuits. Mass flow rates through different circuits are solved to ensure pressure drop through different sub-circuit lengths, of a given circuit are equal. To account for non-uniform distribution of air flow, as well as varying transport and thermal properties and coefficients, each finned-tube macro volume is divided into segments, which are numbered in direction of refrigerant flow.

Each segment of the heat exchanger is treated as a discrete unit of heat transfer. Air velocities are propagated through successive banks of the heat exchanger, as they are on the face of the coil. The presence of thermal resistance can be accounted for through a fouling resistance term. However, the model disregards conduction of heat through finned plates between tubes.

For modeling the refrigerant side heat transfer, the ε-NTU method is used for each segment. When the heat transfer surface temperature is below the dew point temperature of air stream, some moisture condenses out and latent heat transfer occurs. For dehumidification calculation, the method based on enthalpy potential proposed by McQuiston and Parker (1982) is used. For modeling air side, mass energy and humidity is conserved as air propagates through heat exchanger segments. Air side pressure drop is calculated using applicable correlations depending upon various geometric parameters.

Jiang *et al.* (2006) implemented a sub-divided segment approach that allows to track the exact phase transition point inside a segment. This subdivided segment model establishes, iteratively, the length of different phases if there are one or more phase changes within a segment.

5.5 Air Side Propagation

The heat exchanger model requires that air is propagated through a heat exchanger. For a standard configuration, this has been accomplished by Jiang *et al.* (2006). For an inline configuration, air state is propagated downstream, as is, to the logical downstream control volume. For staggered configurations, air state from two upstream control volumes is mixed equally and propagated to the control volume downstream. Clearly, in the case of arbitrary tube layout, neither of the two above-stated laws can be applied.

To implement air side propagation, a mixing law weighted by the interacting face areas of different control volumes was developed. The weighted averages for the mixing law was obtained using the methodology explain in Figure 5-5.

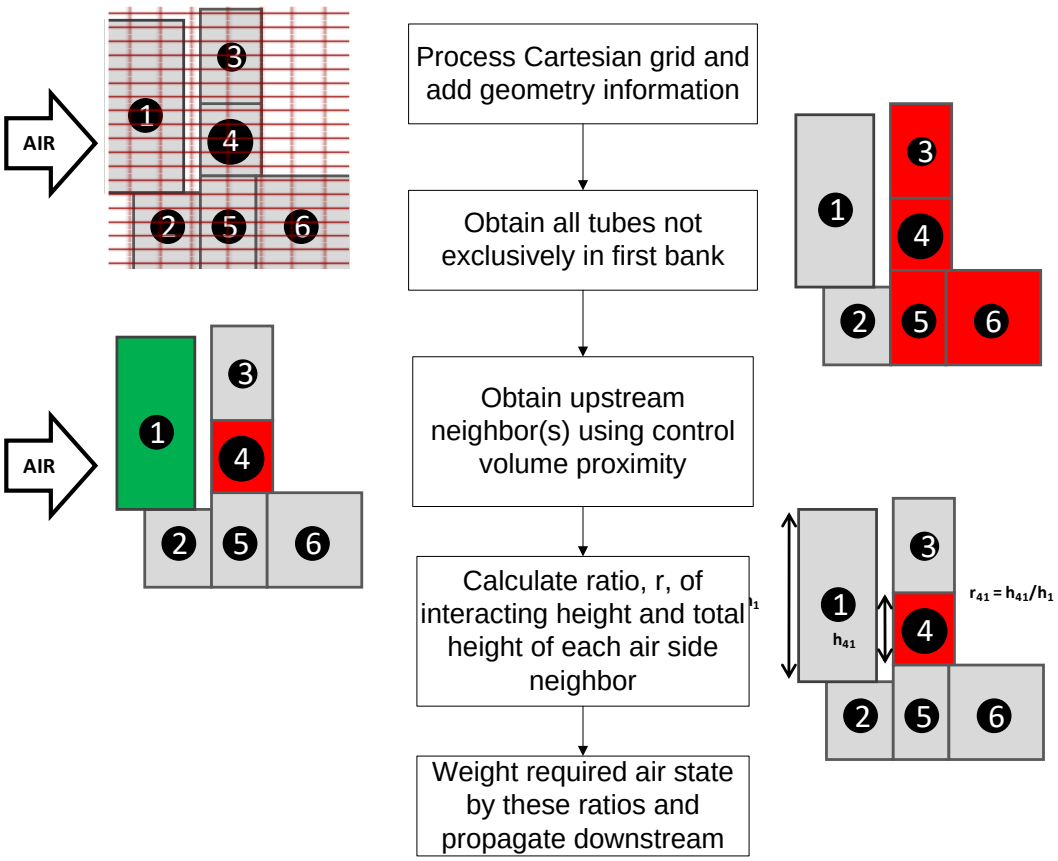

Figure 5-5: Methodology for obtaining weights for mixing of air stream

As illustrated in Figure 5-6, let the mass flow rate entering the exposed faces of tube-1 be mf1, tube-2 be mf2 and tube-3 be mf3. Applying weighted mixing laws based on methodology shown in Equation (5-1) will lead to the following mass flow rates for control volumes that are not exclusively part of the heat exchanger face.

$$
\begin{aligned}
m_3 &= mf_3 + \frac{mf_1 \cdot h_{31}}{h_1} \\
m_4 &= \frac{mf_1 \cdot h_{41}}{h_1} \\
m_5 &= \frac{mf_1 \cdot h_{51}}{h_1} + \frac{mf_2 \cdot h_{52}}{h_2} \\
m_5 &= \frac{m_5 \cdot h_{56}}{h_5}
\end{aligned}
\tag{5-1}
$$

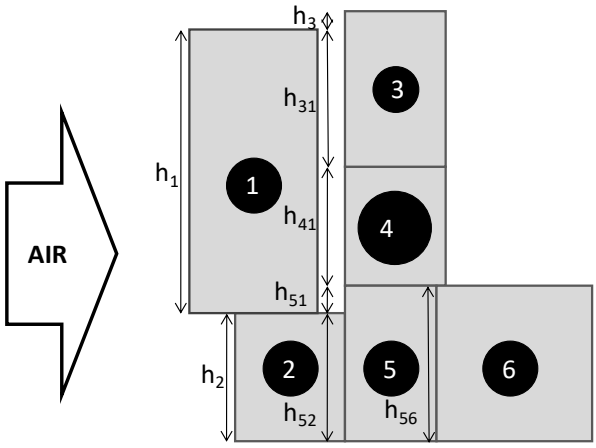

Figure 5-6: Schematic to explain air propagation through heat exchanger

5.6 Robust Wall Temperature and Heat Flux based Solution Scheme

For two-phase flow, empirical refrigerant side heat transfer correlations typically require heat flux as an input. In this case, the heat transfer coefficient is determined iteratively. This is especially important for CO_2 gas cooler. For CO_2 gas cooler, most supercritical HTC correlations need tube wall temperature as an input, thus the wall temperature needs to be guessed first. And many boiling HTC correlations

need heat flux as an input, thus heat flux needs to be guessed in that case. Under certain guess value, the iterations may diverge. In the model of Jiang *et al.* (2006), the successive substitution method is implemented to conduct those iterations. In the new model, golden section search (Kiefer (1953)) is implemented to iterate tube wall temperature and/or heat flux.

Table 5-1 shows a comparison between successive substitution and golden section search to model a CO_2 gas cooler with different supercritical HTC correlations. It can be observed that when CO_2 supercritical HTC correlations (Huai and Koyama (2007), Fang (1999), Pitla *et al.* (2002), Baskov *et al.* (1977)) are used, successive substitution fails to converge, however, Golden Section search can solve all cases. In Figure 5-7, the iteration process of one segment of this CO_2 gas cooler using Huai and Koyama (2007) is plotted. It shows that successive substitution oscillates erratically, while golden section search converges to the solution fast.

Table 5-1: Comparison between Successive Substitution and Golden Section Search to Model a CO_2 Gas Cooler with Different Supercritical HTC Correlations

CO_2 RVHTC Correlation	**Successive Substitution**	**Golden Section**
Yoon *et al.* (2003)	Converge	Converge
Son and Park (2006)	Converge	Converge
Huai and Koyama (2007)	Diverge	Converge
Fang (1999)	Diverge	Converge
Pitla *et al.* (2002)	Diverge	Converge
Baskov *et al.* (1977)	Diverge	Converge

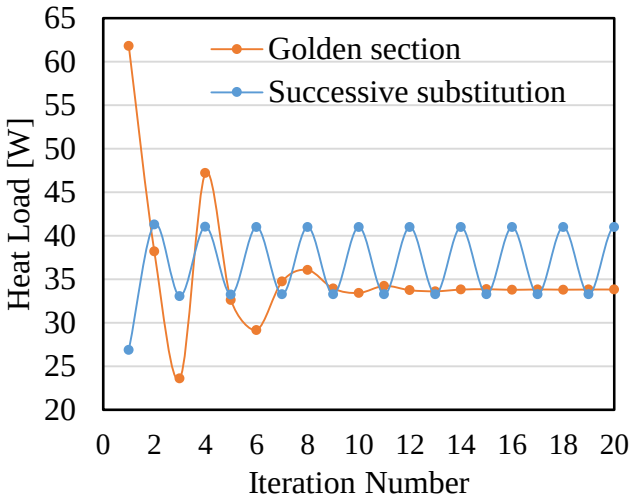

Figure 5-7: Iteration in 1 Segment of CO2 Gas Cooler

5.7 Pressure Drop Calculation

For each segment, the pressure drop consists of frictional, momentum and gravitational pressure drop as shown in Equation (5-2). The frictional refrigerant pressure drop calculation is based on empirical correlations. The momentum pressure drop as shown in Equation (5-3) and gravitational pressure drop as shown in Equation (5-4) are added as compared to Jiang *et al.* (2006)'s model. The pressure drop calculation is independent of heat transfer calculation. If the tubes are connected by headers, the prediction of frictional pressure drop in headers and expansion/contraction pressure drop between header and tubes are also based on empirical pressure drop correlations.

$$\Delta P = \Delta P_{friction} + \Delta P_{momentum} + \Delta P_{gravity} \tag{5-2}$$

$$\Delta P_{momentum} = \left(\frac{1}{\rho_{outlet}} - \frac{1}{\rho_{inlet}}\right) G^2 \tag{5-3}$$

$$\Delta P_{gravity} = \rho_{inlet} g h \tag{5-4}$$

Figure 5-8 demonstrates the new model's capability to account for momentum pressure drop. Five horizontally placed evaporators from industrial sponsors are modeled. As shown in Figure 5-8, the contribution of friction DP and momentum DP for the entire DP are normalized , it indicates that momentum DP is less than 10% of total DP which is consistent with the value in literature.

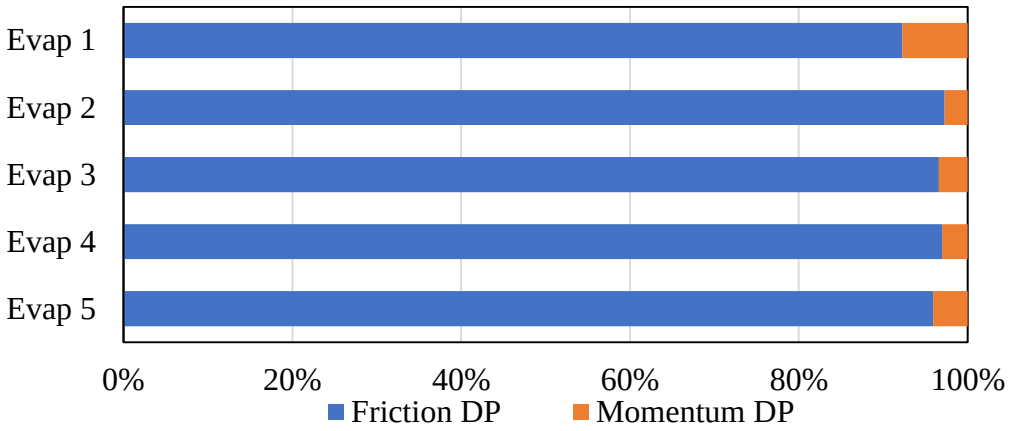

Figure 5-8: Pressure drop prediction for 5 sample evaporators

5.8 Correlation Smoothing with User-defined Boundaries

The approach demonstrated in this section allows one to smoothly join two discontinuous correlations at the transition region. Since heat exchanger models are usually integrated with data reduction tool, cycle simulation tool and optimization tool, which rely on derivative calculation. Therefore, making the model to have continuous and differentiable performance on the valid application range is crucial for these nonlinear solvers or optimizers to work properly.

5.8.1 Discontinuity in single phase correlation

The majority of HX operates in turbulent region, but it's not always the case. For example, a tube-fin heat exchanger is composed of multiple circuits, due to refrigerant maldistribution, different circuits will have different mass flow rate. Some

tubes may operate under laminar to transition regime. Figure 5-9 shows a case study for a 2mm tube, the water temperature is 67 ˚C. Since Dittus and Boelter (1985) and Gnielinski (1976) correlations are developed for turbulent regime, both of them have a sever discontinuity when trying to connect with the laminar flow HTC. One solution to avoid this issue is to use correlation developed for the entire flow regimes, the correlation presented in ARI (2001) is a smooth correlation which is continuous on the entire flow regimes as shown in Figure 5-9.

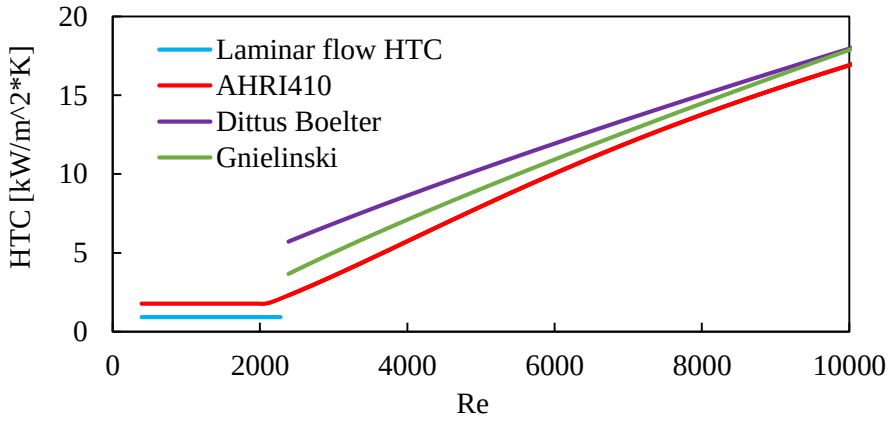

Figure 5-9: Continuities in Single Phase HTC Correlations

In addition to HTC correlation, single phase DP correlations also have discontinuity issue. As shown in Figure 5-10, Blasius (1907) correlation which is only valid for turbulent regime has a significant discontinuity with laminar friction factor. To solve this problem, the first option is to implement the Morrison (2013) correlation which is valid for the entire flow regime. The second option is to apply smoothing between laminar friction correlation and Blasius (1907) correlation. The correlation smoothing technique will be explained in detail in next session. As can be seen, both options show good smoothness at the transition flow regime.

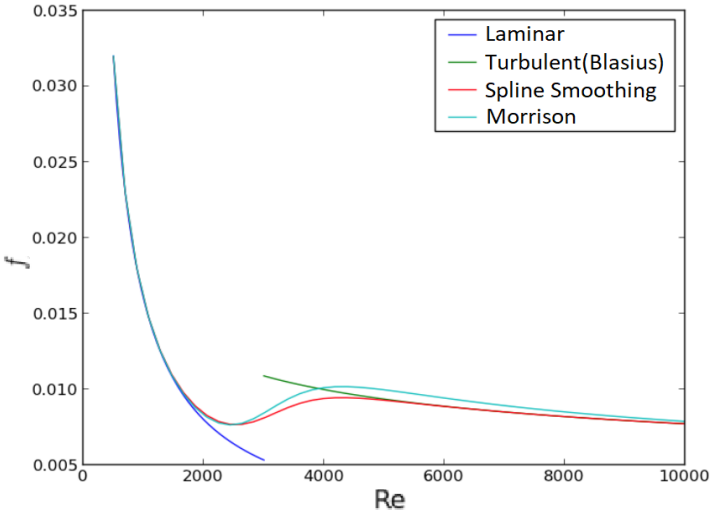

Figure 5-10: Discontinuities in Single Phase DP Correlations

5.8.2 Discontinuity in phase transition regions

The more common discontinuities happen in the correlations at phase transition points. For instance, for a 7.5mm tube, R410A at Tsat=40 ˚C, G=400 kg/m^{2}s, when adopting Churchill (1977) correlation for liquid and vapor phase DP calculation and Friedel (1979) correlation for two-phase DP calculation, the DP prediction is shown in Figure 5-11(a). Similar to the definition of quality in two-phase, the quality definition in single phase is shown in Equation (5-5).

$$Quality = \frac{h - h_l}{h_g - h_l} \tag{5-5}$$

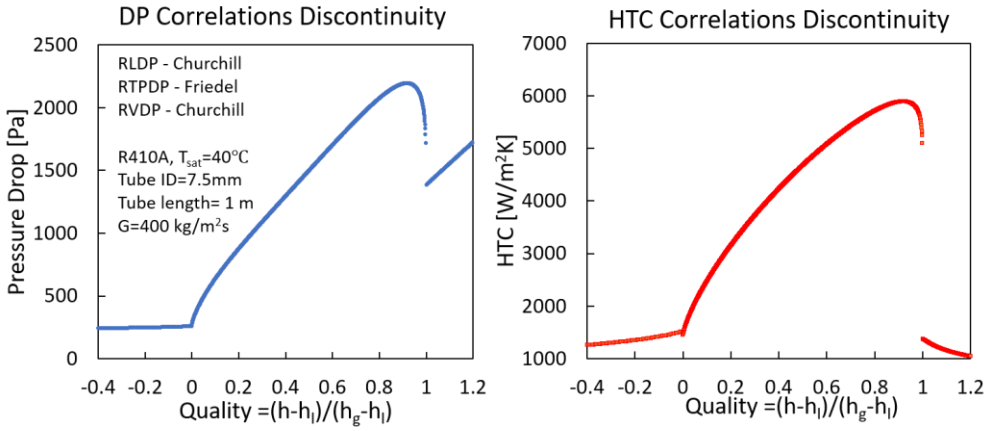

Figure 5-11: Discontinuities in Phase Transition Regions

As an example of HTC correlations, when adopting Gnielinski (1976) correlation for liquid and vapor phase prediction and Shah (2016) for two phase HTC prediction, two discontinuities appear at both phase transition points as shown in Figure 5-11(b).

In general, if there are two functions, $f_1(x)$ and $f_2(x)$, a formula such as $f(x)=(1-\sigma(x)) * f_1(x)+\sigma(x) * f_2(x)$ can be used to smoothly join them. If $\sigma(x)$ is in the form of linear function, it is called linear smoothing, if $\sigma(x)$ is in the form of exponential function, it is called exponential smoothing. Other form of $\sigma(x)$ could also be used, as long as the $\sigma(x)$ can smoothly transition from 0 to 1, or from 1 to 0.

It is worthwhile to explore what is the best smoothing technique in terms of minimizing number of extra correlation evaluation and minimizing number of extra property calls given acceptable prediction accuracy. Three different smoothing method are implemented and benchmarked. The first smoother is linear function, the 2^{nd} smoother is exponential function. The 3^{rd} smoothing is 3-order spline interpolation. The detailed development of spline interpolation is referred to Hall *et al.* (1976) for brevity. As can be seen from Table 5-2 and Figure 5-12, spline smoothing and exponential smoothing (which coincides with spline smoothing on Figure 5-12) show better performance than linear smoothing, because linear smoothing has very sharp turning points, which implies the derivatives at that point is not continuous. However, when testing the derivatives of the smoothened function, the function using spline smoothing is differentiable despite of the larger computational cost as shown in Table 5-2 compared to exponential smoothing. Exponential smoothing though looks continuous in Figure 5-12, it is actually not differentiable at transition points. Since the

discontinuities at phase transition points will cause non-convergence for nonlinear solver/optimizer, spline smoothing is adopted as the smoothing technique in the proposed heat exchanger model and will be used to conduct further analysis.

Table 5-2: Benchmark of Different Smoothing Techniques

Smoothing scheme	Number of extra correlation evaluation	Number of extra property calls
Linear smoothing	1	4 (single phase calls)
Exponential smoothing	1	4 (single phase calls)
Spline smoothing	5	36 (single and 2 phase calls)

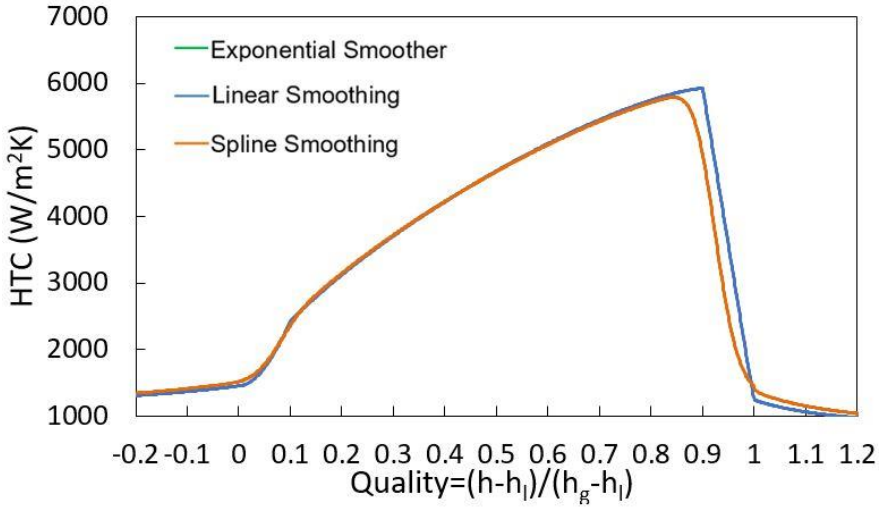

Figure 5-12: Benchmark of Different Smoothing Techniques

For system simulation tool, pressure, enthalpy and mass flow rate are the three variables passed between different components and get iterated by nonlinear solvers. In order to test the performance of correlation smoothing, an R410A outdoor unit from Alabdulkarem *et al.* (2015) is used, when regulating its refrigerant inlet pressure, enthalpy and mass flow rate, the derivative of the outlet enthalpy is observed. The continuity of outlet enthalpy by changing inlet mass flow rate is shown in Figure 5-13, the continuity of outlet enthalpy by changing inlet pressure is shown in Figure 5-14,

the continuity of outlet enthalpy by changing inlet enthalpy is shown in Figure 5-15. Observing 1st order derivatives in below plots, it is obvious that the 1st order derivative with correlation smoothing is continuous, however the model without correlation smoothing has discontinuities.

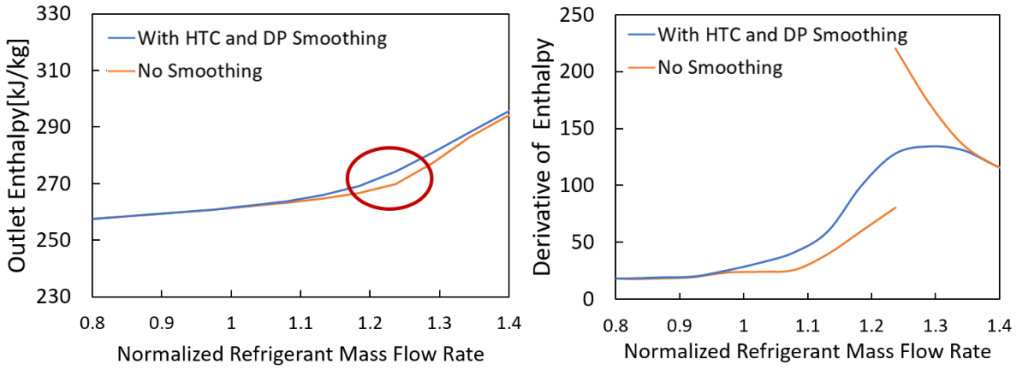

Figure 5-13: Continuity of Outlet Enthalpy Changing Inlet Mass Flow Rate

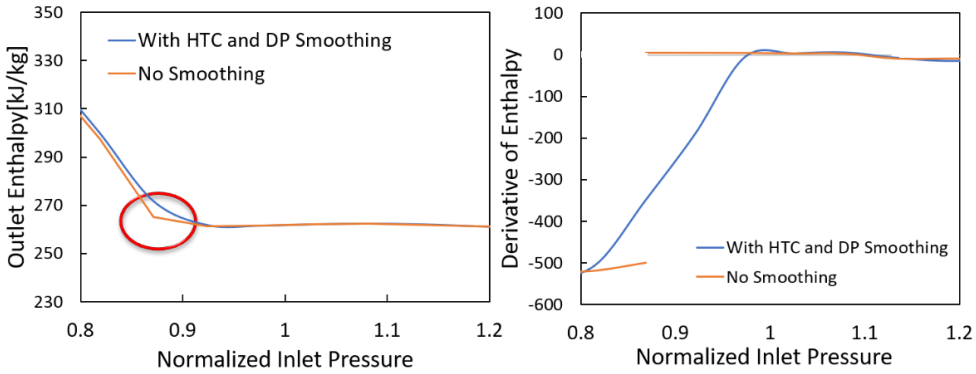

Figure 5-14: Continuity of Outlet Enthalpy Changing Inlet Pressure

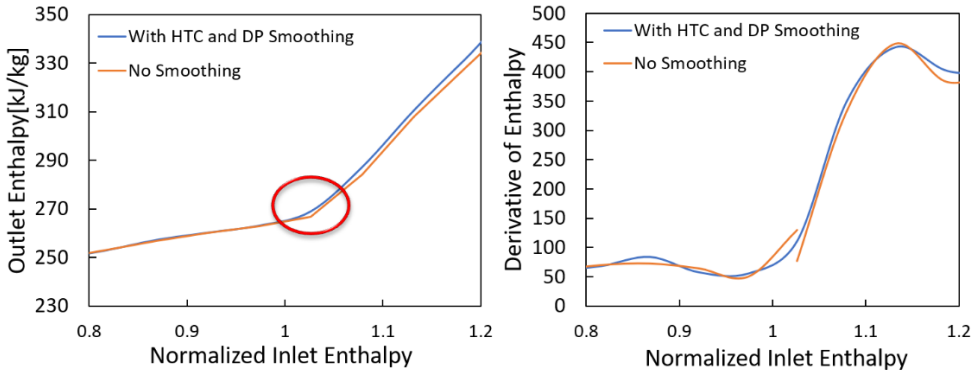

Figure 5-15: Continuity of Outlet Enthalpy Changing Inlet Enthalpy

5.8.3 Smoothing effect on simulation results

As the smoothing has been proven to facilitate nonlinear solver to converge, it is crucial to know its impact on simulation results. As shown in Figure 5-16, 1178 heat exchangers are simulated with and without correlation smoothing, the smoothers are applied for the quality range of $0<x<0.05$, $0.95<x<1.0$. In Figure 5-16(a), the heat exchanger capacity deviation is less than 1.0%. In Figure 5-16(b) Refrigerant DP relative deviation is less than 4.0%. This indicates that the smoothing's impact on prediction accuracy is acceptable.

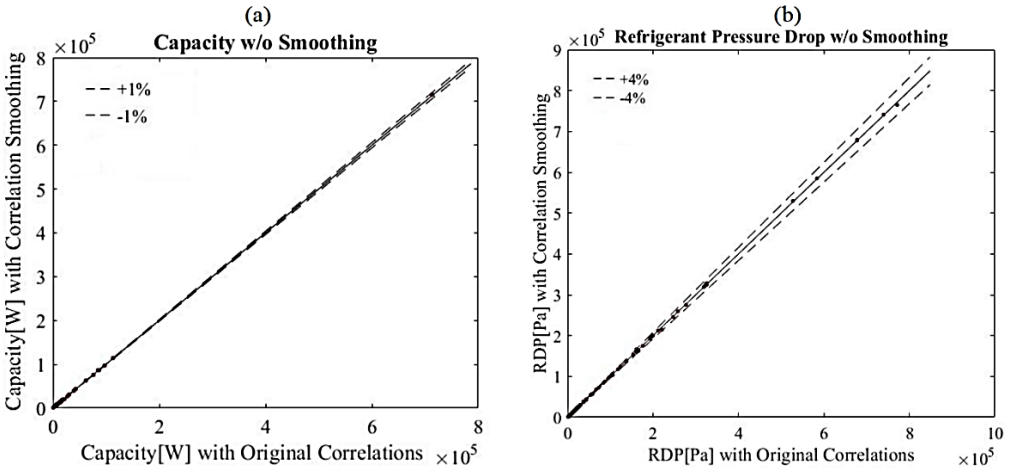

Figure 5-16: Correlation Smoothing Effect on Simulation Results

5.9 Modeling Validation

5.9.1 Conventional geometry tube-fin heat exchanger data

The proposed model is compared against Jiang *et al.* (2006)'s model. This is an important step in verifying the new model because Jiang *et al.* (2006)'s model has been widely validated against experimental data. For the purpose of verification, the proposed model is referred to as the unified tube-fin heat exchanger solver, in short 'UTFSolver'. First, a heat exchanger database is collected, 159,859 conventional tube-fin heat exchangers with different geometries are evaluated by both UTFSolver and

Jiang *et al.* (2006)'s model. This heat exchanger data base includes evaporators, condensers and gas coolers with various tube configurations. There are 22 working fluids used in these heat exchangers. Figure 5-17(a) shows the capacity comparison, Figure 5-17(b) shows the refrigerant DP comparison. It indicates that the new model can reproduce the results from Jiang *et al.* (2006)'s model within the difference of 0.1% in terms of capacity and pressure drop.

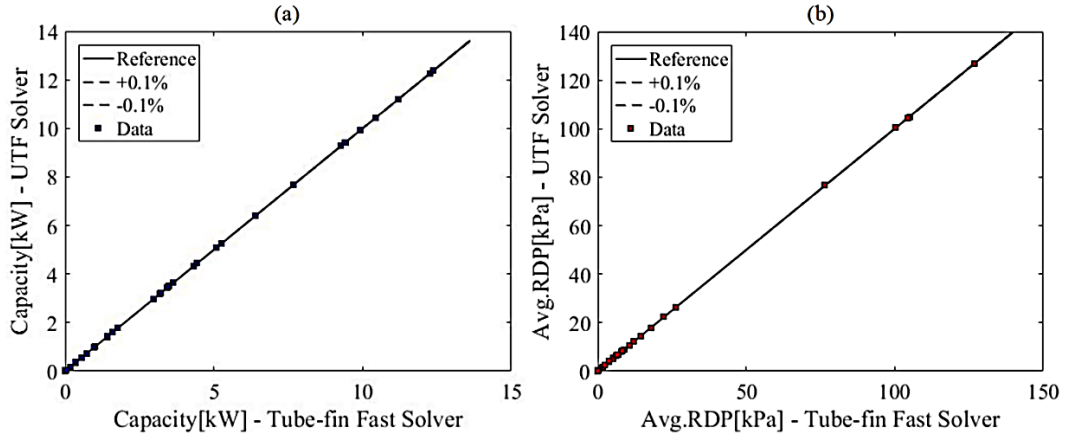

Figure 5-17: Verification of New Model against Jiang *et al.* (2006)'s Model

5.9.2 Variable geometry tube-fin heat exchanger data

One goal to develop the variable geometry tube-fin heat exchanger solver is to model the next generation heat exchanger as shown in Figure 5-18.

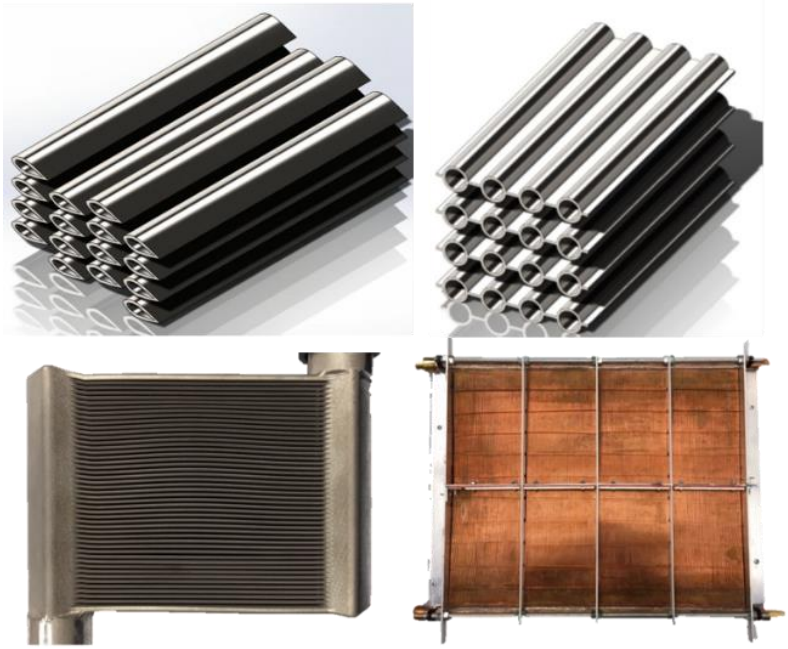

Figure 5-18: Illustration of Next Generation Heat Exchangers

In this regard, 10 next generation heat exchangers are simulated by the new model, the simulation results are compared with experiment data. The detailed geometries and operating conditions for these next generation heat exchangers are referred to Bacellar (2016) for brevity. Figure 5-19(a) shows the Cartesian grid for NTHX-001 generated by the variable geometry heat exchanger model, Figure 5-19(b) shows the capacity validation results, the maximum capacity deviation is below 0.1%.

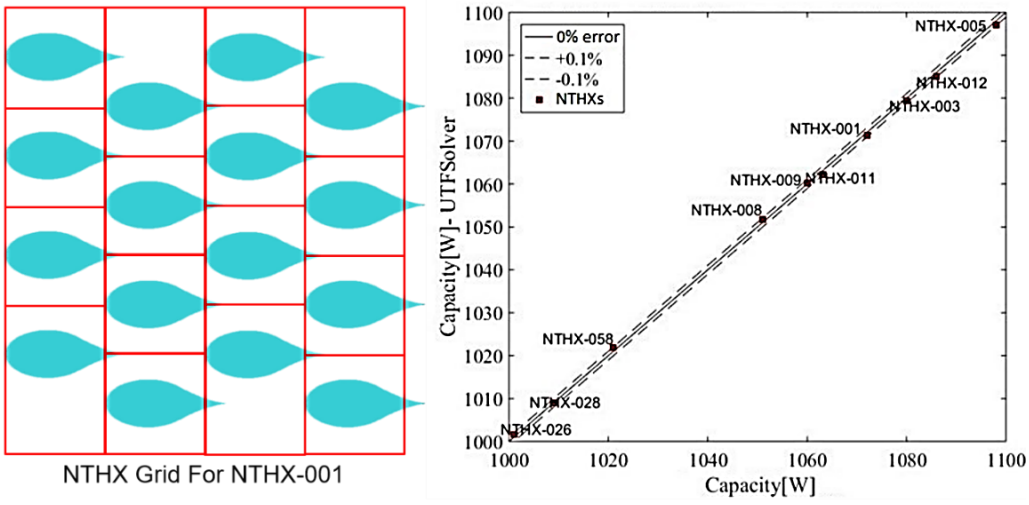

Figure 5-19: (a) Cartesian grid of NTHX-001; (b) Capacity validation for NTHXs

5.10 Summary

In this chapter, a new model for variable geometry tube-fin heat exchanger is developed. This model has the capability of accounting for variable geometric parameters, such as different tube sizes, topology optimized tube shapes, irregular tube layouts and irregular fin dimensions. To improve pressure drop prediction, air and refrigerant momentum and gravitational pressure drop are calculated in addition to friction pressure drop. The new model can simulate the next generation heat exchangers with U-bends or headers to connect tubes. A more robust tube wall temperature and heat flux based solution scheme is integrated in the new model and correlation smoothing with user-define boundaries is implemented to improve the numerical stability. The verification of the new model against existing heat exchanger model shows the new model can reproduce the results from existing model within 0.1% performance deviation. The validation of the new model against next generation heat exchanger test data demonstrates the capability of the new model to simulate next generation heat exchangers, and the deviation between test data and simulation results is within 0.1%.

6 A CFD ASSISTED HEAT EXCHANGER MODEL FOR SIMULATION OF AIR FLOW MAL-DISTRIBUTION FOR AIR-TO-REFRIGERANT HEAT EXCHANGER

6.1 CFD Model

In this chapter, a momentum resistance model is adopted to explore the influence of four geometric parameters (HX depth, HX height, HX apex angle, HX momentum resistance characteristics) and air flow rate on the air velocity distribution and its influence on the heat exchanger performance under dry surface condition are studied. A co-simulation approach integrating the HX model and CFD model is developed. The CFD model is developed using OpenFOAM®(Weller *et al.* (1998)).

In the CFD model, the heat exchanger is modeled using a momentum resistance model, i.e. so-called porous media model (Hooman and Gurgenci, 2010) in which the flow through complex heat exchanger mesh is assumed to depend only on the pressure drop characteristics. The Darcy-Forchheimer law for the momentum resistance model is used in the present work. The model is an extended form of the Darcy's law that accounts for the inertial loss in addition to the viscous loss. It has been commonly applied for flows within porous media where the Reynolds number is higher than 10. For a flow in porous media, the Reynolds number is defined as

$$\mathrm{Re} = \frac{\rho_f u_f L}{\mu_f} \tag{6-1}$$

where ρ_f, μ_f and u_f are the density, dynamic viscosity and specific discharge rate of the fluid, respectively. The characteristic length, L is typically defined as the average grain diameter or pore dimension. The momentum resistance, S_i appears as a source term in the momentum conservation equation as

$$\frac{\partial}{\partial t}(\rho) + \frac{\partial}{\partial x_i}(\rho u_i) = 0 \tag{6-2}$$

$$\frac{\partial}{\partial t}(\gamma \rho u_i) + u_j \frac{\partial}{\partial x_j}(\rho u_i) = -\frac{\partial \rho}{\partial x_i} + \mu \frac{\partial \tau_{ij}}{\partial x_i} + S_i \tag{6-3}$$

$$S_i = -(\mu D_{ij} + \frac{1}{2}\rho \,|\, u_{kk} \,|\, F_{ij}) u_j \tag{6-4}$$

where second order tensors, D_{ij} and F_{ij} are the inverse of permeability and the form drag coefficient (or inertial permeability), respectively. Assuming homogeneous porous medium, the coefficients can be written as scalar matrices, DI_3 and FI_3, where I_3 is the identity matrix of size 3. This is applicable for 2D simulation where the fin surfaces are parallel to the computational domain. The coefficients are derived from the solutions of the pressure drop using the empirical correlations as shown in Table 6-1. The CFD assisted segmented HX model takes the coil specifications and operating conditions as inputs and an appropriate air side pressure drop correlation with valid parameter ranges is chosen. Then the pressure drop values are calculated for a range of velocities that well covers the possible velocity variation within the coil. From this, we can obtain the characteristic momentum resistance coefficients, D and F by building a quadratic function of pressure vs inlet velocity. Thus, the integrated solver makes sure that the correlations are not used outside their proposed range.

Table 6-1: Air Side Pressure Drop Correlations Used in Current Study

Fin types	References
Bare tube	Žukauskas (1972)
Plate fin	Wang and Chi (2000)
Louver fin	Wang *et al.* (1999)
Wavy-louver fin	Wang *et al.* (1998)
Slit fin	Wang *et al.* (2001)

In the proposed approach, the permeability is not directly a function of porosity as in Bejan and Morega (1993) but rather lumped into one value. Also, the porosity in the momentum equation appears only in the time derivative term in the OpenFOAM porous media model. In other words, velocities in all other terms represents superficial velocities, not the true velocity, γu_i i.e., within the porous zone.

The k-omega SST model (Menter (1994)) is used for the turbulence closure. The choice was made for two reasons. First, the k-omega SST model is expected to perform better when there are separation of flow and adverse pressure gradient (Menter *et al.* (2003)) due to the walls introduced by the heat exchanger frame. Second, we observed that the available wall function model for the k-epsilon model in OpenFOAM results in insufficient grid resolution near the high flow curvature region due to its limitation to meet the Y plus value requirement.

The continuity and momentum equations are solved using the SIMPLE scheme (Patankar and Spalding (1974)). The convective terms for the momentum and the turbulence transport equations are discretized using 2nd order upwind scheme while the diffusive terms and the gradients are 2nd order central difference schemes. The explicit non-orthogonal correction scheme is applied to maintain overall second-order accuracy of the diffusive terms.

The computational cost is minimized by assuming a 2-D domain that neglects the tube length direction and is symmetric along the center of the duct with only one of the A-type heat exchanger slab, as shown in Figure 6-1. This is also justified with the observation that the air mal-distribution is predominantly one-dimensional, perpendicular to the coil tubes (Chwalowski *et al.* (1989)). The heat exchanger region

is defined as a block domain where the momentum loss source term applies. The constant velocity and pressure boundary conditions are assigned at the duct inlet and outlet, respectively. The wall boundary conditions are assigned at the apex and bottom of the heat exchanger. The total number of grid cells ranged from 10,000-30,000 for the medium grid resolutions.

Since the integrated solver pursues automated solution procedure for all design cases, there are additional difficulties in determining convergence of the CFD solution. Particularly, when some solutions fail to reach a steady state solution due to turbulence or vortex shedding, the residuals can remain stagnating or oscillating above given convergence criterions. We implemented a local convergence criteria on the velocity and pressure profile in heat exchanger domain to facilitate determination of such cases. The local convergence criteria have been implemented to observe the convergence of numerical solution within the HX area locally since that is what we are mostly concerned of. This was applied after a sufficient number of iterations, it still has difficulty in converging due to oscillatory flow behaviors such as vortex shedding at the rear of the HX apex.

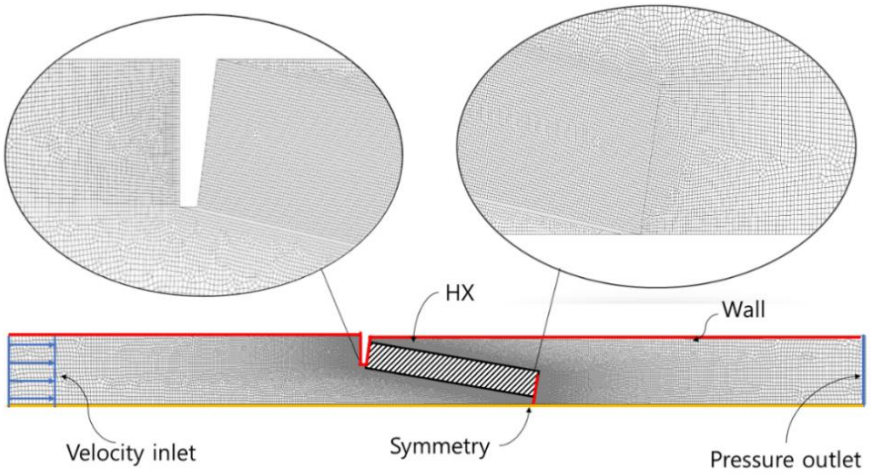

Figure 6-1: Computational Domain and Mesh of the A-Type Heat Exchanger

6.2 Segmented Heat Exchanger and CFD Model Co-simulation

The segmented HX model is the unified tube-fin heat exchanger model as described in Chapter 5. As an overview, the proposed co-simulation approach solves for the air-side velocity profile using OpenFOAM® while the refrigerant side hydraulic equation and energy balance between the refrigerant and the air flow are solved using an epsilon-NTU based segmented HX model. Figure 6-2 shows the flowchart of the approach. In the integrated model, the geometric configurations and the boundary conditions for the CFD solver is provided by the heat transfer model through an input file. These inputs are indicated in Figure 6-3. The input file includes: total air flow rate ($\dot{m}$), heat exchanger depth (D_{HX}), heat exchanger height (H_{HX}), heat exchanger apex angel (θ_{HX}) and momentum resistance characteristic coefficients (D, F) of the heat exchanger fin-and-tube geometry. Based on the inputs, a set of script files and case folders are created to run the CFD solver. After that, the mesh for duct and heat exchanger is created using an open-source meshing tool, Gmsh (Geuzaine and Remacle (2009)). For each case, three sets of meshes with different grid resolutions are created to confirm the grid convergence using the grid convergence index (GCI) value. Appropriate mesh conversion and setup tools are executed prior to running the CFD solver. Once the solver reaches the desired convergence criteria, the normalized heat exchanger face velocity profile is passed on to the segmented HX model to continue with the remaining air-side and refrigerant-side heat transfer and pressure drop calculations. This approach results in a fully automated process within a unified run environment. To this end, the OpenFOAM solver and the segmented HX model are integrated under Windows platform by means of cross-compilation technique (Lee *et*

al. 2018). This reduces the complexity as well as required computational resources by eliminating the use of virtual operating environments.

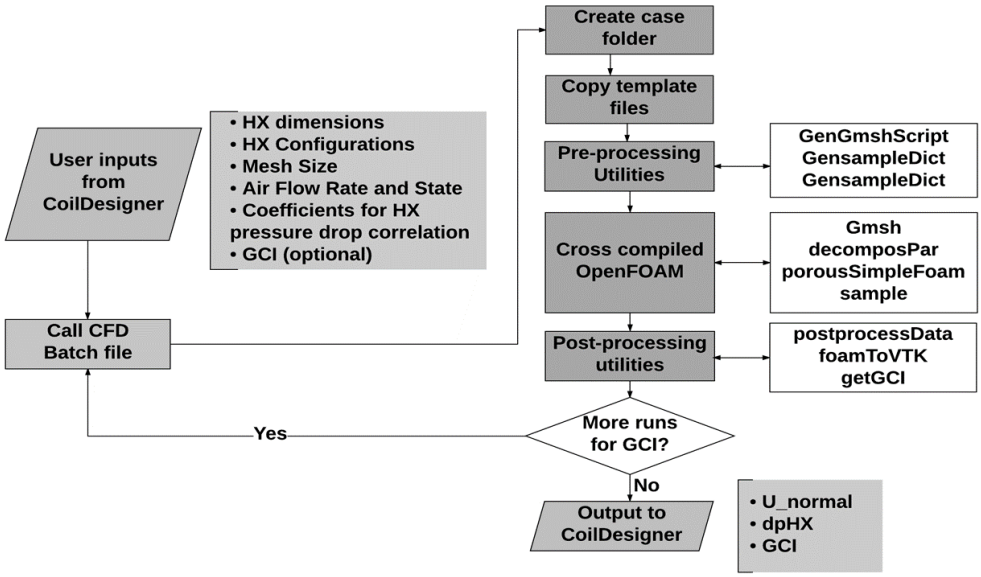

Figure 6-2: Detailed Approach for Integrated CFD Solver with Heat Transfer Model

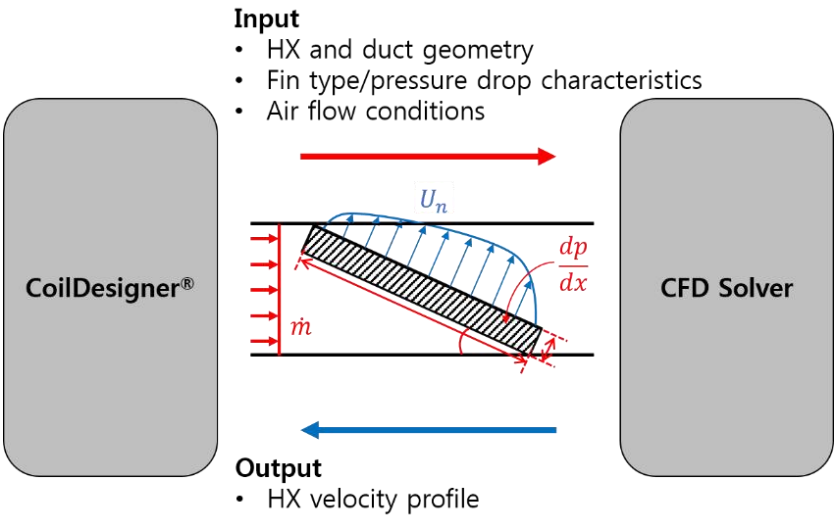

Figure 6-3: Concept for Integrated CFD - HX Model

6.3 Effect of Different Parameters on Air Flow Maldistribution

Parametric studies are performed to investigate the effect of various geometrical parameters and air mass flow rate. The air side correlations and heat exchanger geometry specifications are listed in Table 6-2. They also serve as a verification of the

overall robustness of the integrated model over a wide range of heat exchanger configurations. Furthermore, the applicability of velocity profile scaling based on the sensitivity and similarity of the velocity profiles with respect to each variable is discussed. This is done by translating, scaling and rotating one velocity profile to another case, which is referred as scaling. This is important because the computational cost of a CFD simulation with the momentum resistance model simplification is still two or three orders of magnitude larger than that of the segmented HX model. A typical multivariate multi-objective optimization requires solving for thousands of cases and it is impractical to run CFD simulations for all of them.

Table 6-2 shows the list of variables considered in the parametric study: half apex angle of the heat exchanger, heat exchanger coil depth, heat exchanger coil height, air flow rate (air velocity normal to the coil surface) and different fin types. Again, the pressure drop correlations used to define the momentum resistance characteristic coefficients in

Table 6-3. The baseline value for the velocity was taken as that of the validation case while other parameters were set as the middle values of the parametric study ranges. For each variable in Table 6-2, five sampling points were taken at evenly spaced interval within the parameter range and simulated while other variables were fixed at the baseline value. Note that the heat exchanger depth is usually a discrete parameter, but we can consider any value in the range since the current study assumes a homogenous porous media for a fin-and-tube heat exchanger.

Table 6-2: Variables for Parametric Study

Parameters	Min	Max	Baseline
Half apex angle	10°	40°	25°
HX coil depth	0.052 m	0.104 m	0.078 m
HX coil height	0.317 m	0.736 m	0.527 m
Air velocity	0.75 m/s	4 m/s	2.375 m/s

Table 6-3: Different Fin Types and Momentum Resistance Coefficients for Parametric Study

Fin types	F ($1/m^2$)	D (1/m)
Plate fin	88.8	7546115
Louver fin	199.0	13750699
Bare tube	77.6	1263276
Wavy louver fin	214.0	8775852
Slit fin	108.0	7713807

In fact, it is important to clarify the precise argument of the case studies. In the case studies, the momentum resistance coefficients were derived at the baseline conditions for each fin types using the air side pressure drop correlations in Table 6-1 and we assume that the coils have the homogenous and isotropic momentum resistance coefficients as given in Table 4. Strictly speaking, it cannot be claimed that the parametric study results reflect a specific coil configuration (such as tube pitches, tube diameter, number of tube banks, etc.) because each pressure drop correlation is limited by its validated geometric ranges. Again, this concerns the case studies and the integrated CFD-HX model solver procedure obeys the valid correlation ranges. The grid convergence study shows that the GCI values are below 5% for all simulated cases.

Figure 6-4 shows the effect of heat exchanger apex angle variation on the velocity profile. It can be seen that the velocity profile varies significantly as the apex angle changes. The angle of the brackets at the bottom of the heat exchanger directly reflects the size of recirculating, low velocity region. The lost air flow rate is concentrated near the upper part of the heat exchanger. As expected, the smaller the angle, the larger the velocity mal-distribution and the velocity profile seems to pivot around the center of the heat exchanger. The error in using velocity scaling for changing variables is measured using L2 error norm. Thus, the maximum relative L2 error norm is defined as the error by scaling the velocity profile either from the lower bound case to the upper bound case or the other way around, whichever is higher. The maximum relative L2 error norm is 61.7% for the entire heat exchanger height range ($0 < H_{HX} < 1$) and 39.1% for the middle 80% section ($0.1 < H_{HX} < 0.9$). In general, the size and behavior of the vortices behind the bottom bracket are hard to anticipate and the validity of simply applying rotated the velocity profile to different heat exchanger angles is unknown. Thus, it is apparent that when the angle is changed, a new CFD simulation is needed in order to obtain accurate velocity profile.

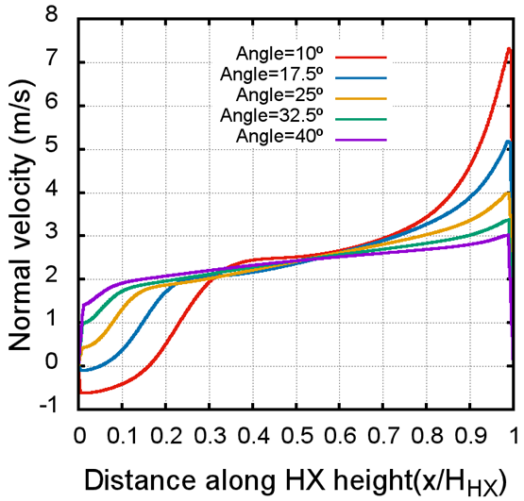

Figure 6-4: Effect of Heat Exchanger Apex Angle on the Velocity Profile

In Figure 6-5 and Figure 6-6, the effects of heat exchanger depth and height are shown, respectively. It is observed that the velocity profiles are quite close to each other within the variable range. In fact, most of the deviations are limited to the wall boundaries. As the height increases, the relative length of the bracket decreases and thus the low velocity region decreases. As the depth increases, the velocity distribution tends to become more uniform due to the dampening effect of momentum resistance model. Also, the wall boundary layer thickness seems insensitive to the heat exchanger depth although the free stream velocity right outside the boundary layer differs significantly. This maximum error norm for varying the heat exchanger depth is 11.3% for the entire heat exchanger height range ($0 < H_{HX} < 1$) whereas for the middle 80% section of the heat exchanger height ($0.1 < H_{HX} < 0.9$) is 5.7%. For varying the heat exchanger height, the maximum L2 error norm is 7.3% for the entire heat exchanger height range ($0 < H_{HX} < 1$) and 5.8% for the middle 80% section ($0.1 < H_{HX} < 0.9$). It indicates the velocity scaling is applicable in these cases.

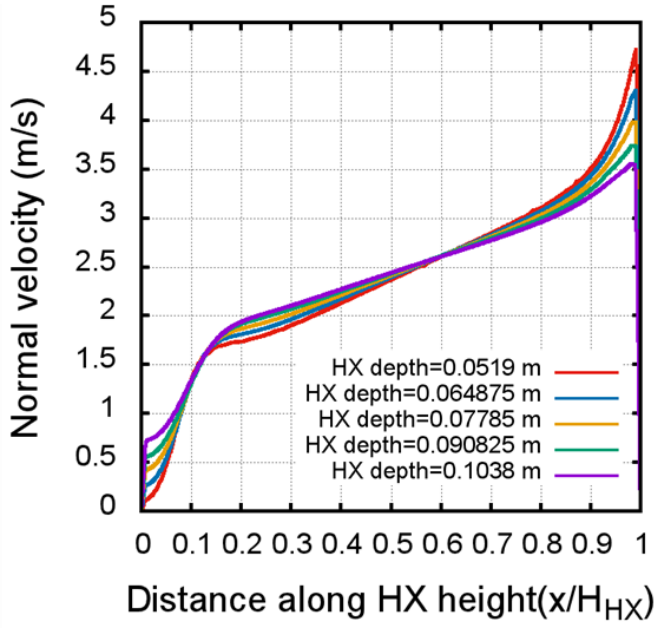

Figure 6-5: Effect of Heat Exchanger Depth on the Velocity Profile

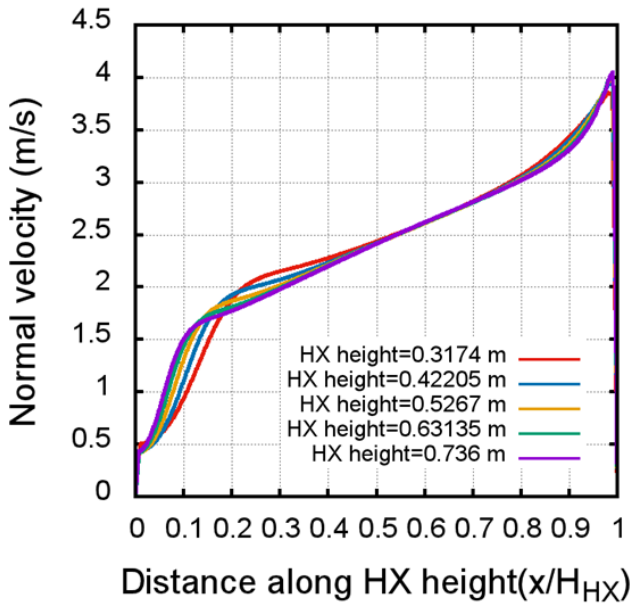

Figure 6-6: Effect of Heat Exchanger Height on the Velocity Profile

The results for varying air flow rates are shown in Figure 6-7. In this figure, the CFD results for each air flow rate are shown in solid line and the discrete markers represents the velocity profile scaled from baseline case (yellow line). We can see that each scaled velocity profiles matches very well with the CFD results for other variable air flow rates. The maximum relative L2 error norm (scaling lowest air flow rate to highest air flow rate) is 13.6 % for the entire heat exchanger height range ($0 < H_{HX} < 1$) and 6% for the middle 80% section ($0.1 < H_{HX} < 0.9$).

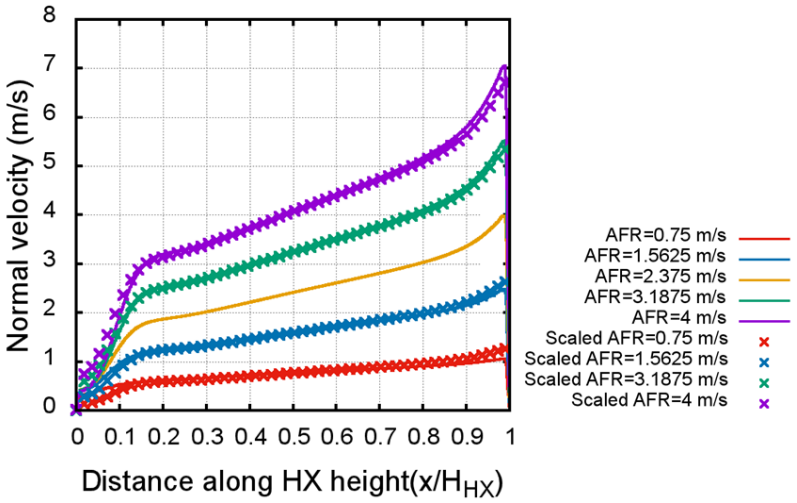

Figure 6-7: Effect of Mass Flow Rate on the Velocity Profile

Lastly, Figure 6-8 shows the effect of different fin types. It can be seen that different fin types (i.e. momentum resistance coefficients) can have substantial effect on the velocity distribution, because of that we don't recommend velocity scaling between different fin geometries. The maximum relative L2 error norm is 22.6% for the entire heat exchanger height range ($0 < H_{HX} < 1$) and 10.4% for the middle 80% section ($0.1 < H_{HX} < 0.9$). Overall, the larger the minimum free flow area per unit volume of a heat exchanger (lower momentum resistance coefficients), the higher the velocity mal-distribution. This is in accord with the previous observation of the dampening effect using momentum resistance model. It is unclear from these cases what the influence of each momentum resistance coefficients, D and F is, but a simple scale analysis for the plate fin case is performed. It is found that both the viscous and inertial terms are in the same order of magnitude. It can also be expected that as the fin geometry becomes coarser, the simplified model is more likely to suffer more from accuracy as the homogeneous assumption become poorer. Thus, investigation on the limit of accuracy for low resistance coefficients will be useful in future study.

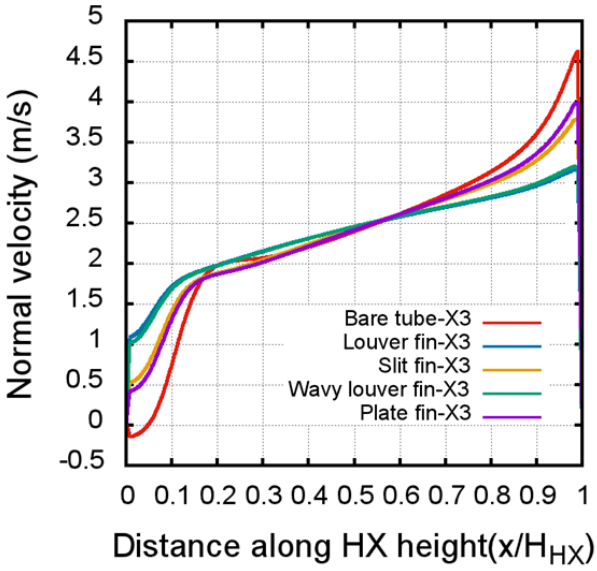

Figure 6-8: Effect of Fin Types on the Velocity Profile

6.4 Effect of Air Maldistribution on Heat Exchanger Performance

In order to demonstrate the effect of air velocity mal-distribution on heat exchanger performance, a R410A condenser by Wang *et al.* (2009) is simulated for a case study. This study uses a heat exchanger model which can calculate refrigerant mass flow mal-distribution in each circuit by equalizing the outlet pressure at merging points, i.e. the outlet pressure in each circuit. For the heat exchanger performance prediction, the inputs are air and refrigerant inlet conditions. The outputs are the heat exchanger performance including capacity, air and refrigerant pressure drop, fluids outlet conditions and refrigerant mass flow rate distribution in each circuit. Table 6-4 shows the refrigerant side heat transfer correlations adopted to simulate this condenser and the air side pressure drop correlations are same as the ones in Table 6-1. Considering the flow and circuit symmetry, only the upper slab is simulated. Table 6-5 shows the inputs for the heat exchanger test conditions and the coil specifications. Table 6-5 only shows the common parameters used in all cases, because the fin type, coil depth, coil height, apex angle and air velocity are the variables changing in the parametric study. The baseline for the variable parameters are the mid-range values of each parameters being investigated. The schematic of heat exchanger simulated is shown in Figure 6-9.

Table 6-4: Refrigerant (R410A) Side Heat Transfer and Pressure Drop Correlations Used for Performance Study

Correlations	References
Single-phase heat transfer	Dittus and Boelter (1985)
Two-phase heat transfer	Shah (2016)
Single-phase pressure drop	Blasius (1907)
Two-phase pressure drop	Xu and Fang (2013)

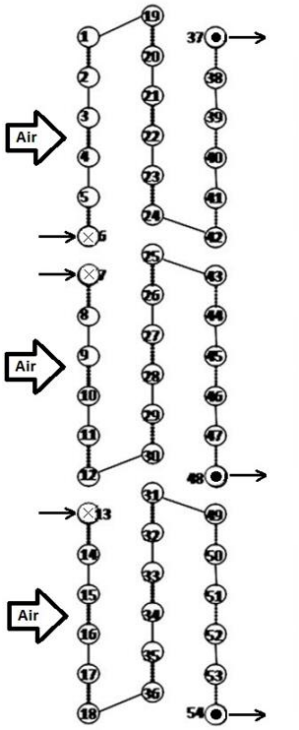

Figure 6-9: Upper Slab of A-coil Used in Simulation

Table 6-5: Heat Exchanger Specifications and Test Conditions for Performance Study

Parameters	Value	Parameters	Value
Tube configuration	Staggered	Air dry bulb [°C] Air wet bulb [°C]	25
Number of tubes per bank	18	Average air velocity [m/s]	0.078
Number of tube banks	3	R410A inlet saturation temperature [°C]	45
Tube OD (mm)	10.5	R410A inlet superheat [K]	20
Tube thickness (mm)	0.55	R410A mass flow rate (1 slab) [g/s]	23.0
Tube vertical spacing (mm)	26.416		
Tube horizontal spacing (mm)	20.32		
Tube length (m)	0.46		

Similar to the parametric studies in previous part, five parameters (fin type, coil depth, coil height, half apex angle and different air velocities) are varied to generate 25 velocity profiles and those profiles are applied to the air side of heat exchangers to see their impact on HX performance. Figure 6-11, Figure 6-12, Figure 6-13 and Figure 6-14 show capacity degradation induced by air flow mal-distribution compared to the uniform air flow distribution case with the same air volume flow rate.

Figure 6-10 shows the effect of fin types. The mal-distribution effect is more severe for bare tube and plate fin than the other 3 fin types where the momentum resistance coefficients are large. Physically, the larger resistance in the fin-tube geometry leads to larger lateral transfer of stream-wise momentum in the coil and tends to damp out the recirculation regions and the overall mal-distribution. The maximum capacity loss observed is 9.75% from bare tube heat exchanger. Figure 6-11 shows the effect of coil depth, it shows that capacity loss decreases with the increase of coil depth, i.e. thick coil can reduce mal-distribution effect. Figure 6-12 shows capacity degradation decreases with increase of coil height, i.e. longer coil height is preferable to have less capacity loss. Figure 6-13 indicates how the heat exchanger performed with different apex angle. As expected from the air flow mal-distribution profile, the apex angle produces the most significant performance degradation. The maximum degradation observed in this case study is 23.54% at 10° apex angle. Figure 6-14 explores the effect of air velocity and it indicates larger air velocity will induce more capacity degradation.

In addition, the air flow mal-distribution also causes refrigerant flow mal-distribution in each circuit. Figure 6-15 illustrates the refrigerant flow mal-distribution

at different apex angle. It is observed that small apex angle can produce severe variation of refrigerant circuit mass flow rate. Comparing Figure 6-13 and Figure 6-15, it can be drawn that capacity degradation also attributes to refrigerant flow mal-distribution. The more severe refrigerant mal-distribution, the larger capacity loss.

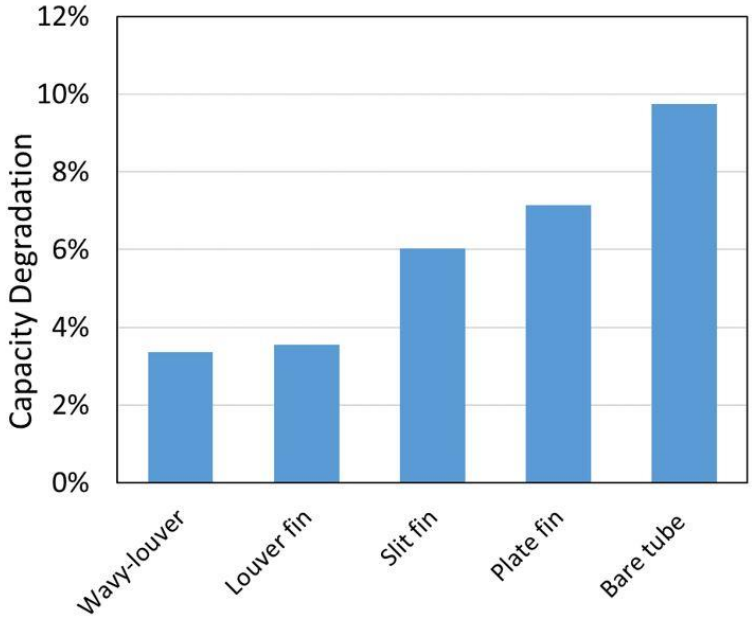

Figure 6-10: Effect of Fin Type on Heat Exchanger Capacity Degradation

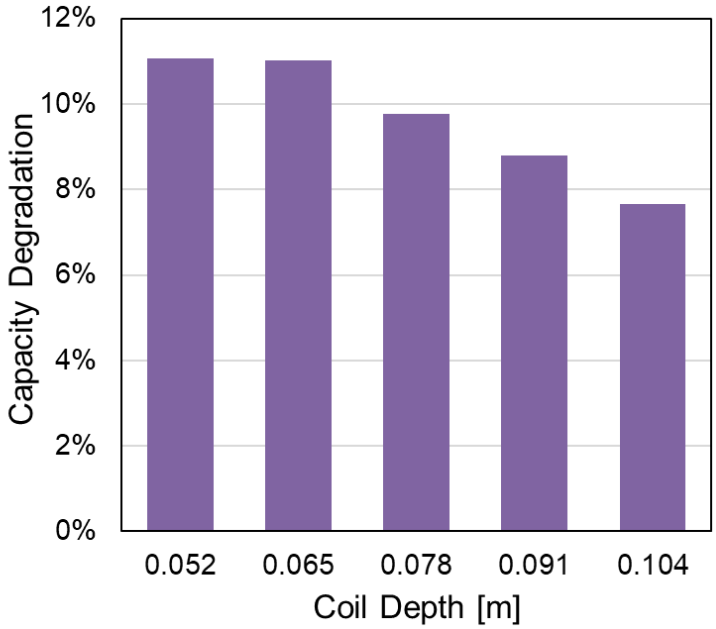

Figure 6-11: Effect of Coil Depth on Heat Exchanger Capacity Degradation

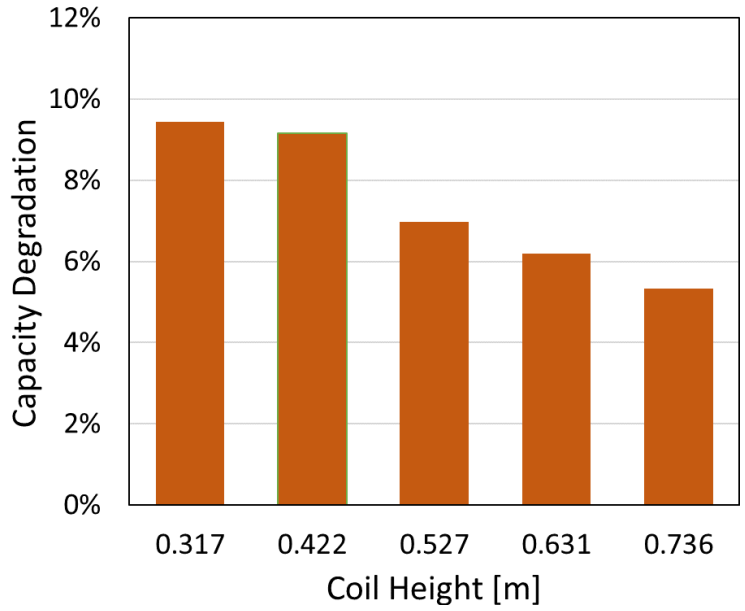

Figure 6-12: Effect of Coil Height on Heat Exchanger Capacity Degradation

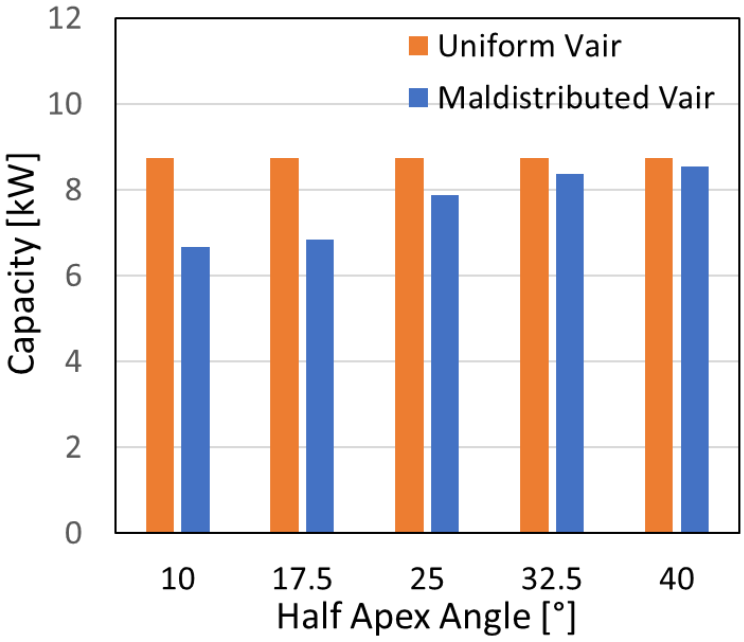

Figure 6-13: Effect of Apex Angle on Heat Exchanger Capacity Degradation

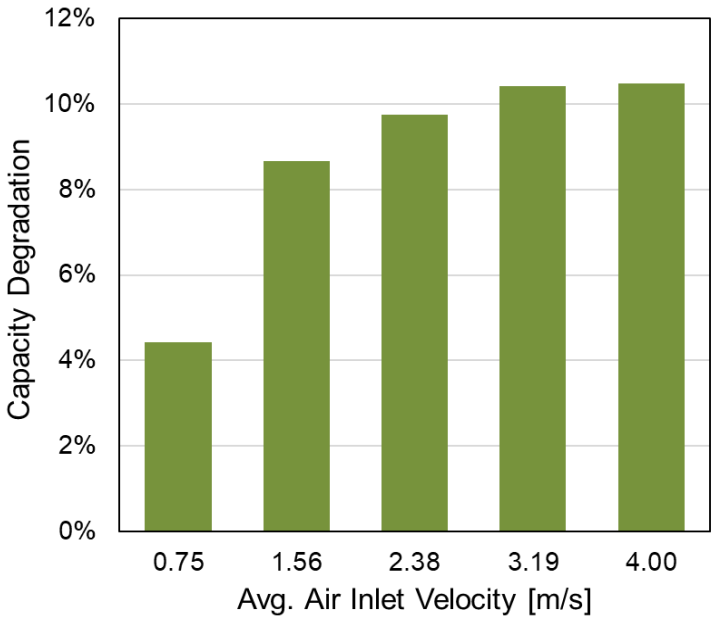

Figure 6-14: Effect of Air Velocity on Heat Exchanger Capacity Degradation

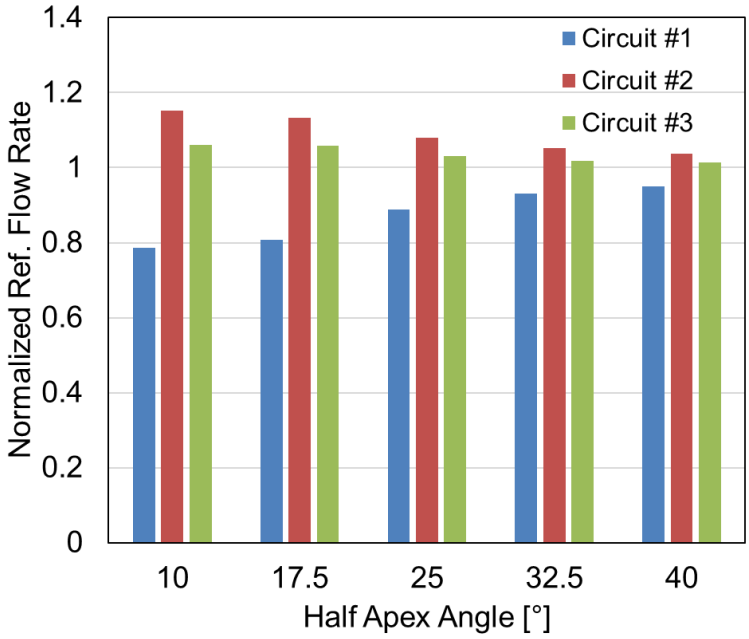

Figure 6-15: Refrigerant Flow Mal-distribution at Different Apex Angle

6.5 Summary

A CFD and heat exchanger co-simulation approach is developed to improve the HX performance prediction by capturing the air velocity mal-distribution at coil face. The CFD simulation process is fully automated using script based open-source CFD

code. Parametric studies have been performed to investigate the effect of HX angle, HX depth, HX height, air flow rate and the different fin types on the velocity profile. The result shows that the HX angle has the most significant influence on the velocity distribution and HX depth, HX height and air flow rate are most insensitive. The momentum resistance coefficients have shown to affect substantial variation in the velocity profile as well. The results show that scaling air velocity profiles by varying heat exchanger height, depth and air flow rate is applicable, however the velocity distribution profile with different apex angle is not scalable.

7 LIST OF MAJOR CONTRIBUTIONS AND FUTURE WORK

7.1 Contributions Resulting from This Research

7.1.1 Tube-fin heat exchanger circuitry optimization using Integer Permutation based Genetic Algorithm

In Chapter 2, a novel Integer Permutation based Genetic Algorithm (IPGA) for optimizing circuitry with manufacturability and operating constraints is developed. The novel genetic operators are designed such that all chromosomes generated by IPGA can be mapped to a valid circuitry. As a result, the proposed algorithm can explore the solution space more efficiently than conventional GA. A constraint-dominated sorting technique is used in the fitness assignment stage to handle manufacturability constraints. An exhaustive search on a small heat exchanger proves IPGA can find optimal or near-optimal circuitries using relatively small population size and low number of iterations. Overall, a 2.4-14.6% increase in heat exchange capacity compared to the baseline circuitry design is observed by applying IPGA to an A-shaped indoor unit. At the end of Chapter 2, comparison with other optimization methods in literature shows that IPGA finds better designs exhibiting higher capacity, less pressure drop and better manufacturability.

7.1.2 Tube-fin heat exchanger circuitry optimization problem formulation for improved performance under multiple air velocity profiles

Since air-to-refrigerant heat exchangers are typically confined in packaged units along with a fan, the airflow distribution on the face of the HXs is a dominant factor influencing its performance. This poses a design challenge as heat exchangers are typically designed by assuming a uniform airflow rate or a single known airflow distribution profile. For each airflow profile, a typical circuitry optimization algorithm can generate a completely different optimal refrigerant circuitry. Therefore, a circuitry

design that can guarantee an acceptable minimum performance under various airflow distributions is required. Section 3.1 presents three new circuitry optimization problem formulations. The objective values are obtained by assessing the heat exchanger performance under a limited number of operating conditions (i.e. several typical airflow distribution profiles obtained from experimental measurements). The Integer Permutation based Genetic Algorithm developed in Chapter 2 is used to obtain the optimal circuitry. In addition to this problem formulation with the goal of maximizing the worst case capacity, another two problem formulations (one with the objective to maximize the average capacity and the other with the objective to minimize the standard deviation of capacities) are also examined. The comparison between the optimal circuitries obtained from the new problem formulations and the optimal circuitry from single optimization under uniform airflow distribution shows that the optimal circuitry designs from new problem formulations are more resilient to multiple airflow maldistribution profiles. At the end of Section 3.1, it is demonstrated that, by implementing the new problem formulations on an A-type indoor unit in a real vapor compression cycle, the optimal circuitry design can improve evaporator cooling capacity by 5.1% compared to the baseline and system COP by 4.8% compared to the vapor compression cycle using the baseline heat exchanger as its evaporator.

7.1.3 Tube-fin heat exchanger circuitry optimization problem formulation for improved performance under frosting conditions

Frost accumulation on tube-fin heat exchanger leads to reduction in evaporator capacity and deteriorates cycle efficiency. The conventional counter-flow heat exchanger circuitry has the disadvantage that more frost tends to accumulate in the first few banks exposed to the incoming air. This frost concentration makes the air side flow

resistance increase rapidly, thus reduces the air flow rate and evaporator capacity under constant fan power. In Section 3.2, IPGA is used with a new problem formulation to obtain optimal circuitry under frosting conditions. A dynamic HX model with the capability to account for non-uniform frost growth on a fan-supplied coil is used to assess the performance of optimal circuitry. The new problem formulation yields better circuitry designs with larger HX capacity, more uniform frost distribution, less air flow path blockage, and therefore longer evaporator operation time between defrost operations.

7.1.4 Tube-fin heat exchanger circuitry optimization problem formulation for heat exchangers used as condensers and evaporators in heat pump applications

The previous circuitry optimization studies reported in literature have been performed on heat exchangers under a specific operating condition, either working as a condenser or an evaporator. However, an optimal circuitry obtained under the Air Conditioning (AC) mode cannot guarantee optimal performance if it is used in the Heat Pump (HP) mode. This necessitates a new optimization problem formulation whose optimal designs offer optimal performance in both AC and HP modes. Section 3.3 implements a bi-objective problem formulation. The comparison between the bi-objective optimal design and the single objective optimal design solely optimized under air-conditioning mode shows that the bi-objective optimal design is more resilient to variations in the operating conditions. As a result, the cooling capacity of the bi-objective optimal increases by 2.0% compared to the baseline circuitry when the heat exchanger works under air-conditioning mode, while the heating capacity of the same coil increases by 2.2% when it works as a condenser under heat pump mode. In contrast, the capacity of the single objective optimal design obtained under AC mode degrades

10% when it is used under heat pump mode. Use of this bi-objective circuitry optimization problem formulation can help assure a certain minimum acceptable performance of heat exchangers in reversible heat pumps during both cooling and heating mode usage in early design stages.

7.1.5 Multi-bank microchannel heat exchanger pass optimization using Integer Permutation based Genetic Algorithm

Microchannel heat exchangers are increasingly applied in heat pump applications due to their compactness, high heat transfer effectiveness and reduced charge. Similar to the circuitry of tube-fin heat exchanger, the performance of MCHX is strongly influenced by its pass arrangement. For multi-bank MCHX, pass arrangement optimization is particularly challenging. So far, very few studies on MCHX pass arrangements have appeared in the literature, and no study presents an optimization algorithm to solve this problem. Chapter 4 presents an integer permutation based Genetic Algorithm for multi-bank MCHX pass optimization. Different from tube-fin heat exchanger circuitry optimization, the manufacturability aspect has been implemented as the working principle of the GA operators. That is, instead of using manufacturability constraints to add penalty on those infeasible designs generated by GA, all genetic operators in the MCHX pass arrangement optimization framework are designed such that all individuals generated by GA can be decoded as feasible designs which can guarantee manufacturability. This method significantly improves the efficiency of the MCHX pass arrangement optimization algorithm. Case studies show that the proposed MCHX pass arrangement optimization algorithm yields optimal MCHX designs with 8.1-10.3% improved capacity than baseline MCHXs.

7.1.6 Development of the variable geometry air-to-refrigerant heat exchanger model with capability to simulate next generation heat exchanger and predict airflow maldistribution

This thesis presents work to develop a first-principle based tube-fin heat exchanger model. This model allows evaluation and design of the cutting-edge variable geometry tube-fin heat exchangers, therefore pushing the design envelope with further enhanced performance and minimized cost. It features improved pressure drop prediction by accounting for momentum and gravitational pressure drop. For evaporator predictions, it incorporates multiple dehumidification methods and provides option to use fin surface temperature in addition to tube surface temperature. To improve the numerical stability, it implements correlation smoothing with user-defined boundaries. The detail of this heat exchanger model is explained in Chapter 5.

This heat exchanger model integrates an in-house OpenFOAM® based CFD model that allows simulation of air flow maldistribution at the frontal face of heat exchanger, therefore the HX performance prediction accuracy is further improved. This OpenFOAM® based CFD model and the integration work are explained in Chapter 6.

7.2 Summary of Major Contributions

1. Integer permutation based air-to-refrigerant heat exchanger flow path optimization algorithm has the following contributions:

• A novel integer permutation-based Genetic Algorithm to optimize tube-fin HX circuitries and microchannel HX pass configurations

• Effective chromosome representation and genetic operators to map genotype to valid phenotype (circuitry/pass configuration) were developed

• Hybrid initialization approaches to maintain diversity and feasibility of initial individuals and to facilitate convergence were developed

• Options to add manufacturability constraints such that the optimal design can be manufactured in a cost-effective manner are provided

• IPGA for tube-fin heat exchanger circuitry optimization results in 2.4-14.6% capacity improvement compared to the baseline. This capability facilitates the industry transition to new lower Global Warming Potential refrigerants, without requiring expensive re-tooling of fin dies, and accounting for the performance variation through circuitry manipulation only.

• IPGA for microchannel heat exchanger pass arrangement optimization results in 8.1-10.3% performance improvement compared to the baseline.

2. Different applications of the proposed Integer Permutation based Genetic Algorithm have been investigated, these applications include:

• A new circuitry optimization formulation to generate optimal designs to compensate performance degradation due to air flow maldistribution. This formulation is applied to a case study. The results show 5.1% capacity improvement and 4.8% COP improvement compared to the baseline

• A circuitry optimization formulation to obtain improved HX performance under frosting conditions is implemented and the results demonstrate a 11.3% capacity improvement and 5.1% COP improvement compared to the baseline

• A bi-objective optimization formulation to generate HX circuitry design with stable performance under both cooling and heating operating modes in reversible heat pump is implemented and results show a 12.1% effective capacity improvement and 7.6% COP improvement compared to the cooling optimized design

3. A new heat exchanger model to predict performance of air-to-refrigerant heat exchangers with generalized geometries is developed. This model has the following contributions:

• Capability to model next generation heat exchanger with topology optimized tubes, variable tube size, and the option to use header or U-bends to connect tubes

• Capability to support multiple fluid groups in the same heat exchanger

• Capability to calculate air and refrigerant gravitational and momentum pressure drop in addition to friction pressure drop to improve pressure drop prediction

• Correlation smoothing with user-defined boundaries is implemented to enhance numerical stability

7.3 List of Publications

The following peer-reviewed journal papers were published as outcome of the research conducted in this dissertation:

1. Li, Z., Aute, V. and Ling, J., 2019. Tube-fin Heat Exchanger Circuitry Optimization Using Integer Permutation Based Genetic Algorithm. International Journal of Refrigeration. 103: 135-144.
2. Lee, M. S., Li, Z., Ling, J. and Aute, V., 2018. A CFD Assisted Segmented Control Volume Based Heat Exchanger Model for Simulation of Air-to-refrigerant Heat Exchanger with Air Flow Mal-Distribution. Applied Thermal Engineering 131: 230-243.
3. Huang, Z., Li, Z., Hwang, Y. and Radermacher, R., 2016. Application of Entransy Dissipation Based Thermal Resistance to Design Optimization of a Novel Finless Evaporator. Science China Technological Sciences 59(10): 1486-1493.

The following peer-reviewed conference papers were published as outcome of the research conducted in this dissertation:

1. Li, Z., Ling, J. and Aute, V., 2019. Multi-Bank Microchannel Heat Exchanger Pass Arrangement Optimization Using Integer Permutation Based Genetic Algorithm. 25th IIR Int. Congress of Refrigeration. Montreal, Canada.
2. Li, Z., Qiao, H. and Aute, V., 2019. Tube-Fin Heat Exchanger Circuitry Optimization for Improved Performance under Frosting Conditions. 13th International Modelica Conference. Regensburg, Germany. Paper-85.
3. Li, Z., Ling, J. and Aute, V., 2019. Refrigerant Circuitry Optimization of Heat Exchangers Used as Condensers and Evaporators in Heat Pump Applications. 9th Int. Conf. on Compressor and Refrigeration. Xi'An, China.
4. Li, Z., Ling, J. and Aute, V., 2018. A Review of Two-Phase Heat Transfer and Pressure Drop Correlations for Natural Refrigerants in Small Diameter Tubes. 13th IIR Gustav Lorentzen Conference. Valencia, Spain.
5. Li, Z., Ling, J., Aute, V. and Radermacher, R., 2017. Investigation of Port Level Refrigerant Flow Maldistribution in Microchannel Heat Exchanger. 12th IEA Heat Pump Conference. Rotterdam, Netherlands.
6. Li, Z., Ling, J. and Aute, V., 2018. Tube-Fin Heat Exchanger Circuitry Optimization for Multiple Airflow Maldistribution Profiles. 17th International Refrigeration and Air Conditioning Conference. Purdue, USA.

7. Li, Z. and Aute, V., 2018. Optimization of Heat Exchanger Flow Paths Using a Novel Integer Permutation Based Genetic Algorithm. EngOpt 2018 the 6th Int. Conf. on Engineering Optimization, Lisboa, Portugal.
8. Mehendale, S., Li, Z. and Aute, V., 2016. Refrigerant Circuit Optimization of Dual-Mode Single-Row Microchannel Heat Exchangers Used for R410a Heat Pumps. 16th International Refrigeration and Air Conditioning Conference. Purdue, USA.

7.4 Future Work

The following research tasks could further improve the understanding of heat exchanger design especially refrigerant flow path design:

- Explore real-life applications of microchannel heat exchanger pass arrangement optimization algorithm, such as its application to resist the impact of air flow maldistribution, the application of optimal pass arrangement under frosting condition and its application in reversible heat pump. These applications have been explored for tube-fin heat exchanger circuitry optimization, but not for microchannel heat exchanger pass arrangement optimization
- For a large heat exchanger which consists of a number of tubes, the impact of changing a small number of tube connections on heat exchanger performance should be considered in the optimization. The robust optimization considering the uncertainty of heat exchanger circuitry is a topic worth of studying in future
- Conduct refrigerant flow path optimization in system level, the studies conducted in this thesis are mainly focused on heat exchanger component level. There is a

great potential that this algorithm can significantly improve the system efficiency if IPGA is integrated with system level simulation tool

- Integrate the developed refrigerant flow path optimization algorithm into a comprehensive air-to-refrigerant heat exchanger design optimization framework. The goal is to optimize refrigerant flow path as well as other structural parameters such as tube shape, tube hydraulic diameter, fin type, fin density, number of tube banks all at once. The expected optimal heat exchanger is a variable geometry next generation heat exchanger with irregular tube layout, irregular fin dimensions, topology optimized tube shapes and optimal refrigerant flow path to offer optimal performance within the available design space.

REFERENCES

[1] Abdelaziz, O., Singh, V., Aute, V. and Radermacher, R., 2008. A-type Heat Exchanger Simulation Using 2-D CFD for Airside Heat Transfer and Pressure Drop. 12th International Refrigeration and Air Conditioning Conference at Purdue, USA.

[2] Aganda, A., Coney, J. and Sheppard, C., 2000. Airflow Maldistribution and the Performance of a Packaged Air Conditioning Unit Evaporator. Applied Thermal Engineering 20(6): 515-528.

[3] AHRI, 2008. Standard 210/240-2008. Performance Rating of Unitary Air Conditioning and Air-Source Heat Pump Equipment. Air-Conditioning and Refrigeration Institute. Arlington, VA.

[4] Alabdulkarem, A., Eldeeb, R., Hwang, Y., Aute, V., et al., 2015. Testing, Simulation and Soft-Optimization of R410a Low-Gwp Alternatives in Heat Pump System. International Journal of Refrigeration 60: 106-117.

[5] Aljuwayhel, N., Reindl, D., Klein, S. and Nellis, G., 2007. Comparison of Parallel- and Counter- Flow Circuiting in an Industrial Evaporator under Frosting Conditions. International Journal of Refrigeration 30(8): 1347-1357.

[6] ARI, 2001. Standard 410–2001: Forced-Circulation Air-Cooling and Air-Heating Coils. Air-Conditioning and Refrigeration Institute. Arlington, VA.

[7] Bacellar, D., 2016. Airside Passive Heat Transfer Enhancement, Using Multi-Scale Analysis and Shape Optimization, for Compact Heat Exchangers with Small Characteristic Lengths. (Ph.D. Thesis)

[8] Bacellar, D., Aute, V., Huang, Z. and Radermacher, R., 2017. Design Optimization and Validation of High-Performance Heat Exchangers Using Approximation Assisted Optimization and Additive Manufacturing. Science and Technology for the Built Environment 23(6): 896-911.

[9] Badhrinath, K. and Rao, J., 1994. Bi-Level Models for Optimum Designs Which Are Insensitive to Perturbations in Variables and Parameters. Advances in Design Automation 69(2): 15-23.

[10] Bahman, A. M. and Groll, E. A., 2016. Second-Law Analysis to Improve the Energy Efficiency of Environmental Control Unit. International Refrigeration and Air Conditioning Conference. Purdue, USA.

[11] Bahman, A. M. and Groll, E. A., 2017. Application of Interleaved Circuitry to Improve Evaporator Effectiveness and COP of a Packaged AC System. International Journal of Refrigeration 79(Supplement C): 114-129.

[12] Balling, R. J., Free, J. C. and Parkinson, A. R., 1986. Consideration of Worst-Case Manufacturing Tolerances in Design Optimization. Journal of Mechanisms, Transmissions, and Automation in Design 108(4): 438-441.

[13] Baskov, V. L., Kuraeva, I. V. and Protopopov, V. S., 1977. Heat Transfer with the Turbulent Flow of a Liquid at Supercritical Pressure in Tubes under Cooling Conditions. High Temperature 15.1: 81-86.

[14] Bejan, A. and Morega, A. M., 1993. Optimal Arrays of Pin Fins and Plate Fins in Laminar Forced Convection. Journal of Heat Transfer 115(1): 75-81.

[15] Belegundu, A. D. and Zhang, S., 1992. Robustness of Design through Minimum Sensitivity. Journal of Mechanical Design 114(2): 213-217.

[16] Bigot, G., Palandre, L. and Clodic, D., 2000. Optimized Design of Heat Exchangers for "Reversible" Heat Pump Using R-407C. International Refrigeration and Air Conditioning Conference. Purdue, USA.

[17] Blasius, H., 1907. Grenzschichten in Flüssigkeiten Mit Kleiner Reibung, Druck von BG Teubner.

[18] Branke, J., Year. Reducing the Sampling Variance When Searching for Robust Solutions. Proceedings of the 3rd Annual Conference on Genetic and Evolutionary Computation, Morgan Kaufmann Publishers Inc.

[19] Casson, V., Cavallini, A., Cecchinato, L. and Del Col, D., 2002. Peformance of Finned Coil Condensers Optimized for New HFC Refrigerants/Discussion. ASHRAE Transactions 108: 517.

[20] Choi, K. and Youn, B., 2002. On Probabilistic Approaches for Reliability-Based Design Optimization (RBDO). 9th AIAA/ISSMO Symposium on Multidisciplinary Analysis and Optimization.

[21] Churchill, S. W., 1977. Friction-Factor Equation Spans All Fluid-Flow Regimes. Chemical Engineering 84(24): 91-92.

[22] Chwalowski, M., Didion, D. and Domanski, P., 1989. Verification of Evaporator Computer Models and Analysis of Performance of an Evaporator Coil. ASHRAE Transactions 95: 1229-1236.

[23] Coit, D. W. and Smith, A. E., 1996. Penalty Guided Genetic Search for Reliability Design Optimization. Computers & Industrial Engineering 30(4): 895-904.

[24] Deb, K., 2000. An Efficient Constraint Handling Method for Genetic Algorithms. Computer Methods in Applied Mechanics and Engineering 186(2): 311-338.

[25] Deb, K., 2001. Multi-Objective Optimization Using Evolutionary Algorithms, John Wiley & Sons.

[26] Deb, K., 2012. Optimization for Engineering Design: Algorithms and Examples, PHI Learning Pvt. Ltd.

[27] Dittus, F. and Boelter, L., 1985. Heat Transfer in Automobile Radiators of the Tubular Type. International Communications in Heat and Mass Transfer 12(1): 3-22.

[28] Do, K. H., Min, J. Y. and Kim, S. J., 2007. Thermal Optimization of an Internally Finned Tube Using Analytical Solutions Based on a Porous Medium Approach. Journal of Heat Transfer 129(10): 1408-1416.

[29] Domanski, P., 2003. Evap-Cond, Simulation Models for Finned Tube Heat Exchangers. National Institute of Standards and Technology Building and Fire Research Laboratory, Gaithersburg, MD, USA.

[30] Domanski, P. A., 1991. Simulation of an Evaporator with Nonuniform One-Dimensional Air Distribution. ASHRAE Transactions.

[31] Domanski, P. A., Yashar, D., Kaufman, K. A. and Michalski, R. S., 2004. An Optimized Design of Finned-Tube Evaporators Using the Learnable Evolution Model. HVAC&R Research 10(2): 201-211.

[32] Domanski, P. A., Yashar, D. and Kim, M., 2005. Performance of a Finned-Tube Evaporator Optimized for Different Refrigerants and Its Effect on System Efficiency. International Journal of Refrigeration 28(6): 820-827.

[33] Du, X. and Chen, W., 2000. Towards a Better Understanding of Modeling Feasibility Robustness in Engineering Design. Journal of Mechanical Design 122(4): 385-394.

[34] Fang, X., 1999. Modeling and Analysis of Gas Coolers, Air Conditioning and Refrigeration Center. College of Engineering. University of Illinois at Urbana-Champaign.

[35] Friedel, L., 1979. Improved Friction Pressure Drop Correlation for Horizontal and Vertical Two-Phase Pipe Flow. Proceedings of European Two-Phase Flow Group Meet., Ispra, Italy, 1979.

[36] Geuzaine, C. and Remacle, J. F., 2009. Gmsh: A 3-D Finite Element Mesh Generator with Built-in Pre-and Post-Processing Facilities. International Journal for Numerical Methods in Engineering 79(11): 1309-1331.

[37] Gnielinski, V., 1976. New Equations for Heat and Mass Transfer in Turbulent Pipe and Channel Flow. International Chemistry Engineering 16(2): 359-368.

[38] Goldberg, D. E., 1989. Genetic Algorithms in Search, Optimization, and Machine Learning. New York, Addison-Wesley.

[39] Gong, J., Gao, T., Yuan, X. and Huang, D., 2008. Effects of Air Flow Maldistribution on Refrigeration System Dynamics of Air Source Heat Pump Chiller under Frosting Conditions. Energy Conversion and Management 49(6): 1645-1651.

[40] Gunawan, S. and Azarm, S., 2004. Non-Gradient Based Parameter Sensitivity Estimation for Single Objective Robust Design Optimization. Journal of Mechanical Design 126(3): 395-402.

[41] Hall, C. A. and Meyer, W. W., 1976. Optimal Error Bounds for Cubic Spline Interpolation. Journal of Approximation Theory 16(2): 105-122.

[42] Hermann, P., 1962. Simulation of Steam Generation in a Heat Exchanger. IRE Transactions on Electronic Computers(1): 53-57.

[43] Heun, M. K. and Dunn, W. E., 1996. Principles of Refrigerant Circuiting with Application to Microchannel Condensers. Part 2: The Pressure-Drop Effect and the Cross-Flow Heat Exchanger Effect. ASHRAE Transaction.

[44] Hirokawa, N. and Fujita, K., Year. Mini-Max Type Formulation of Strict Robust Design Optimization under Correlative Variation. ASME 2002 International Design Engineering Technical Conference.

[45] Hooman, K. and Gurgenci, H., 2010. Porous Medium Modeling of Air-Cooled Condensers. Transport in Porous Media 84(2): 257-273.

[46] Huai, X. and Koyama, S., 2007. Heat Transfer Characteristics of Supercritical Co2 Flow in Small-Channeled Structures. Experimental Heat Transfer 20(1): 19-33.

[47] Huang, L., Aute, V. and Radermacher, R., 2015. A Survey of Optimization Formulations and Techniques for the Design of Heat Exchangers Using Lower Gwp Refrigerants. 2015 ASHRAE Winter Conference, Paper # CH-15-C039.

[48] Hughes, E. J., Year. Evolutionary Multi-Objective Ranking with Uncertainty and Noise. International Conference on Evolutionary Multi-Criterion Optimization, Springer.

[49] Imke, U., 2004. Porous Media Simplified Simulation of Single-and Two-Phase Flow Heat Transfer in Micro-Channel Heat Exchangers. Chemical Engineering Journal 101(1-3): 295-302.

[50] Jiang, H., Aute, V. and Radermacher, R., 2002. A User-Friendly Simulation and Optimization Tool for Design of Coils. International Refrigeration and Air Conditioning Conference. Purdue, USA.

[51] Jiang, H., Aute, V. and Radermacher, R., 2006. CoilDesigner: a General-purpose Simulation and Design Tool for Air-to-refrigerant Heat Exchangers. International Journal of Refrigeration 29(4): 601-610.

[52] Jin, R., Du, X. and Chen, W., 2003. The Use of Metamodeling Techniques for Optimization under Uncertainty. Structural and Multidisciplinary Optimization 25(2): 99-116.

[53] Jung, D., McLinden, M., Radermacher, R. and Didion, D., 1989. A Study of Flow Boiling Heat Transfer with Refrigerant Mixtures. International Journal of Heat and Mass Transfer 32(9): 1751-1764.

[54] Jung, D. and Radermacher, R., 1989. Prediction of Pressure Drop During Horizontal Annular Flow Boiling of Pure and Mixed Refrigerants. International Journal of Heat and Mass Transfer 32(12): 2435-2446.

[55] Kærn, M. R., Brix, W., Elmegaard, B. and Larsen, L. F. S., 2011. Performance of Residential Air-Conditioning Systems with Flow Maldistribution in Fin-and-Tube Evaporators. International Journal of Refrigeration 34(3): 696-706.

[56] Kærn, M. R., Elmegaard, B. and Larsen, L. F. S., 2013. Comparison of Fin-and-Tube Interlaced and Face Split Evaporators with Flow Maldistribution and Compensation. International Journal of Refrigeration 36(1): 203-214.

[57] Kærn, M. R. and Tiedemann, T., 2012. Compensation of Airflow Maldistribution in Fin-and-Tube Evaporators. International Refrigeration and Air Conditioning Conference. Purdue, USA.

[58] Kargupta, H., Deb, K. and Goldberg, D. E., Year. Ordering Genetic Algorithms and Deception. PPSN, Citeseer.

[59] Katz, D. L. and Briggs, D. E., 1965. A Bright Future for Computers in Heat Transfer. Chemical Engineerings Progress 61191-96.

[60] Kiefer, J., 1953. Sequential Minimax Search for a Maximum. Proceedings of the American Mathematical Society 4(3): 502-506.

[61] Kim, N.-H., Yun, J.-H. and Webb, R., 1997. Heat Transfer and Friction Correlations for Wavy Plate Fin-and-Tube Heat Exchangers. Journal of heat transfer 119(3): 560-567.

[62] Kim, S. and Kim, D., 1999. Forced Convection in Microstructures for Electronic Equipment Cooling. Journal of Heat Transfer 121(3): 639-645.

[63] Kim, S. J., Yoo, J. W. and Jang, S. P., 2002. Thermal Optimization of a Circular-Sectored Finned Tube Using a Porous Medium Approach. Journal of Heat Transfer 124(6): 1026-1033.

[64] Kirby, E. S., Bullard, C. W. and Dunn, W. E., 1998. Effect of Airflow Nonuniformity on Evaporator Performance/Discussion. ASHRAE Transactions 104: 755.

[65] Kritikos, K., Albanakis, C., Missirlis, D., Vlahostergios, Z., et al., 2010. Investigation of the Thermal Efficiency of a Staggered Elliptic-tube Heat Exchanger for Aeroengine Applications. Applied Thermal Engineering 30(2-3): 134-142.

[66] Lee, J. and Domanski, P. A., 1997. Impact of Air and Refrigerant Maldistributions on the Performance of Finned-tube Evaporators with R-22 and R-407C. NIST Report.

[67] Lee, K.-H. and Park, G.-J., 2001. Robust Optimization Considering Tolerances of Design Variables. Computers & Structures 79(1): 77-86.

[68] Lee, K. and Lee, T. H., Year. Fuzzy Multi-objective Optimization of an Automotive Seat Using Response Surface Model and Reliability Method. Proceedings of the 4th World Congress of Structural and Multidisciplinary Optimization.

[69] Lee, M. S., Li, Z., Ling, J. and Aute, V., 2018. A CFD Assisted Segmented Control Volume Based Heat Exchanger Model for Simulation of Air-to-refrigerant Heat Exchanger with Air Flow Mal-distribution. Applied Thermal Engineering 131: 230-243.

[70] Lee, W. J., Kim, H. J. and Jeong, J. H., 2016. Method for Determining the Optimum Number of Circuits for a Fin-tube Condenser in a Heat Pump. International Journal of Heat and Mass Transfer 98: 462-471.

[71] Li, J. and Pega, H., 2018. An Experimentally Validated Model for Microchannel Condensers with Separation Circuiting. 17th International Refrigeration and Air Conditioning Conference, Purdue, USA.

[72] Li, M., Azarm, S. and Aute, V., Year. A Multi-Objective Genetic Algorithm for Robust Design Optimization. Proceedings of the 7th Annual Conference on Genetic and Evolutionary Computation.

[73] Li, M., Azarm, S. and Boyars, A., 2006. A New Deterministic Approach Using Sensitivity Region Measures for Multi-Objective Robust and Feasibility Robust Design Optimization. Journal of Mechanical Design 128(4): 874-883.

[74] Li, Z. and Aute, V., 2018. Optimization of Heat Exchanger Flow Paths Using a Novel Integer Permutation Based Genetic Algorithm. EngOpt 2018 Proceedings of the 6th International Conference on Engineering Optimization, Lisboa, Portugal.

[75] Li, Z., Ling, J. and Aute, V., 2018. Tube-Fin Heat Exchanger Circuitry Optimization for Multiple Airflow Maldistribution Profiles. 17th International Refrigeration and Air Conditioning Conference. Purdue, USA.

[76] Li, Z., Ling, J. and Aute, V., 2018. Tube-Fin Heat Exchanger Circuitry Optimization Using Integer Permutation Based Genetic Algorithm. 17th International Refrigeration and Air Conditioning Conference. Purdue, USA.

[77] Liang, S., Wong, T. and Nathan, G., 2001. Numerical and Experimental Studies of Refrigerant Circuitry of Evaporator Coils. International Journal of Refrigeration 24(8): 823-833.

[78] Liu, J., Wei, W., Ding, G., Zhang, C., et al., 2004. A General Steady State Mathematical Model for Fin-and-Tube Heat Exchanger Based on Graph Theory. International Journal of Refrigeration 27(8): 965-973.

[79] Malhammar, A., 1988. Monitoring Frost Growth in Evaporators Is a Complex Process. Australian Refrigeration, Air Conditioning and Heat.

[80] Martínez-Ballester, S., Corberán, J.-M. and Gonzálvez-Maciá, J., 2013. Numerical Model for Microchannel Condensers and Gas Coolers: Part Ii–Simulation Studies and Model Comparison. International Journal of Refrigeration 36(1): 191-202.

[81] McQuiston, F. C. and Parker, J. D., 1982. Heating, Ventilating, and Air Conditioning: Analysis and Design. Wiley.

[82] Mehendale, S., 2013. Principles of Refrigerant Circuiting in Single Row Microchannel Evaporators. ASME 2013 11th International Conference on Nanochannels, Microchannels, and Minichannels, ASME.

[83] Mehendale, S., Li, Z. and Aute, V., 2016. Refrigerant Circuit Optimization of Dual-Mode Single-Row Microchannel Heat Exchangers Used for R410A Heat Pumps. International Refrigeration and Air Conditioning Conference. Purdue, USA.

[84] Menter, F. R., 1994. Two-Equation Eddy-Viscosity Turbulence Models for Engineering Applications. AIAA journal 32(8): 1598-1605.

[85] Menter, F. R., Kuntz, M. and Langtry, R., 2003. Ten Years of Industrial Experience with the Sst Turbulence Model. Turbulence, heat and mass transfer 4(1): 625-632.

[86] Min, J. and Webb, R. L., 2004. Numerical Analyses of Effects of Tube Shape on Performance of a Finned Tube Heat Exchanger. Journal of Enhanced Heat Transfer 11(1).

[87] Morrison, F. A., 2013. Data Correlation for Friction Factor in Smooth Pipes. Department of Chemical Engineering, Michigan Technological University, Houghton, MI 49931.

[88] Müller-Steinhagen, H. and Heck, K., 1986. A Simple Friction Pressure Drop Correlation for Two-Phase Flow in Pipes. Chemical Engineering and Processing: Process Intensification 20(6): 297-308.

[89] Ogawa, K., Tanaka, N. and Takeshita, M., 1993. Performance Improvement of Plate Fin-and-Tube Heat Exchangers under Frosting Conditions. ASHRAE Transactions.

[90] Oliet, C., Perez-Segarra, C., Danov, S. and Oliva, A., 2007. Numerical Simulation of Dehumidifying Fin-and-Tube Heat Exchangers: Semi-Analytical Modelling and Experimental Comparison. International Journal of Refrigeration 30(7): 1266-1277.

[91] Parkinson, A., Sorensen, C. and Pourhassan, N., 1993. A General Approach for Robust Optimal Design. Journal of Mechanical Design 115(1): 74-80.

[92] Patankar, S. and Spalding, D., 1974. A Calculation Procedure for the Transient and Steady-State Behavior of Shell-and-Tube Heat Exchangers. Chapter in Heat Exchangers: Design and Theory Sourcebook.

[93] Payne, W. V. and Domanski, P. A., 2003. Potential Benefits of Smart Refrigerant Distributors. NIST Report.

[94] Pitla, S. S., Groll, E. A. and Ramadhyani, S., 2002. New Correlation to Predict the Heat Transfer Coefficient During In-tube Cooling of Turbulent Supercritical CO_2. International Journal of Refrigeration 25(7): 887-895.

[95] Ploskas, N., Laughman, C., Raghunathan, A. U. and Sahinidis, N. V., 2018. Optimization of Circuitry Arrangements for Heat Exchangers Using Derivative-free Optimization. Chemical Engineering Research and Design.

[96] Press, W. H., Teukolsky, S. A., Vetterling, W. T. and Flannery, B. P., 2007. Numerical Recipes 3rd Edition: The Art of Scientific Computing, Cambridge University Press.

[97] Qiao, H., Aute, V. and Radermacher, R., 2015. Transient Modeling of a Flash Tank Vapor Injection Heat Pump System–Part I: Model Development. International Journal of Refrigeration 49: 169-182.

[98] Qiao, H., Aute, V. and Radermacher, R., 2017. Dynamic Modeling and Characteristic Analysis of a Two-stage Vapor Injection Heat Pump System under Frosting Conditions. International Journal of Refrigeration 84: 181-197.

[99] Renaud, J., 1997. Automatic Differentiation in Robust Optimization. AIAA Journal 35(6): 1072-1079.

[100] Rossetti, A., Minetto, S. and Marinetti, S., 2015. A Simplified Thermal Cfd Approach to Fins and Tube Heat Exchanger: Application to Maldistributed Airflow on an Open Display Cabinet. International Journal of Refrigeration 57: 208-215.

[101] Rossi, T. M. and Braun, J. E., 1995. Computer Models for the Development, Evaluation, and Implementation of Fault Detection and Diagnostic Methods for HVAC Equipment. Report No. : HL95-13(A),1995.

[102] Sanders, C. T., 1974. The Influence of Frost Formation and Defrosting on the Performance of Air Coolers. (Ph.D. Thesis)

[103] Sarfraz, O. and Bradshaw, C. R., 2019. A Novel Technique for Computationally Efficient Consideration of Cross-Fin Conduction in Fin-and-Tube Heat Exchanger Models. International Journal of Refrigeration 107: 73-83.

[104] Schwentker, R., Aute, V., Radermacher, R. and Mercer, K., Year. Simulation and Design Tool for Microchannel Heat Exchangers. Fifth International Conference on Enhanced, Compact, and Ultra-Compact Heat Exchangers,.

[105] Shah, M. M., 2016. Comprehensive Correlations for Heat Transfer During Condensation in Conventional and Mini/Micro Channels in All Orientations. International Journal of Refrigeration 67: 22-41.

[106] Shah, M. M., 2017. Unified Correlation for Heat Transfer During Boiling in Plain Mini/Micro and Conventional Channels. International Journal of Refrigeration 74: 606-626.

[107] Shen, B., Groll, E. and Braun, J., 2004. Acmodel: A Steady-State System Simulation Model for Unitary Air Conditioners and Heat Pumps. USNC/IIR Short Course on Simulation Tools for Vapor Compression Systems and Component Analysis. International Refrigeration and Air Conditioning Conference. Purdue, USA.

[108] Shi, Y., Ji, J. and Zhang, C., 2010. Semiporous Media Approach for Numerical Simulation of Flow through Large-Scale Sparse Tubular Heat Exchangers. HVAC&R Research 16(5): 617-628.

[109] Singh, V., Abdelaziz, O., Aute, V. and Radermacher, R., 2011. Simulation of Air-to-refrigerant Fin-and-tube Heat Exchanger with CFD-based Air Propagation. International Journal of Refrigeration 34(8): 1883-1897.

[110] Singh, V., Aute, V. and Radermacher, R., 2009. A Heat Exchanger Model for Air-to-refrigerant Fin-and-tube Heat Exchanger with Arbitrary Fin Sheet. International Journal of Refrigeration 32(7): 1724-1735.

[111] Son, C. and Park, S., 2006. An Experimental Study on Heat Transfer and Pressure Drop Characteristics of Carbon Dioxide During Gas Cooling Process in a Horizontal Tube. International Journal of Refrigeration 29(4): 539-546.

[112] Spears, W. and Jong, K., 1998. The Role of Mutation and Recombination in Evolutionary Algorithms. (Ph.D. Thesis)

[113] Sundaresan, S., 1993. A Robust Optimization Procedure with Variations on Design Variables and Constraints. ASME, Advances in Design Automation.

[114] Sundaresan, S., Ishii, K. and Houser, D. R., 1992. Design Optimization for Robustness Using Performance Simulation Programs. Engineering Optimization 20(3): 163-178.

[115] Taguchi, G., 1978. Performance Analysis Design. The International Journal of Production Research 16(6): 521-530.

[116] Tsutsui, S. and Ghosh, A., 1997. Genetic Algorithms with a Robust Solution Searching Scheme. IEEE Transactions on Evolutionary Computation 1(3): 201-208.

[117] Waltrich, P. J., Barbosa Jr, J. R. and Hermes, C. J., 2011. COP-based Optimization of Accelerated Flow Evaporators for Household Refrigeration Applications. Applied Thermal Engineering 31(1): 129-135.

[118] Wang, C. and Chi, K., 2000. Heat Transfer and Friction Characteristics of Plain Fin-and-Tube Heat Exchangers, Part I: New Experimental Data. International Journal of Heat and Mass Transfer 43(15): 2681-2691.

[119] Wang, C., Jang, J., Lai, C. and Chang, Y., 1999. Effect of Circuit Arrangement on the Performance of Air-Cooled Condensers. International Journal of Refrigeration 22(4): 275-282.

[120] Wang, C., Lee, C., Chang, C. and Lin, S., 1999. Heat Transfer and Friction Correlation for Compact Louvered Fin-and-Tube Heat Exchangers. International Journal of Heat and Mass Transfer 42(11): 1945-1956.

[121] Wang, C., Lee, W. and Sheu, W., 2001. A Comparative Study of Compact Enhanced Fin-and-tube Heat Exchangers. International Journal of Heat and Mass Transfer 44(18): 3565-3573.

[122] Wang, C., Tsai, Y. and Lu, D., 1998. Comprehensive Study of Convex-louver and Wavy Fin-and-tube Heat Exchangers. Journal of Thermophysics and Heat Transfer 12(3): 423-430.

[123] Wang, X., Hwang, Y. and Radermacher, R., 2009. Two-stage Heat Pump System with Vapor-Injected Scroll Compressor Using R410A as a Refrigerant. International Journal of Refrigeration 32(6): 1442-1451.

[124] Weller, H. G., Tabor, G., Jasak, H. and Fureby, C., 1998. A Tensorial Approach to Computational Continuum Mechanics Using Object-Oriented Techniques. Computers in Physics 12(6): 620-631.

[125] Winkler, J., Aute, V. and Radermacher, R., 2006. Component-based Vapor Compression Simulation Tool with Integrated Multi-objective Optimization Routines. International Refrigeration and Air Conditioning Conference. Purdue, USA.

[126] Wu, Z., Ding, G., Wang, K. and Fukaya, M., 2008a. Knowledge-based Evolution Method for Optimizing Refrigerant Circuitry of Fin-and-tube Heat Exchangers. HVAC&R Research 14(3): 435-452.

[127] Wu, Z., Ding, G., Wang, K. and Fukaya, M., 2008b. Application of a Genetic Algorithm to Optimize the Refrigerant Circuit of Fin-and-tube Heat Exchangers for Maximum Heat Transfer or Shortest Tube. International Journal of Thermal Sciences 47(8): 985-997.

[128] Xu, Y. and Fang, X., 2013. A New Correlation of Two-phase Frictional Pressure Drop for Condensing Flow in Pipes. Nuclear Engineering and Design 263: 87-96.

[129] Yashar, D., Cho, H. and Domanski, P., 2008. Measurement of Air-velocity Profiles for Finned-tube Heat Exchangers Using Particle Image Velocimetry. NIST Report.

[130] Yashar, D. and Cho, H., 2007. Air-Side Velocity Distribution in Finned-tube Heat Exchangers. NIST Report.

[131] Yashar, D. and Domanski, P., 2009. Particle Image Velocimetry Measurements and Cfd-Based Predictions of Air Distribution at Evaporator Inlet and Outlet. NIST Report.

[132] Yashar, D. and Domanski, P., 2010. Air Flow Distribution through an a-Shaped Evaporator under Dry and Wet Coil Conditions. International Refrigeration and Air Conditioning Conference. Purdue, USA.

[133] Yashar, D., Domanski, P. and Cho, H., 2014. An Experimental and Computational Study of Approach Air Distribution for Slanted and a-Shaped Finned-Tube Heat Exchangers. HVAC&R Research 20(5): 498-507.

[134] Ye, L., Tong, M. W. and Zeng, X., 2009. Design and Analysis of Multiple Parallel-Pass Condensers. International Journal of Refrigeration 32(6): 1153-1161.

[135] Yoon, S., Kim, J., Hwang, Y., Kim, M., et al., 2003. Heat Transfer and Pressure Drop Characteristics During the in-Tube Cooling Process of Carbon Dioxide in the Supercritical Region. International Journal of Refrigeration 26(8): 857-864.

[136] Yu, J. and Ishii, K., 1998. Design for Robustness Based on Manufacturing Variation Patterns. Journal of Mechanical Design 120(2): 196-202.

[137] Zhu, J. and Ting, K., 2001. Performance Distribution Analysis and Robust Design. Journal of Mechanical Design 123(1): 11-17.

[138] Žukauskas, A., 1972. Heat Transfer from Tubes in Crossflow. Advances in Heat Transfer, Elsevier. 8: 93-160.